

EUROPEAN ORGANISATION FOR NUCLEAR RESEARCH (CERN)



Submitted to: JHEP

CERN-PH-2016-079
7th June 2016

Measurement of the double-differential high-mass Drell–Yan cross section in pp collisions at $\sqrt{s} = 8$ TeV with the ATLAS detector

The ATLAS Collaboration

Abstract

This paper presents a measurement of the double-differential cross section for the Drell–Yan $Z/\gamma^* \rightarrow \ell^+ \ell^-$ and photon-induced $\gamma\gamma \rightarrow \ell^+ \ell^-$ processes where ℓ is an electron or muon. The measurement is performed for invariant masses of the lepton pairs, $m_{\ell\ell}$, between 116 GeV and 1500 GeV using a sample of 20.3 fb^{-1} of pp collisions data at centre-of-mass energy of $\sqrt{s} = 8$ TeV collected by the ATLAS detector at the LHC in 2012. The data are presented double differentially in invariant mass and absolute dilepton rapidity as well as in invariant mass and absolute pseudorapidity separation of the lepton pair. The single-differential cross section as a function of $m_{\ell\ell}$ is also reported. The electron and muon channel measurements are combined and a total experimental precision of better than 1% is achieved at low $m_{\ell\ell}$. A comparison to next-to-next-to-leading order perturbative QCD predictions using several recent parton distribution functions and including next-to-leading order electroweak effects indicates the potential of the data to constrain parton distribution functions. In particular, a large impact of the data on the photon PDF is demonstrated.

Contents

1	Introduction	3
2	ATLAS detector	4
3	Simulated event samples	4
4	Event selection	5
4.1	Electron channel	6
4.2	Muon channel	7
5	Background estimate	7
5.1	Multijet and $W+jets$ background estimate in the electron channel	8
5.2	Multijet and $W+jets$ background estimate in the muon channel	10
6	Cross-section measurement	12
7	Systematic uncertainties	13
7.1	Electron channel	14
7.1.1	Multijet and $W+jets$ background	14
7.1.2	Energy scale and resolution	15
7.1.3	Reconstruction, identification and isolation efficiency	15
7.1.4	Trigger efficiency	16
7.2	Muon channel	16
7.2.1	Reconstruction efficiency	16
7.2.2	Momentum scale and resolution	16
7.2.3	Isolation and impact parameter efficiency	16
7.2.4	Multijet and $W+jets$ background	17
7.2.5	Trigger efficiency	17
7.3	Systematic uncertainties common to both channels	17
7.3.1	Top and diboson background	17
7.3.2	Luminosity	18
7.3.3	MC statistics and MC modelling	18
7.3.4	Bin-by-bin correction	18
7.3.5	PDF uncertainty	18
8	Results	19
9	Comparison to theoretical predictions	26
10	Conclusion	31
Appendix		33

1 Introduction

The Drell–Yan (DY) process [1] of lepton pair production in hadronic interactions, $pp \rightarrow Z/\gamma^* + X$ with $Z/\gamma^* \rightarrow \ell^+\ell^-$, is a powerful tool in understanding the nature of partonic interactions and of hadronic structure in detail. The study of this process has been fundamental in developing theoretical perturbative calculations of quantum chromodynamics (QCD) which are now performed at next-to-next-to-leading-order (NNLO) accuracy [2–5]. Measurements from the Large Hadron Collider (LHC) of neutral- and charged-current Drell–Yan processes mediated by Z/γ^* and W exchange respectively at centre-of-mass energies of $\sqrt{s} = 7$ TeV and 8 TeV have been recently published by the ATLAS [6–8], CMS [9–12] and LHCb [13–17] collaborations. These data provide new constraints on the parton distribution functions (PDFs) of the proton, some of which have been used in recent global PDF fits [18–20].

Although on-shell Z and W boson measurements provide the greatest experimental precision, they are restricted in the kinematic range of partonic momentum fraction x , and four-momentum transfer $Q = m_{\ell\ell}$, the invariant mass of the dilepton pair. Off-shell measurements provide complementary constraints in a wider range of x and Q . In the neutral-current case, the off-shell measurements are dominated by the electromagnetic quark couplings to the virtual photon γ^* , whereas the on-shell measurements are dominated by the weak axial and vector couplings of the quarks to the Z boson. Therefore, the measurements have different sensitivity to the up-type and down-type quarks. At large $m_{\ell\ell}$ the measurements offer constraints on the large- x antiquark PDFs which are poorly known. In addition, off-shell measurements may also be sensitive to the largely unconstrained photon PDF [7, 8, 21, 22] through the photon-induced (PI) process $\gamma\gamma \rightarrow \ell^+\ell^-$.

Neutral-current DY data at higher masses can also be used to determine the running of the electroweak (EW) gauge couplings above the weak scale, and to set model-independent limits on new states with electroweak quantum numbers [23]. In particular, at the highest invariant masses accessible at the LHC, the observed dilepton spectrum may be sensitive to new physics, which could manifest itself as a resonance or a broad modification to the continuum spectrum. Such searches performed by the ATLAS and CMS experiments [24–26] have so far not found any significant deviations from the Standard Model, and the largest systematic uncertainty on the derived exclusion limits arises from the lack of knowledge of the PDFs at high x . Since at leading order the parton momentum fractions from the two protons (1 or 2) are given by $x_{1,2} = (m_{\ell\ell}/\sqrt{s}) e^{\pm y_{\ell\ell}}$, where $y_{\ell\ell}$ is the dilepton rapidity, it can be seen that the large x region is accessible at large $m_{\ell\ell}$ in the case of central production ($y_{\ell\ell} = 0$), as well as at lower $m_{\ell\ell}$ and large $y_{\ell\ell}$. Therefore, a double-differential measurement of the Drell–Yan cross section in $m_{\ell\ell}$ and $y_{\ell\ell}$ provides PDF constraints in a new kinematic region which is expected to be unaffected by the manifestation of potential new physics at the highest invariant mass.

This article reports two inclusive double-differential cross-section measurements for the process $pp \rightarrow \ell^+\ell^- + X$. The first measurement is reported as a function of $m_{\ell\ell}$ and absolute dilepton rapidity $|y_{\ell\ell}|$, and the second as a function of $m_{\ell\ell}$ and absolute dilepton pseudorapidity separation $|\Delta\eta_{\ell\ell}|$. These measurements are sensitive to the proton PDFs, the PI process, and higher-order electroweak corrections, which have different kinematic dependencies. In particular, the t -channel PI process is expected to contribute at large $|\Delta\eta_{\ell\ell}|$, small $|y_{\ell\ell}|$ and large $m_{\ell\ell}$. Therefore, measurements as a function of various kinematic distributions are needed to disentangle the different contributions [27]. For completeness the inclusive single-differential measurement $d\sigma/dm_{\ell\ell}$ is also provided. The measurements are performed using pp collision data collected at $\sqrt{s} = 8$ TeV in both electron and muon channels. The data cover the kinematic region of $116 \leq m_{\ell\ell} \leq 1500$ GeV and access partonic momentum fractions from 10^{-3} up to $x \sim 1$. The integrated luminosity of the data sample is 20.3 fb^{-1} , a factor five larger than used in the previous ATLAS

measurement [7] at $\sqrt{s} = 7$ TeV performed in the electron channel only. Therefore, the results reported here have a substantially better precision than earlier results.

2 ATLAS detector

The ATLAS detector [28] consists of an inner tracking detector (ID) surrounded by a thin superconducting solenoid, electromagnetic and hadronic calorimeters, and a muon spectrometer (MS). Charged particles in the pseudorapidity¹ range $|\eta| < 2.5$ are reconstructed with the ID, which consists of layers of silicon pixel and microstrip detectors and a straw-tube transition-radiation tracker having coverage within $|\eta| < 2.0$. The ID is immersed in a 2 T magnetic field provided by the solenoid. The latter is surrounded by a hermetic calorimeter that covers $|\eta| < 4.9$ and provides three-dimensional reconstruction of particle showers. The electromagnetic calorimeter is a liquid-argon sampling calorimeter, which uses lead absorbers for $|\eta| < 3.2$ and copper absorbers in the very forward region. The hadronic sampling calorimeter uses plastic scintillator tiles as the active material and steel absorbers in the region $|\eta| < 1.7$. In the region $1.5 < |\eta| < 4.9$, liquid argon is used as active material, with copper or/and tungsten absorbers. Outside the calorimeters, air-core toroids supply the magnetic field for the MS. There, three stations of precision chambers allow the accurate measurement of muon track curvature in the region $|\eta| < 2.7$. The majority of these precision chambers are composed of drift tubes, while cathode-strip chambers provide coverage in the inner stations of the forward region for $2.0 < |\eta| < 2.7$. Additional muon chambers installed between the inner and middle stations of the forward region and commissioned prior to the 2012 run improve measurements in the transition region of $1.05 < |\eta| < 1.35$ where the outer stations have no coverage. Muon triggering is possible in the range $|\eta| < 2.4$, using resistive-plate chambers in the central region that also provide a measurement of the coordinate out of the bending plane, and thin-gap chambers in the forward region. A three-level trigger system [29] selects events to be recorded for offline analysis.

3 Simulated event samples

Monte Carlo (MC) simulation samples are used to model the expected signal and background yields, with the exception of certain data-driven background estimates. The MC samples are normalised using the highest-order cross-section predictions available in perturbation theory.

The DY process is generated at next-to-leading order (NLO) using PowHEG [30–33] and the CT10 PDF [34], with PYTHIA 8 [35] to model parton showering and hadronisation. To estimate systematic uncertainties in the event modelling an alternative sample is simulated using the same PDF but the MC@NLO [36–38] generator with HERWIG++ [39]. The Z/γ^* differential cross section as a function of mass has been calculated at next-to-next-to-leading order (NNLO) in perturbative QCD (pQCD) using FEWZ 3.1 [5, 40, 41] with the MSTW2008NNLO PDF [42]. The calculation includes NLO electroweak (EW) corrections beyond final-state photon radiation (FSR). A mass-dependent K -factor used to scale the Z/γ^* MC sample is obtained from the ratio of the calculated NNLO pQCD cross section with the additional EW corrections,

¹ ATLAS uses a right-handed coordinate system with its origin at the nominal interaction point in the centre of the detector and the z -axis along the beam pipe. The x -axis points from the interaction point to the centre of the LHC ring, and the y -axis points upward. Cylindrical coordinates (r, ϕ) are used in the transverse plane, ϕ being the azimuthal angle around the beam pipe. The pseudorapidity is defined in terms of the polar angle θ as $\eta = -\ln \tan(\theta/2)$.

to the cross section from the PowHEG sample. It is found to deviate from unity by 3.5–2.0% across the measured range in $m_{\ell\ell}$.

The photon-induced (PI) process, $\gamma\gamma \rightarrow \ell^+\ell^-$, is simulated at leading-order using PYTHIA 8 and the MRST2004qed PDF [21]. The MC yield is scaled by a factor of 0.7 in order to match the NLO calculations of SANC [43, 44].

The background from $t\bar{t}$ production is the dominant background with isolated prompt leptons from electroweak boson decays. It is estimated at NLO using PowHEG and the CT10 PDF, with PYTHIA 6 [45] for parton showering and hadronisation. Two further MC samples for $t\bar{t}$ and single top (Wt) production in association with a W boson are modelled by MC@NLO and the CT10 PDF, with HERWIG [46, 47] for parton showering and hadronisation. The MC@NLO $t\bar{t}$ sample is used for estimating systematic uncertainties only. The $t\bar{t}$ MC samples are normalised to a cross section of $\sigma_{t\bar{t}} = 253^{+13}_{-15}$ pb for a top-quark mass of 172.5 GeV. This is calculated at NNLO in QCD including resummation of next-to-next-to-leading logarithmic soft-gluon terms with Top++2.0 [48–53]. The PDF and α_S uncertainties on the $t\bar{t}$ cross section are calculated using the PDF4LHC prescription [54] with the MSTW2008 68% CL NNLO [42, 55], CT10 NNLO [34, 56] and NNPDF2.3 [57] PDF error sets added in quadrature to the scale uncertainty. Varying the top-quark mass by ± 1 GeV leads to an additional systematic uncertainty of +8 pb and -7 pb, which is also added in quadrature. The single-top background in association with a W boson has a cross section of $\sigma_{Wt} = 22.4 \pm 1.5$ pb [58]. Given that the Wt contribution is small compared to the $t\bar{t}$ cross section, an overall uncertainty of 6% is estimated on the top-quark background.

Further important background contributions are due to diboson (WW , WZ and ZZ) production with decays to final states with at least two leptons. The diboson processes are generated at leading order (LO) with HERWIG, using the CTEQ6L1 PDF [59]. The WZ and ZZ cross-section values used are 20.3 ± 0.8 pb and 7.2 ± 0.3 pb respectively, as calculated at NLO with MCFM [60, 61] and the CT10 PDF. The WW cross section is assumed to be 70.4 ± 7 pb, derived by scaling the MCFM value of 58.7 pb by a factor of 1.20 ± 0.12 . This scale factor and its uncertainty correspond to an approximate mean of the two scale factors for WW production with zero and one extra jet, as discussed in ref. [62]. They are consistent with the recent ATLAS measurement of the WW cross section at $\sqrt{s} = 8$ TeV, which yields a value of 71.1 ± 1.1 (stat) $^{+5.7}_{-5.0}$ (sys) ± 1.4 pb[63].

All MC samples used in the analysis include the effects of FSR, multiple interactions per bunch crossing (“pile-up”), and detector simulation. FSR is simulated using Photos [64], except for samples hadronised by HERWIG++ which includes a native FSR simulation. The effects of pile-up are accounted for by overlaying simulated minimum-bias events [65]. The interactions of particles with the detector are modelled using a full ATLAS detector simulation [65] based on GEANT4 [66]. Finally, several corrections are applied to the simulated samples, accounting for differences between data and simulation in the lepton trigger, reconstruction, identification, and isolation efficiencies as well as lepton resolution and muon momentum scale.

An overview of the simulated event samples is given in table 1.

4 Event selection

Events are required to be recorded during stable beam condition periods and must pass detector and data-quality requirements. Due to differences in the detector response to electrons and muons the selection is optimised separately for each channel and is described in the following.

Process	Generator	Parton shower	Generator PDF	Model parameters (“Tune”)
Drell–Yan	POWHEG	PYTHIA 8.162	CT10	AU2 [67]
Drell–Yan PI	MC@NLO 4.09 PYTHIA 8.170	HERWIG++ 2.6.3 PYTHIA 8.170	CT10 MRST2004qed	UE-EE-3 [39] 4C [68]
$t\bar{t}$	POWHEG	PYTHIA 6.427.2	CT10	AUET2 [69]
$t\bar{t}$	MC@NLO 4.06	HERWIG 6.520	CT10	AUET2
Wt	MC@NLO 4.06	HERWIG 6.520	CT10	AUET2
Diboson	HERWIG 6.520	HERWIG 6.520	CTEQ6L1	AUET2

Table 1: Overview of simulated event samples used.

4.1 Electron channel

The electron data are collected by a trigger which uses calorimetric information to identify two compact electromagnetic energy depositions. Identification algorithms use calorimeter shower shape information to find candidate electron pairs with a minimum transverse energy of 35 GeV and 25 GeV for the leading and subleading electron. The candidate electron pairs are not matched to inner detector tracks in the trigger allowing the same trigger to be used for the multijet and W +jets data-driven background estimation studies, where a background-enriched sample is required.

Electrons are reconstructed by clustering energy deposits in the electromagnetic calorimeter using a sliding-window algorithm. These clusters are then matched to tracks reconstructed in the inner detector. The calorimeter provides the energy measurement and the track is used to determine the angular information of the electron trajectory. An energy scale correction determined from $Z \rightarrow e^+e^-$, $W \rightarrow ev$, and $J/\psi \rightarrow e^+e^-$ decays [70] is applied to data. Candidates are required to have a pseudorapidity within the inner detector tracking region, $|\eta^e| < 2.47$, excluding a region, $1.37 < |\eta^e| < 1.52$, where the transition between the barrel and endcap electromagnetic calorimeters is not well modelled in the simulation. Each candidate is required to satisfy the “medium” electron identification [71, 72] criteria based on calorimetric shower shapes and track parameters.

Leptons produced in the Drell–Yan process are expected to be well isolated from energy depositions not associated with the lepton. The degree of isolation for electrons is defined as the scalar sum of transverse energy, $\sum E_T$, of additional energy contained in a cone of size $\Delta R = \sqrt{(\Delta\phi)^2 + (\Delta\eta)^2}$ around the electron, omitting the electron transverse energy E_T^e . This calorimetric isolation is required to satisfy $\sum E_T(\Delta R = 0.4) < 0.007 \cdot E_T^e + 5$ GeV for the leading electron, and $\sum E_T(\Delta R = 0.4) < 0.022 \cdot E_T^e + 6$ GeV for the subleading electron, in order to retain a high efficiency of approximately 99% per electron over a large range in E_T^e .

Candidate events are required to have at least two electrons with $E_T^e > 30$ GeV and at least one of the electrons satisfying $E_T^e > 40$ GeV to ensure the selected electron is on the efficiency plateau of the trigger. The invariant mass of the pair is required to be in the range $116 \leq m_{ee} \leq 1500$ GeV. The absolute difference in pseudorapidity between the two electrons, $|\Delta\eta_{ee}|$, is restricted to be less than 3.5 in order to suppress the multijet background which is dominated by t -channel processes. No charge requirements are placed on the lepton pair.

4.2 Muon channel

Candidate events in the muon channel are collected using two triggers, each requiring a single muon, but with different transverse momentum thresholds as measured in the higher-level trigger system. A high-threshold trigger demands that the muon transverse momentum be above 36 GeV and collects most of the data sample. A supplementary low-threshold trigger requires an isolated muon with transverse momentum above 24 GeV. The isolation for muons is defined using the scalar sum of transverse momenta, $\sum p_T$, of additional tracks divided by p_T^μ , the transverse momentum of the muon. This provides a good discriminant against the multijet background arising from the semileptonic decays of heavy quarks. This isolation definition is implemented in the low-threshold trigger in which the candidate muons are required to satisfy $\sum p_T(\Delta R = 0.2)/p_T^\mu < 0.12$.

Muons are identified by tracks reconstructed in the muon spectrometer matched to tracks reconstructed in the inner detector and must satisfy $|\eta^\mu| < 2.4$. In addition they must pass the “medium” identification criteria [73], based on requirements on the number of hits in the different inner detector and muon spectrometer subsystems, as well as the significance of the charge / momentum ratio imbalance between the ID and MS measurements. Background from multijet events is efficiently suppressed by imposing the isolation condition $\sum p_T(\Delta R = 0.2)/p_T^\mu < 0.1$. A small contribution of cosmic-ray muons is removed by requiring the magnitude of the longitudinal impact parameter to the primary interaction vertex, z_0 , to be less than 10 mm. The primary interaction vertex is taken to be the one with the largest sum of squared transverse momenta of all associated tracks.

Events are selected if they contain at least two oppositely charged muons with $p_T^\mu > 30$ GeV and at least one of the muons satisfies $p_T^\mu > 40$ GeV in order to have the same phase space as in the electron channel measurement. Finally the dilepton invariant mass is required to be in the range $116 \leq m_{\mu\mu} \leq 1500$ GeV. No requirement is placed on $|\Delta\eta_{\mu\mu}|$.

5 Background estimate

The background from processes with two or more isolated final-state leptons of the same flavour is derived from MC simulation. The processes with non-negligible contributions are $t\bar{t}$, Wt (hereafter termed the top-quark background) and diboson (WW , WZ and ZZ) production, see table 1. The background arising from the $Z/\gamma^* \rightarrow \tau\tau$ process is predicted using MC simulation and found to be negligible.

Background contributions from events where at least one final-state jet or photon passes the electron or muon selection criteria are determined using data. This includes contributions from light- and heavy-flavour multijet processes, and $\gamma +$ jet production, referred to hereafter as the multijet background. Additional contributions are due to $W +$ jets processes and $t\bar{t}$ and Wt production with less than two isolated final-state leptons, referred to hereafter as $W +$ jets background. The data-driven estimates are described in detail below.

The number of expected events is calculated as the sum of the data-driven and simulated background estimates, and the expected event yield predicted by the DY and PI MC simulations. As can be seen in figures 1–5, good agreement is found in both the ee and $\mu\mu$ channels comparing data and expectation for the η^ℓ and p_T^ℓ distributions of the leptons, as well as for the distributions in invariant mass, rapidity and $\Delta\eta_{\ell\ell}$. The background contributions are stacked in order of increasing importance. In the electron channel the top-quark, multijet and diboson contributions to the expectation are found to be approximately 9%,

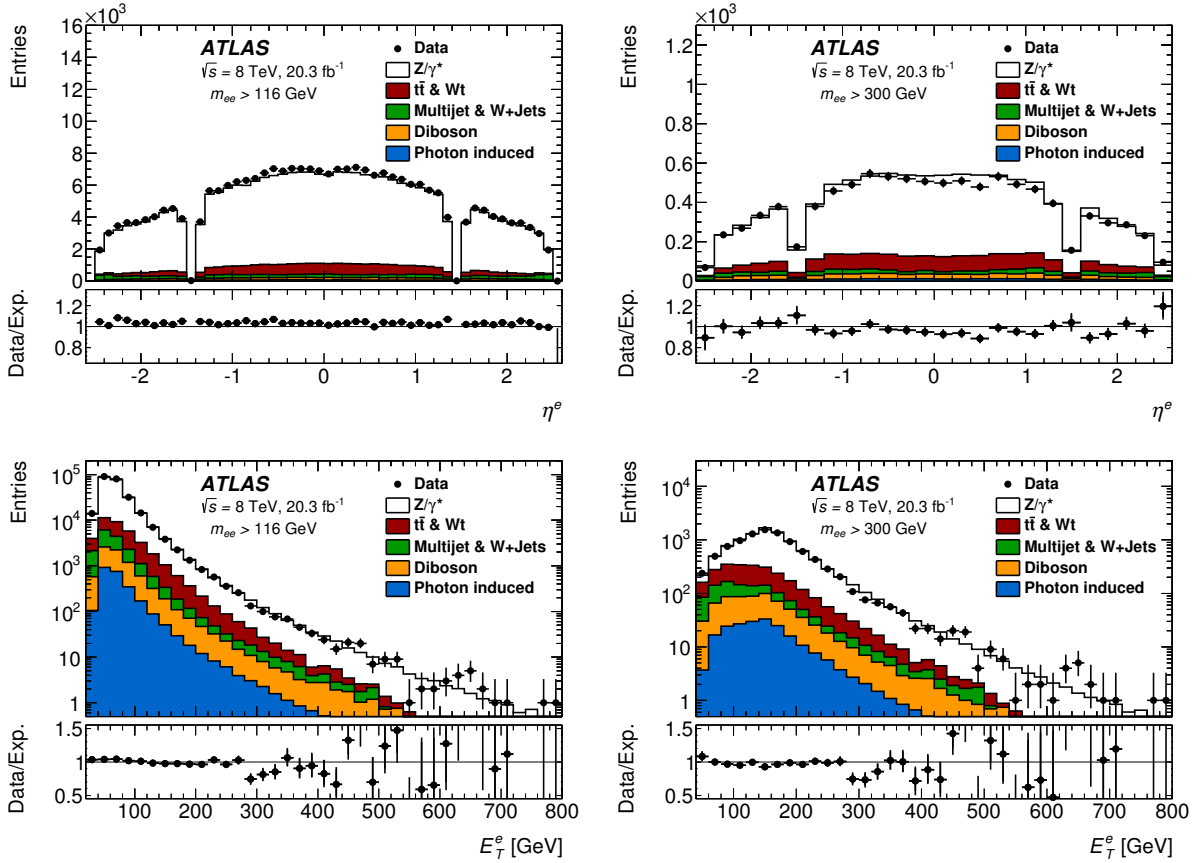


Figure 1: Distribution of electron pseudorapidity η^e (upper plots) and transverse energy E_T^e (lower plots) for invariant masses $m_{ee} > 116$ GeV (left plots), and $m_{ee} > 300$ GeV (right plots), shown for data (solid points) and expectation (stacked histogram) after the complete selection. The lower panels show the ratio of data with its statistical uncertainty to the expectation.

4% and 2% respectively in the phase space of the measurement. In the muon channel the top-quark and diboson backgrounds constitute about 9% and 2% of the total expectation, whereas the multijet contribution is below 1% everywhere. The predicted PI contribution is 1% for both channels but can reach as much as 16% in the bin at highest $m_{\ell\ell}$ and largest $\Delta\eta_{\ell\ell}$.

5.1 Multijet and $W+jets$ background estimate in the electron channel

The probability that a jet is misidentified as an electron (the “fake rate”) is determined as a function of transverse energy, E_T and pseudorapidity, η , of the electron candidate using background-enriched data samples. These samples are recorded using a set of single-jet triggers with E_T thresholds in the range 25–360 GeV. In each of these samples, the fake rate f_1 (f_2) is calculated as the fraction of leading (subleading) electron candidates that pass the nominal electron identification and leading (subleading) electron isolation requirements, with respect to the entire sample of “loose” electron candidates. The loose candidates satisfy only a subset of the nominal electron identification criteria. To reject prompt-electron contributions from W decays or the DY process, events are vetoed in the following cases: if

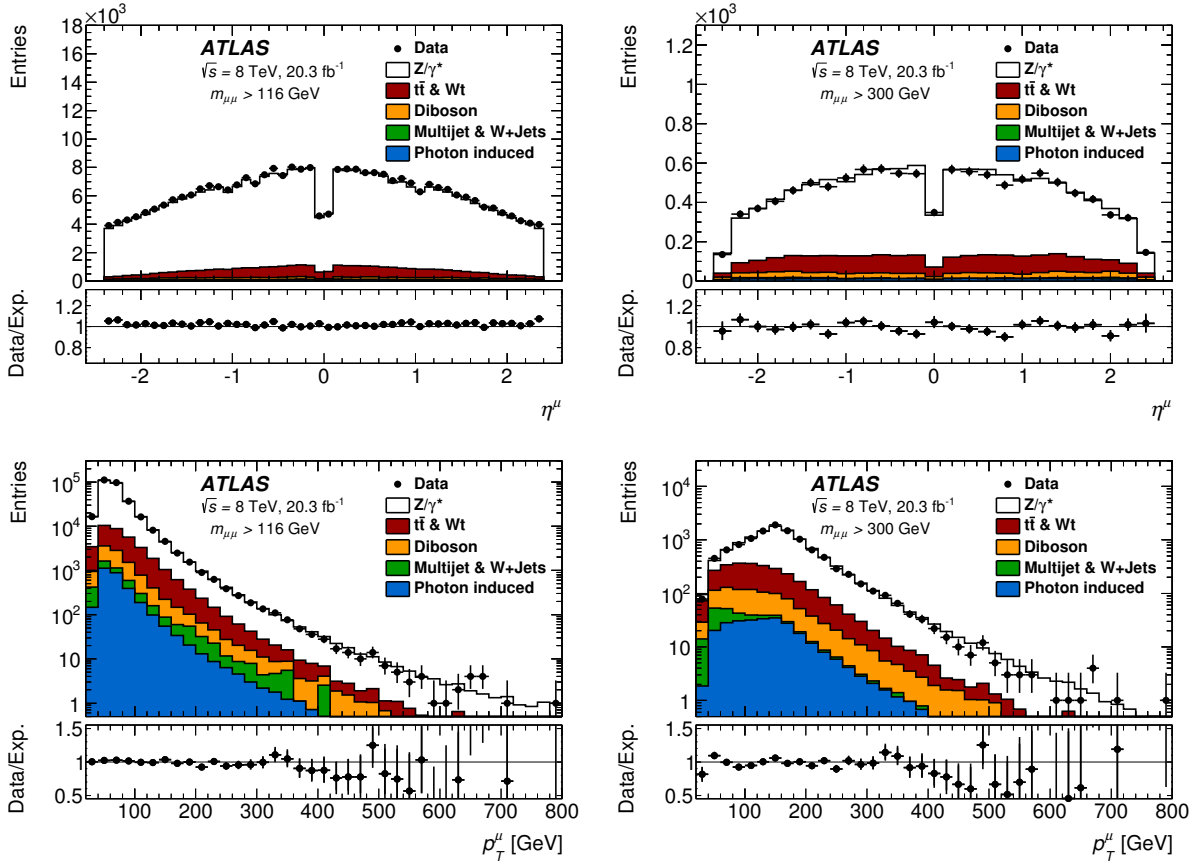


Figure 2: Distribution of muon pseudorapidity η^μ (upper plots) and transverse momentum p_T^μ (lower plots) for invariant masses $m_{\mu\mu} > 116$ GeV (left plots), and $m_{\mu\mu} > 300$ GeV (right plots), shown for data (solid points) and expectation (stacked histogram) after the complete selection. The lower panels show the ratio of data with its statistical uncertainty to the expectation.

the missing transverse momentum [74] is larger than 25 GeV, if they contain two identified electrons satisfying strict criteria or if they contain two electrons satisfying less strict criteria but with an invariant mass between 71 GeV and 111 GeV. A weighted average of the fake rates obtained from the jet samples is then calculated.

In addition to the fake rate, the probability r_1 (r_2) that a prompt electron in this loose selection satisfies the nominal electron identification and leading (subleading) isolation requirements is used in evaluating this background. This probability is taken from the MC simulation as a function of E_T and η . Potential differences between data and simulated samples in lepton identification and isolation efficiencies are accounted for by applying scale factors [72] to the simulation, which are generally close to unity.

A system of equations is used to solve for the unknown contribution to the background from events with one or more fake electrons in the sample triggered with the default analysis trigger. The relation between the number of true paired objects N_{ab} , with $E_T^a > E_T^b$ and $a, b \in \{R, F\}$, and the number of measured pairs

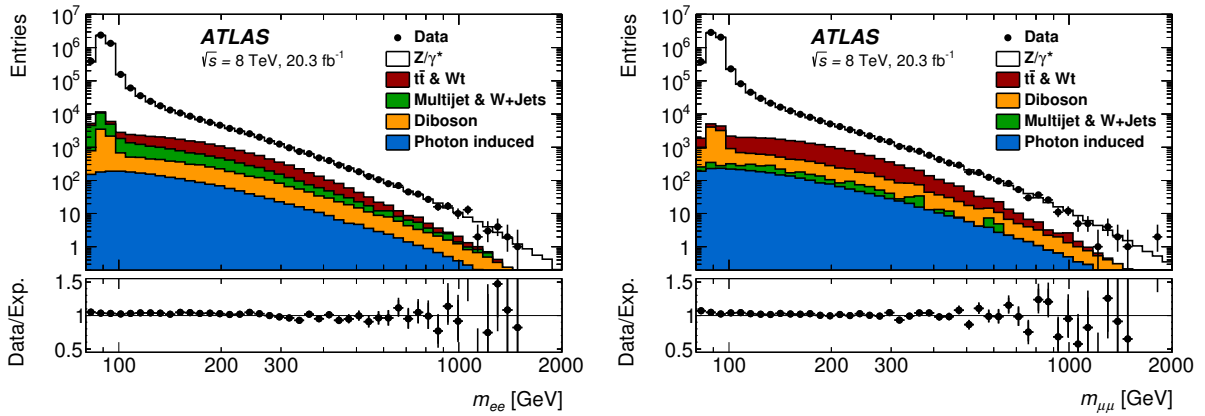


Figure 3: The invariant mass ($m_{\ell\ell}$) distribution after event selection for the electron selection (left) and muon selection (right), shown for data (solid points) compared to the expectation (stacked histogram). The lower panels show the ratio of data with its statistical uncertainty to the expectation.

N_{xy} , with $x, y \in \{T, L\}$, can be written as:

$$\begin{pmatrix} N_{TT} \\ N_{TL} \\ N_{LT} \\ N_{LL} \end{pmatrix} = \begin{pmatrix} r_1 r_2 & r_1 f_2 & f_1 r_2 & f_1 f_2 \\ r_1(1 - r_2) & r_1(1 - f_2) & f_1(1 - r_2) & f_1(1 - f_2) \\ (1 - r_1)r_2 & (1 - r_1)f_2 & (1 - f_1)r_2 & (1 - f_1)f_2 \\ (1 - r_1)(1 - r_2) & (1 - r_1)(1 - f_2) & (1 - f_1)(1 - r_2) & (1 - f_1)(1 - f_2) \end{pmatrix} \begin{pmatrix} N_{RR} \\ N_{RF} \\ N_{FR} \\ N_{FF} \end{pmatrix}. \quad (1)$$

The subscripts R and F refer to prompt electrons and fake electrons (jets) respectively. The subscript T refers to electrons that pass the nominal selection. The subscript L corresponds to electrons that pass the loose requirements described above but fail the nominal requirements.

The background originating from pairs of objects with at least one fake electron ($N_{TT}^{\text{Multijet\&W+jets}}$) in the total number of pairs, where both objects are reconstructed as signal-like (i.e. contribute to N_{TT}) is given by:

$$N_{TT}^{\text{Multijet\&W+jets}} = r_1 f_2 N_{RF} + f_1 r_2 N_{FR} + f_1 f_2 N_{FF}. \quad (2)$$

The number of true paired objects on the right-hand side of equation (2) can be expressed in terms of measurable quantities (N_{TT} , N_{TL} , N_{LT} , N_{LL}) by inverting the matrix in equation (1). The normalisation and shape of the background in each variable of interest are automatically derived by using the measurable quantities as a function of that same variable. The estimated multijet background over the full invariant mass range is found to be about 3%.

5.2 Multijet and W +jets background estimate in the muon channel

The multijet background remaining after the complete event selection in the muon channel is largely due to heavy flavour b - and c -quark decays, and is estimated using a data-driven technique in two s-eps-converted-to.pdf. This method also accounts for any potential W +jets background, however, the contribution of this component is expected to be negligible. First the normalisation of the multijet background in each $m_{\mu\mu}$ bin is determined, and then the shape in the $|y_{\mu\mu}|$ and in $|\Delta\eta_{\mu\mu}|$ variables is estimated.

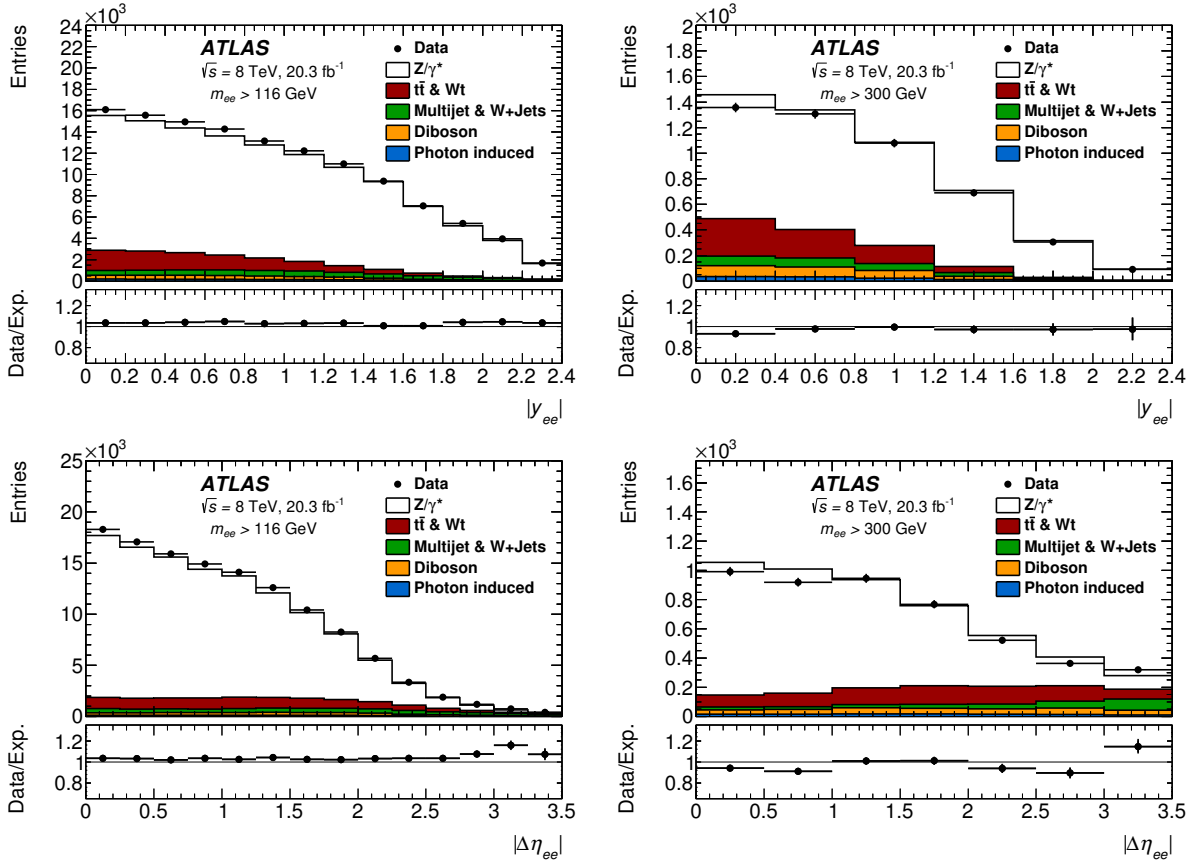


Figure 4: Distribution of absolute dielectron rapidity $|y_{ee}|$ (upper plots) and absolute dielectron pseudorapidity separation $|\Delta\eta_{ee}|$ (lower plots) for invariant mass $m_{ee} > 116$ GeV (left plots), and $m_{ee} > 300$ GeV (right plots), shown for data (solid points) and expectation (stacked histogram) after the complete selection. The lower panels show the ratio of data with its statistical uncertainty to the expectation.

The background in each invariant mass region is determined using three orthogonal control regions with inverted muon isolation requirements, and/or inverted muon-pair charge requirements. The two variables are largely uncorrelated for the multijet background. In each control region the contamination from signal, top-quark, and diboson background is subtracted using simulation. The yield of multijet events in the signal region is predicted using the constraint that the yield ratio of opposite-charge to same-charge muon pairs is identical in the isolated and non-isolated regions. A comparison of the isolation distribution for muons in events with either same-charge and opposite-charge muon pairs shows a small linear deviation of up to 10% when extrapolated into the isolated signal region. This is found to be independent of $m_{\mu\mu}$, and is corrected for. For the region $m_{\mu\mu} > 500$ GeV there are insufficient same-charge isolated muon pairs to give a reliable estimate. Therefore, the background yield in the region $m_{\mu\mu} < 500$ GeV is fitted to two alternative functional forms and extrapolated to larger $m_{\mu\mu}$ where the averaged prediction is taken as the estimate of the background yield. The $|y_{\mu\mu}|$ and $|\Delta\eta_{\mu\mu}|$ dependence of the background in each $m_{\mu\mu}$ region is obtained from a multijet-enriched data control region in which pairs of same-charge and opposite-charge muons satisfy $\sum p_T(\Delta R = 0.2)/p_T^\mu > 0.1$. Signal, top-quark and diboson contamination in this control region is subtracted using MC simulation. The resulting $|y_{\mu\mu}|$ and $|\Delta\eta_{\mu\mu}|$ spectra in each $m_{\mu\mu}$ region are normalised to the yield obtained in the first step. For $m_{\mu\mu} > 500$ GeV the $|y_{\mu\mu}|$ or $|\Delta\eta_{\mu\mu}|$ shape is taken

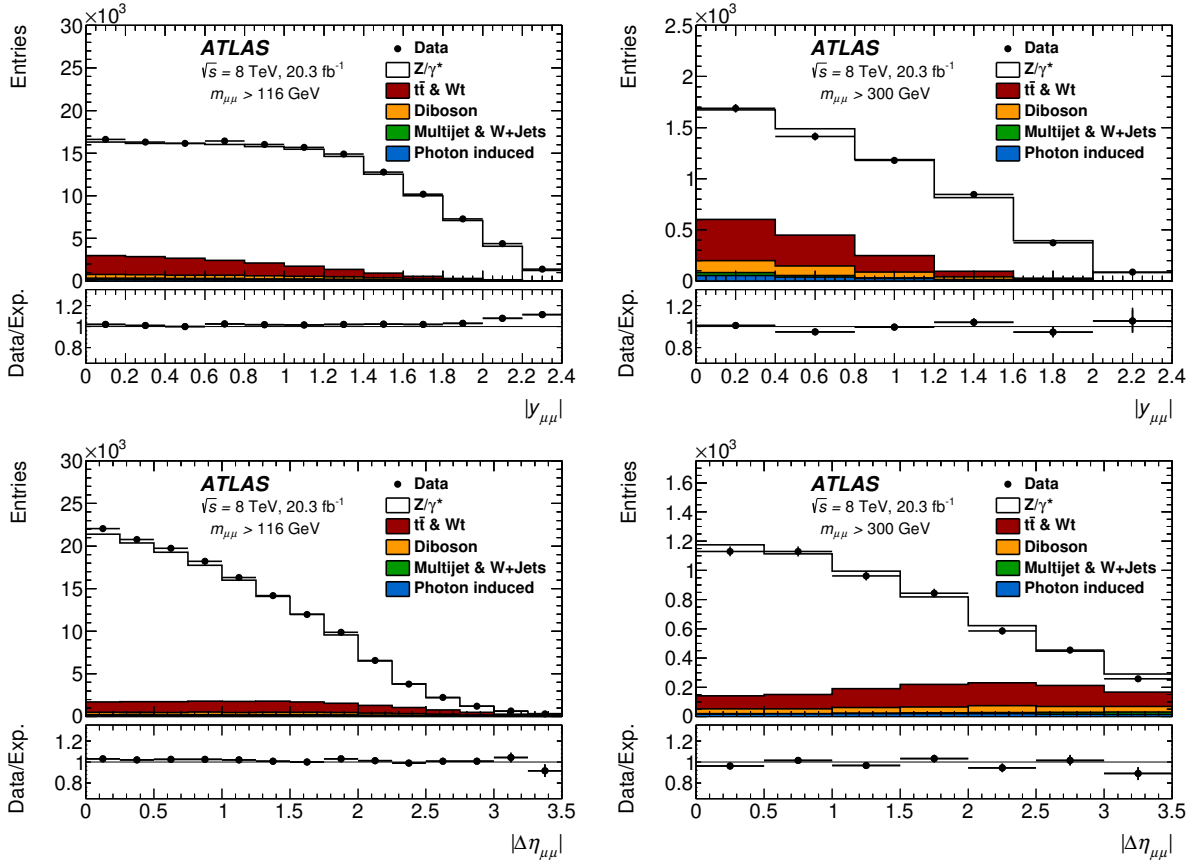


Figure 5: Distribution of absolute dimuon rapidity $|y_{\mu\mu}|$ (upper plots) and absolute dimuon pseudorapidity separation $|\Delta\eta_{\mu\mu}|$ (lower plots) for invariant mass $m_{\mu\mu} > 116$ GeV (left plots), and $m_{\mu\mu} > 300$ GeV (right plots), shown for data (solid points) and expectation (stacked histogram) after the complete selection. The lower panels show the ratio of data with its statistical uncertainty to the expectation.

from the region $300 < m_{\mu\mu} < 500$ GeV. Overall the total multijet background varies from 1% to 0.1% over the complete invariant mass range.

6 Cross-section measurement

The Drell–Yan cross section, including the irreducible contribution from the PI process, is measured differentially in 12 bins of m_{ee} from 116 GeV to 1500 GeV, as well as double-differentially in five bins of m_{ee} as a function of $|y_{ee}|$ and $|\Delta\eta_{ee}|$. The results are presented in the fiducial region of the measurement, in which the leading (subleading) lepton has a $p_T^\ell > 40$ GeV ($p_T^\ell > 30$ GeV) and both leptons are within $|\eta^\ell| < 2.5$. The kinematic variables are defined by the leptons before FSR, i.e. the results are given at the Born-level in QED. Results at the “dressed” level, where leptons after FSR are recombined with radiated photons within a cone of $\Delta R = 0.1$, are obtained by multiplying the Born-level results with the dressed correction factors k_{dressed} , provided in tables 6–11 in the appendix. These correction factors are obtained from the Powheg and Pythia 8 MC samples for the DY and PI processes, respectively.

The double-differential cross section as a function of invariant mass and rapidity is calculated as

$$\frac{d^2\sigma}{dm_{\ell\ell} dy_{\ell\ell}} = \frac{N_{\text{data}} - N_{\text{bkg}}}{C_{\text{DY}} \mathcal{L}_{\text{int}}} \frac{1}{\Delta_{m_{\ell\ell}} 2\Delta_{|y_{\ell\ell}|}}, \quad (3)$$

where N_{data} is the number of candidate events observed in a given bin of $m_{\ell\ell}$ and $|y_{\ell\ell}|$ of width $\Delta_{m_{\ell\ell}}$ and $\Delta_{|y_{\ell\ell}|}$ respectively. The total background in that bin is denoted as N_{bkg} and \mathcal{L}_{int} is the integrated luminosity. The factor of two in the denominator accounts for the modulus in the rapidity bin width. The double-differential cross section as a function of mass and $|\Delta\eta_{\ell\ell}|$ and the single-differential measurement as a function of invariant mass are defined accordingly.

The factor, C_{DY} , takes into account the efficiency of the signal selection and bin migration effects. It is defined as the number of MC generated events that pass the signal selection in a certain measurement bin calculated from the reconstructed lepton kinematics divided by the total number of generated events within the fiducial region, in the corresponding bin, calculated from Born-level or dressed-level lepton kinematics. It is obtained from the Drell–Yan and PI MC samples after correction for differences in the reconstruction, identification, trigger, and isolation efficiencies between data and simulation, as well as for momentum scale and resolution mismodelling effects. In general the C_{DY} factors are found to be in the range 60–80% across the measured kinematic range.

The C_{DY} factor also includes extrapolations over the small regions that are excluded for reconstructed electron ($1.37 < |\eta^e| < 1.52$ and $2.47 < |\eta^e| < 2.5$) or muon ($2.4 < |\eta^\mu| < 2.5$) candidates. In the electron channel, the fiducial cross section measurements as a function of m_{ee} and $|y_{ee}|$, and the single-differential measurement, are extrapolated over the unmeasured region $|\Delta\eta_{ee}| > 3.5$. The extrapolation correction is included in the C_{DY} factor. No such extrapolation is required for the double-differential measurement as function of mass and $|\Delta\eta_{ee}|$ which only extends to $|\Delta\eta_{ee}| = 3$.

The Born-level bin purity is defined as the fraction of reconstructed MC signal events in a given bin which were also generated in the same bin using Born-level lepton kinematics. An analogous definition is used for the dressed-level bin purity. The bin purities are found to be typically above 85%, and above 75% everywhere. This ensures that the bin migration effects are small, and the corrections applied to account for bin migrations have small uncertainties.

7 Systematic uncertainties

The systematic uncertainties on the measurements are discussed separately for those sources which arise only in the electron channel, those which arise only in the muon channel, and those which are common to both measurements. In each section the sources are discussed in order of importance, with the largest sources of uncertainty listed first. Each source is classified as being correlated or uncorrelated between measurement bins in a single channel. The uncorrelated sources are propagated using the pseudo-experiment method in which the correction factors used to improve the modelling of data by the simulation are randomly shifted in an ensemble of pseudo-experiments according to the mean and standard deviation of the correction factor. The resulting uncertainty on the measured cross section is determined from the variance of the measurements for the ensemble. The correlated contributions are propagated by the offset method in which the values from each source are coherently shifted upwards and downwards by one standard deviation and the magnitude of the change in the measurement is computed. The sign of the uncertainty corresponds to a one standard deviation upward shift of the uncertainty source.

7.1 Electron channel

The systematic uncertainties on the cross section that are unique to the electron channel are dominated by the uncertainties in the determination of the multijet and $W+jets$ background described in section 5.1, and in the electron energy scale. In addition, a large contribution to the uncertainty also arises from the top-quark and diboson background subtraction, and is discussed in section 7.3.

All correlated and uncorrelated contributions to the systematic uncertainties are given in each bin of the measurement in tables 6, 7, and 8 of the appendix.

7.1.1 Multijet and $W+jets$ background

In order to derive the uncertainty on the data-driven background estimate described in section 5.1, the default “matrix method” is altered by assuming $r_1 = r_2 = 1$. This second matrix method leads to a simplification of the matrix in equation (1), but also necessitates the use of MC corrections to account for the identification and isolation inefficiencies of real electrons. Large MC corrections can be avoided in a third matrix method where the contamination from real electrons is reduced. The subscript L in equation (1) now corresponds to electrons that pass the loose requirements but fail the requirement on the matching between track and cluster, instead of failing the full identification and isolation requirements.

In addition, two alternative background-enriched samples are obtained using a tag-and-probe technique on the jet-triggered sample and on the sample triggered by the default analysis triggers, requiring the tag to fail certain aspects of the electron identification depending on the trigger. Furthermore, the event should have a missing transverse momentum smaller than 25 GeV, the probe needs to have the same charge as the tag and the invariant mass of the tag-and-probe pair needs to be outside the Z mass window from 71 to 111 GeV.

The default and the two additional matrix methods are each used in conjunction with the default and the two alternative background-enriched samples, leading to a default and eight alternative background estimates. Out of the eight alternative background estimates those two are identified that in general, i.e. in almost all bins except for fluctuations, yield the largest and smallest background contribution. In each bin, the average absolute difference between those two and the default background estimate is used as a systematic uncertainty on the method.

Another systematic uncertainty can arise if fake rates are different for the various processes contributing to this background, and if the relative contributions of these processes differ between the data samples from which the fake rates are measured and the data sample to which the fake rates are applied. For example, jets originating from bottom quarks have a higher fake rate than light-quark jets, but the effect of this is negligible as the number of b -jets is small and similar in both samples. However, as an additional check the background is recalculated using all nine methods discussed above, but with separate fake rates for different background processes. As the mean of these nine methods is in agreement with the default background estimate no additional systematic uncertainty is applied.

The uncertainty on the default fake-rate calculation is derived by varying the requirements used to suppress real electron contamination in the data sample used to measure the fake rate. The largest deviation of about 5% on the background occurs when the value of the missing transverse energy requirement is

changed. It is added in quadrature to the systematic uncertainty on the method to obtain the full systematic uncertainty ($\delta_{\text{cor}}^{\text{mult.}}$) on the cross section that is correlated between bins. The value of $\delta_{\text{cor}}^{\text{mult.}}$ is found to be around 1%, rising to almost 4% at large $|\Delta\eta_{ee}|$.

The uncorrelated part consists of the statistical uncertainty on the fake rates, which results in an uncertainty on the background of at most 5%, and of the statistical uncertainty from the sample to which the fake rates are applied. These two sources are added in quadrature and yield the uncertainty ($\delta_{\text{unc}}^{\text{mult.}}$) on the cross section that is uncorrelated between bins and is typically less than 0.5%, increasing to 3% at large $|\Delta\eta_{ee}|$.

7.1.2 Energy scale and resolution

The electron energy scale and resolution as well as the corresponding uncertainties are determined using $Z \rightarrow e^+e^-$, $W \rightarrow ev$, and $J/\psi \rightarrow e^+e^-$ decays [70]. The uncertainty on the energy scale is separated into 14 uncorrelated systematic sources as well as one statistical component. The statistical uncertainty on the energy scale is found to be negligible. Adding the effects of the 14 sources of uncertainty on the energy scale in quadrature after propagating to the measured cross sections, the combined uncertainty is denoted as $\delta_{\text{cor}}^{\text{Escale}}$, and is 1–4% for $m_{ee} > 200$ GeV, but is better than 0.5% at lower m_{ee} and central rapidity.

The uncertainty on the energy resolution is separated into seven uncorrelated systematic sources which are propagated to the cross-section measurements individually and then quadratically summed. This combined uncertainty is denoted as $\delta_{\text{cor}}^{\text{Eres}}$ and is typically 0.1–0.2% everywhere except at large $|y_{ee}|$ or large $|\Delta\eta_{ee}|$.

7.1.3 Reconstruction, identification and isolation efficiency

The reconstruction and identification efficiencies of electrons are determined from data for electrons with E_T^e up to about 100 GeV, using various tag-and-probe methods in Z and J/ψ decays, following the prescription of ref. [71] with certain improvements and adjustments for the 2012 conditions [72]. In order to extend the measurement range of the identification efficiency, the tag-and-probe method using the isolation distribution of the probe for the discrimination between signal and background in $Z \rightarrow e^+e^-$ decays [72] is carried out up to about 500 GeV in E_T . Within statistical uncertainties, the identification efficiencies are found to be stable and consistent with the one derived in the last bin ($E_T^e > 80$ GeV) in ref. [72].

The differences between the measured reconstruction and identification efficiencies and their values in MC simulation are taken as η - and E_T -dependent scale factors with which the C_{DY} factor derived from simulation is corrected. Similarly, scale factors for the isolation requirements on the leading and sub-leading electron are derived using a tag-and-probe method in $Z \rightarrow e^+e^-$ decays. They are applied as a function of E_T^e only, as the η dependence is negligible.

The uncertainties on the cross section due to the systematic uncertainties on the scale factors for the electron reconstruction, identification and isolation as well as the statistical uncertainty on the isolation are denoted as $\delta_{\text{cor}}^{\text{reco}}$, $\delta_{\text{cor}}^{\text{id}}$, $\delta_{\text{cor}}^{\text{iso}}$ and $\delta_{\text{unc}}^{\text{iso}}$ respectively. Of these, the largest component is $\delta_{\text{cor}}^{\text{id}}$, which is found to be 0.5–1% everywhere. The uncertainty $\delta_{\text{cor}}^{\text{reco}}$ is generally below 0.3% and better than 1% everywhere. Both components of the isolation efficiency uncertainty are found to be 0.2% or better for $m_{ee} < 300$ GeV.

7.1.4 Trigger efficiency

The trigger efficiency is measured in data and in the MC simulation using a tag-and-probe method in $Z \rightarrow e^+e^-$ decays. The differences as a function of E_T^e are found to be smaller than 1% everywhere, with no dependence on η . Therefore, E_T^e -dependent scale factors are used to correct C_{DY} . The uncertainty on the cross section due to the statistical ($\delta_{\text{unc}}^{\text{trig}}$) and systematic ($\delta_{\text{cor}}^{\text{trig}}$) uncertainties on the trigger efficiency are each found to be 0.1% or better for $m_{ee} < 300$ GeV.

7.2 Muon channel

Uncertainties related to the muon trigger, reconstruction, isolation and impact parameter efficiencies, as well as the muon momentum scale and resolution are all studied using the $Z \rightarrow \mu^+\mu^-$ process and a tag-and-probe method. Of these, the largest contribution to the measurement precision arises from the reconstruction efficiency modelling, and the muon momentum scale calibration. However, the top-quark and diboson background subtraction is also a dominant source of uncertainty, and is discussed in section 7.3. A detailed breakdown of the uncertainties is provided in tables 9, 10 and 11 in the appendix.

7.2.1 Reconstruction efficiency

This is the dominant source of muon-related correlated systematic uncertainty and is dominated at large p_T^μ by the uncertainty in contributions from catastrophic muon energy loss via bremsstrahlung [73]. When propagated to the cross section this source is found to be typically 0.5%, rising to 1% at the highest p_T^μ . This contribution is denoted as $\delta_{\text{cor}}^{\text{reco}}$.

7.2.2 Momentum scale and resolution

The corrections on muon momentum scale and resolution are obtained from fits to the $Z \rightarrow \mu^+\mu^-$ line-shape with scale and resolution parameters in local η^μ and ϕ^μ regions, separately for muon tracks reconstructed in the ID and the MS [73]. Uncertainties arising from the methodology result in a correlated systematic uncertainty on the measured cross sections of typically 0.4%. These contributions are listed as $\delta_{\text{cor}}^{\text{pT}}$ for the momentum scale, and $\delta_{\text{cor}}^{\text{MSres}}$ and $\delta_{\text{cor}}^{\text{IDres}}$ for the MS and ID resolution uncertainties respectively.

7.2.3 Isolation and impact parameter efficiency

Modelling of the muon isolation and impact parameter selection efficiencies can give rise to additional systematic uncertainties and are estimated together. The sources considered include the remaining background contamination, the residual variation in η^μ , and a possible bias from the event topology estimated by varying the azimuthal opening angle between the two muons used in the tag-and-probe method. The resulting correlated cross-section uncertainty is found to be typically 0.1%, rising to 0.5% at large $m_{\mu\mu}$. This contribution is labelled as $\delta_{\text{cor}}^{\text{iso}}$.

7.2.4 Multijet and $W+jets$ background

The uncertainty on the multijet background estimation consists of several sources. The statistical uncertainty of the control regions is propagated in the appropriate way and can be significant, in particular from the isolated same-sign control sample. The subtracted top-quark and diboson contamination in the control regions is varied within the theoretical cross section uncertainties given in section 3. The subtracted signal contamination is varied by $\pm 5\%$. The extrapolation uncertainty in the multijet estimate at large invariant mass is estimated taking half the difference between the two extrapolation functions and is the largest contribution to the uncertainty in this region. The uncertainty in the shape of the $|y_{\mu\mu}|$ and $|\Delta\eta_{\mu\mu}|$ spectra is determined from the RMS of these distributions in regions of small, moderate and large non-isolation of the muon pairs obtained from the control regions. This component typically dominates the uncertainty at large $|y_{\mu\mu}|$ and small $|\Delta\eta_{\mu\mu}|$. These sources are combined into correlated and uncorrelated components, where the latter is due to the statistical uncertainty of the method, and are denoted as $\delta_{\text{cor}}^{\text{mult.}}$ and $\delta_{\text{unc}}^{\text{mult.}}$. The combined uncertainty in the background estimation ranges from 20% at low $m_{\mu\mu}$ to above 100% at the highest $m_{\mu\mu}$, however when propagated onto the cross section measurements it is below 1% in all double differential measurement bins.

7.2.5 Trigger efficiency

The trigger efficiency corrections obtained using the tag-and-probe method as described in ref. [75] are parameterised in terms of muon pseudorapidity η^μ , azimuthal angle ϕ^μ , and electric charge. The uncertainty sources considered are the background contamination, a possible residual dependence on muon p_T^μ , and an uncertainty based on the event topology. This results in a correlated uncertainty on the measured cross sections of 0.1% and is denoted as $\delta_{\text{cor}}^{\text{trig.}}$.

7.3 Systematic uncertainties common to both channels

The systematic uncertainties common to both channels are derived using identical methods and are assumed to be fully correlated between the channels. They are dominated by the uncertainty on the $t\bar{t}$ background and the luminosity. The statistical uncertainties of the MC samples used are uncorrelated between the measurement channels.

7.3.1 Top and diboson background

In most of the phase space the largest background in both the electron and the muon channel is due to top-quark production. The normalisation uncertainty on this background is taken to be 6% as already described in section 3. The top-quark background is dominated by $t\bar{t}$ production, which is modelled using two different MC generators, see table 1. No systematic differences have been found when comparing the distributions in dilepton invariant mass, rapidity and $\Delta\eta$. Another important background is due to diboson (WW , WZ and ZZ) production. The normalisation uncertainties are about 10% (see section 3).

To further validate the normalisation and shape of the $t\bar{t}$ and diboson simulations used in this analysis, a data control region is defined by an opposite-charge electron–muon pair selection that is chosen to match the nominal muon and electron pair selections as closely as possible. This selection strongly suppresses the Drell–Yan process and leads to a sample with about an 80% contribution from top-quark production

at lower invariant masses, decreasing to about 50% for the highest masses. The remaining events are mainly due to diboson production. As no systematic differences are found comparing dilepton invariant mass, rapidity and $\Delta\eta$ distributions in data and simulation no further uncertainties are assigned. The normalisation uncertainties of the top ($\delta_{\text{cor}}^{\text{top}}$) and diboson ($\delta_{\text{cor}}^{\text{diboson}}$) backgrounds as well as the statistical uncertainty of both simulations combined ($\delta_{\text{unc}}^{\text{bgMC}}$) are given in the appendix.

7.3.2 Luminosity

The uncertainty on the integrated luminosity is 1.9%, which is derived by following the methodology detailed in ref. [76].

7.3.3 MC statistics and MC modelling

The bin-by-bin correction factor C_{DY} is calculated from the Drell–Yan and PI MC samples as already described in section 6. In order to check for a potential model dependence, two different Drell–Yan samples are generated, see table 1, and no systematic differences have been found for C_{DY} as a function of invariant mass, rapidity and $\Delta\eta$. Similarly, a negligible influence on these distributions is found when assigning a 40% uncertainty to the cross section of the PI MC sample. This value is derived by calculating the PI contribution in a constituent and a current quark mass scheme [21], and taking the magnitude of the difference between either scheme and their average [7]. The statistical uncertainty due to the finite number of signal MC events used in the calculation of C_{DY} is denoted as $\delta_{\text{unc}}^{\text{MC}}$.

7.3.4 Bin-by-bin correction

The bin-by-bin correction used in the calculation of the cross section is compared to an iterative Bayesian unfolding technique [77] as implemented in the program RooUnfold [78]. The differences between these two approaches are found to be negligible.

7.3.5 PDF uncertainty

As discussed in section 6, the C_{DY} correction factor also includes a small extrapolation from the measured region to the fiducial region. This acceptance correction is about 13% for electrons and 5% for muons, but can be larger in certain bins of the two-dimensional cross-section measurement. The PDF uncertainties due to the acceptance correction are estimated using the CT10 PDF eigenvector set at 68% confidence level (CL). They are found to be negligible, with uncertainties of the order of 0.1% or below for most cross-section measurement bins, and below 0.2% everywhere.

8 Results

The measured Born-level fiducial cross sections for the electron and muon channel analyses are in good agreement with one another and each achieve a precision of 1% at low $m_{\ell\ell}$ where they are dominated by the experimental systematic uncertainties. For $m_{\ell\ell} \gtrsim 400$ GeV the statistical uncertainty of the data samples dominates the measurement precision. The measurements are presented in tables 6–11 of the appendix, including the systematic uncertainties (excluding the luminosity measurement uncertainty) separated into those which are point-to-point correlated and those which are uncorrelated.

The two measurement channels are defined with a common fiducial region given in section 6, therefore, they can be combined to further reduce the statistical uncertainty. A further reduction in the total uncertainty is also achieved by taking into account systematic uncertainties which are not correlated between the two measurement channels. A χ^2 minimisation technique is used to perform the combination of the cross sections [79–81]. This method introduces a free nuisance parameter for each correlated systematic error source which contributes to the total χ^2 , and therefore gives results that are different from a simple weighted average. The combination is performed separately for each differential cross-section measurement. The sources of uncertainty considered are discussed in section 7, some of which consist of several contributions. However, for ease of presentation only the major sources are reported in tables 6–11 giving a total of 35 nuisance parameters. Only the normalisation uncertainties of the $t\bar{t}$ and diboson backgrounds are correlated between the channels, using two common nuisance parameters. After the minimisation, no nuisance parameter is shifted by more than one standard deviation. The χ^2 per degree of freedom, χ^2/dof , is found to be $14.2/12 = 1.19$ for the single-differential cross section, $53.1/48 = 1.11$ for the cross sections differential in $m_{\ell\ell}$ and $|y_{\ell\ell}|$, and $59.3/47 = 1.26$ for the cross sections differential in $m_{\ell\ell}$ and $|\Delta\eta_{\ell\ell}|$.

The combined fiducial cross sections are presented in tables 2, 3 and 4. The combination procedure yields orthogonal systematic uncertainty sources, as listed in the tables, which are formed of linear combinations of the original uncertainties. The combined cross sections have an improved precision across the kinematic range, where at low $m_{\ell\ell}$ an accuracy of better than 1% is attained. The double-differential cross sections have an accuracy of between 1% and 7% throughout the kinematic range of the measurements.

The results of the combination are shown in figures 6–8. In each figure the upper panels show the measured Born-level cross sections for the electron channel, muon channel and the combination. The ratio of the individual channels to the combined measurement is also shown as well as the pulls from the two channels, defined as the single-channel measurement subtracted from the combined result in units of the uncertainty. No coherent trends between the measurements are observed and the pulls are found to be typically below two standard deviations, and everywhere below three standard deviations.

The single-differential cross section shown in figure 6 falls rapidly over five orders of magnitude as $m_{\ell\ell}$ increases by about a factor of ten. In figure 7 the cross sections differential in $m_{\ell\ell}$ and $|y_{\ell\ell}|$ show a marked narrowing of the rapidity plateau width as $m_{\ell\ell}$ increases. The measurements obtained as a function of $|\Delta\eta_{\ell\ell}|$ and $m_{\ell\ell}$ are shown in figure 8. For all $m_{\ell\ell}$, the cross sections are largest where the absolute magnitude of the lepton pseudorapidity separation is close to zero, and are observed to fall as the separation increases.

m_{τ} (GeV)	δ^{33S} [pb/mm]	δ^{33S} [fb/mm]	δ^{33S} [fb/mm]	δ^{33S}				δ^{33S}				δ^{33S}				δ^{33S}			
				$\delta_{\text{Cor}}^{\text{33S}}$ [%]															
116-130	2.28×10^{-1}	0.34	0.53	6.3	0.12	-0.24	0.08	-0.03	0.00	0.00	0.01	0.00	0.00	0.00	-0.00	0.00	0.00	-0.05	
130-150	1.04×10^{-2}	0.44	0.67	0.80	0.13	0.38	-0.00	-0.03	-0.01	-0.00	-0.00	-0.00	-0.00	-0.00	-0.01	-0.01	-0.04	-0.07	
150-175	4.98×10^{-2}	0.57	0.91	0.18	0.56	0.01	-0.00	-0.03	-0.01	-0.00	-0.00	-0.00	-0.00	-0.00	-0.01	-0.01	-0.06	-0.09	
175-200	2.54×10^{-2}	0.81	1.18	1.43	0.25	0.74	-0.00	-0.06	-0.07	-0.01	-0.00	-0.00	-0.00	-0.00	-0.02	-0.02	-0.12	-0.16	
200-230	1.37×10^{-2}	1.02	1.42	1.75	0.32	0.98	-0.02	-0.09	-0.01	-0.00	-0.00	-0.00	-0.00	-0.00	-0.03	-0.03	-0.16	-0.21	
230-260	7.89×10^{-3}	1.36	1.59	2.09	0.43	0.99	-0.01	-0.12	-0.08	-0.00	-0.07	-0.00	-0.00	-0.00	-0.04	-0.04	-0.18	-0.22	
260-300	4.45×10^{-3}	1.58	1.67	2.30	0.46	1.00	-0.02	-0.11	-0.05	-0.01	-0.09	-0.00	-0.00	-0.00	-0.05	-0.05	-0.20	-0.24	
300-380	1.87×10^{-3}	1.73	1.80	2.50	0.56	1.12	-0.02	-0.11	-0.09	0.01	-0.09	-0.00	-0.00	-0.00	-0.07	-0.07	-0.23	-0.28	
380-500	6.20×10^{-4}	2.42	1.71	2.96	0.63	1.03	-0.00	-0.10	-0.04	0.14	-0.07	-0.00	-0.00	-0.00	-0.08	-0.08	-0.25	-0.30	
500-700	1.53×10^{-4}	3.65	1.68	4.02	0.57	0.88	-0.00	-0.14	0.04	0.04	-0.10	-0.00	-0.00	-0.00	-0.05	-0.05	-0.35	-0.41	
700-1000	2.66×10^{-5}	6.98	1.75	7.22	0.57	0.73	-0.00	-0.13	0.07	0.07	-0.13	-0.00	-0.00	-0.00	-0.07	-0.07	-0.40	-0.47	
1000-1500	2.26×10^{-6}	17.05	2.95	17.31	0.53	0.70	-0.00	-0.01	-0.01	-0.01	-0.01	-0.00	-0.00	-0.00	-0.08	-0.08	-0.32	-0.37	

Table 2: The combined Born-level single-differential cross section $\frac{d\sigma}{dm_{\ell\ell}}$. The measurements are listed together with the statistical (δ^{stat}), systematic (δ^{sys}) and total (δ^{tot}) uncertainties. In addition the contributions from the individual correlated ($\delta_{\text{cor}}^{\text{l}} - \delta_{\text{cor}}^{35}$) and uncorrelated (δ^{unc}) systematic error sources are also provided. The luminosity uncertainty of 1.9% is not shown and not included in the overall systematic and total uncertainties.

m_{eff}	μ_{eff}	Unitary	δ^{exp}	δ^{exp}	δ^{corr}												δ^{corr}														
					δ^{exp}	δ^{exp}	δ^{exp}	δ^{exp}	δ^{exp}	δ^{exp}	δ^{exp}	δ^{exp}	δ^{exp}	δ^{exp}	δ^{exp}	δ^{exp}	δ^{exp}	δ^{exp}	δ^{exp}	δ^{exp}	δ^{exp}	δ^{exp}	δ^{exp}	δ^{exp}	δ^{exp}	δ^{exp}					
116-150	0.9-0.2	4.18-0.10 ⁺	1.81	0.62	1.02	1.20	0.00	0.02	-0.03	0.01	0.06	-0.07	-0.01	0.02	0.02	0.01	0.15	-0.05	-0.02	-0.08	0.09	-0.21	0.13	-0.19	0.09	0.15	0.04	0.25	0.03		
116-150	0.6-0.4	4.08-0.10 ⁺	1.82	0.63	1.04	1.21	0.00	0.01	0.06	-0.08	-0.05	-0.07	-0.00	0.02	0.04	0.02	0.14	-0.16	-0.01	0.00	-0.08	-0.05	0.10	-0.19	0.14	-0.12	-0.01	0.02	-0.06	0.03	
116-150	0.4-0.2	4.04-0.10 ⁺	1.83	0.62	1.04	1.21	0.00	0.01	0.06	-0.08	-0.05	-0.07	-0.00	0.02	0.04	0.02	0.13	-0.16	-0.01	0.00	-0.08	-0.05	0.10	-0.19	0.14	-0.12	-0.01	0.02	-0.06	0.03	
116-150	0.5-0.4	4.04-0.10 ⁺	1.84	0.59	1.01	1.22	0.01	0.01	0.03	-0.02	-0.02	-0.06	-0.07	-0.04	-0.01	0.01	0.13	-0.14	-0.04	-0.04	-0.06	0.01	-0.16	0.05	-0.18	0.06	-0.05	0.01	0.05	0.04	
116-150	0.5-0.4	3.97-0.10 ⁺	1.84	0.59	1.01	1.22	0.01	0.01	0.03	-0.02	-0.02	-0.06	-0.07	-0.04	-0.01	0.01	0.13	-0.14	-0.04	-0.04	-0.06	0.01	-0.16	0.05	-0.18	0.06	-0.05	0.01	0.05	0.04	
116-150	1.1-1.2	3.95-10 ⁺	1.84	0.56	1.01	1.22	0.02	0.00	0.04	-0.01	-0.03	-0.06	-0.07	-0.04	-0.01	0.01	0.09	-0.12	-0.04	-0.04	-0.05	0.05	-0.13	0.06	-0.18	0.07	-0.05	0.01	0.06	0.04	
116-150	1.1-1.4	3.84-0.10 ⁺	1.84	0.58	1.02	1.23	0.02	0.00	0.04	-0.01	-0.03	-0.06	-0.07	-0.04	-0.01	0.02	0.09	-0.12	-0.05	-0.05	-0.06	0.06	-0.13	0.05	-0.19	0.08	-0.06	0.01	0.06	0.04	
116-150	1.4-1.6	3.48-0.10 ⁺	1.80	0.89	0.58	1.06	0.24	0.01	0.03	-0.01	-0.03	-0.06	-0.07	-0.04	-0.01	0.02	0.03	-0.11	-0.05	-0.05	-0.06	0.01	-0.10	0.01	-0.17	0.04	-0.08	0.01	0.05	0.06	
116-150	1.6-1.8	2.92-0.10 ⁺	1.81	1.00	0.64	1.28	0.02	0.00	0.04	-0.01	-0.03	-0.06	-0.07	-0.04	-0.01	0.02	0.03	-0.11	-0.05	-0.05	-0.06	0.01	-0.10	0.01	-0.17	0.04	-0.08	0.01	0.05	0.06	
116-150	1.8-2.0	2.29-0.10 ⁺	1.82	1.14	0.70	1.29	0.02	0.00	0.04	-0.01	-0.03	-0.06	-0.07	-0.04	-0.01	0.02	0.03	-0.11	-0.05	-0.05	-0.06	0.01	-0.10	0.01	-0.17	0.04	-0.08	0.01	0.05	0.06	
116-150	2.2-2.4	1.74-0.10 ⁺	1.82	1.16	0.75	1.29	0.02	0.00	0.04	-0.01	-0.03	-0.06	-0.07	-0.04	-0.01	0.02	0.03	-0.11	-0.05	-0.05	-0.06	0.01	-0.10	0.01	-0.17	0.04	-0.08	0.01	0.05	0.06	
116-150	2.4-2.6	1.23-0.10 ⁺	1.83	1.16	0.75	1.29	0.02	0.00	0.04	-0.01	-0.03	-0.06	-0.07	-0.04	-0.01	0.02	0.03	-0.11	-0.05	-0.05	-0.06	0.01	-0.10	0.01	-0.17	0.04	-0.08	0.01	0.05	0.06	
150-200	0.3-0.2	10.48-0.10 ⁺	1.41	1.31	1.93	0.32	-0.03	0.00	0.04	-0.05	-0.06	-0.13	-0.07	-0.01	0.00	0.10	-0.07	-0.12	-0.00	-0.02	-0.03	-0.27	-0.13	-0.19	-0.09	-0.03	-0.07	-0.03	-0.07		
150-200	0.2-0.4	10.48-0.10 ⁺	1.40	1.34	1.72	1.81	1.9	0.33	-0.03	0.00	0.04	-0.05	-0.06	-0.13	-0.07	-0.01	0.00	0.10	-0.07	-0.12	-0.00	-0.02	-0.03	-0.27	-0.13	-0.19	-0.09	-0.03	-0.07	-0.03	-0.07
150-200	0.4-0.6	10.33-0.10 ⁺	1.42	1.28	1.87	1.93	1.97	0.30	-0.03	0.00	0.04	-0.05	-0.06	-0.12	-0.07	-0.01	0.00	0.10	-0.07	-0.12	-0.00	-0.02	-0.03	-0.26	-0.12	-0.18	-0.08	-0.02	-0.06	-0.03	-0.07
150-200	0.6-0.8	10.33-0.10 ⁺	1.39	1.11	1.78	0.32	0.01	0.03	0.04	-0.02	-0.06	-0.09	-0.07	-0.04	-0.01	0.08	-0.05	-0.15	-0.02	-0.03	-0.04	-0.23	-0.09	-0.15	-0.06	-0.02	-0.06	-0.03	-0.07		
150-200	0.8-1.0	10.22-0.10 ⁺	1.42	1.02	1.75	0.33	0.01	0.03	0.04	-0.02	-0.06	-0.09	-0.07	-0.04	-0.01	0.07	-0.05	-0.15	-0.02	-0.03	-0.04	-0.22	-0.08	-0.14	-0.05	-0.02	-0.06	-0.03	-0.07		
150-200	1.0-1.2	10.22-0.10 ⁺	1.38	0.92	1.72	0.33	0.01	0.03	0.04	-0.02	-0.06	-0.09	-0.07	-0.04	-0.01	0.07	-0.05	-0.15	-0.02	-0.03	-0.04	-0.21	-0.07	-0.13	-0.04	-0.02	-0.06	-0.03	-0.07		
150-200	1.2-1.4	10.12-0.10 ⁺	1.47	0.80	1.60	1.72	0.33	0.01	0.03	0.04	-0.02	-0.06	-0.09	-0.07	-0.04	-0.01	0.07	-0.05	-0.15	-0.02	-0.03	-0.04	-0.20	-0.06	-0.12	-0.03	-0.02	-0.06	-0.03	-0.07	
150-200	1.4-1.6	10.11-0.10 ⁺	1.50	0.78	1.68	1.72	0.33	0.01	0.03	0.04	-0.02	-0.06	-0.09	-0.07	-0.04	-0.01	0.07	-0.05	-0.15	-0.02	-0.03	-0.04	-0.19	-0.05	-0.11	-0.02	-0.02	-0.06	-0.03	-0.07	
150-200	1.6-1.8	10.09-0.10 ⁺	1.53	0.78	1.68	1.72	0.33	0.01	0.03	0.04	-0.02	-0.06	-0.09	-0.07	-0.04	-0.01	0.07	-0.05	-0.15	-0.02	-0.03	-0.04	-0.18	-0.04	-0.10	-0.02	-0.02	-0.06	-0.03	-0.07	
150-200	1.8-2.0	10.08-0.10 ⁺	1.53	0.78	1.68	1.72	0.33	0.01	0.03	0.04	-0.02	-0.06	-0.09	-0.07	-0.04	-0.01	0.07	-0.05	-0.15	-0.02	-0.03	-0.04	-0.17	-0.04	-0.10	-0.02	-0.02	-0.06	-0.03	-0.07	
200-300	0.2-0.4	2.42-0.10 ⁺	2.21	2.06	3.03	0.56	-0.00	0.06	0.02	-0.08	0.04	-0.10	-0.09	-0.01	0.18	0.08	-0.07	-0.14	-0.01	-0.03	-0.04	-0.48	-0.13	-0.19	-0.06	-0.03	-0.07	-0.03	-0.07		
200-300	0.4-0.6	2.39-0.10 ⁺	2.21	2.06	3.03	0.56	-0.00	0.06	0.02	-0.08	0.04	-0.10	-0.09	-0.01	0.14	0.06	-0.07	-0.14	-0.01	-0.03	-0.04	-0.47	-0.12	-0.18	-0.06	-0.03	-0.07	-0.03	-0.07		
200-300	0.6-0.8	2.38-0.10 ⁺	1.95	2.01	2.91	0.56	-0.01	0.06	0.02	-0.08	0.04	-0.10	-0.09	-0.01	0.14	0.06	-0.07	-0.14	-0.01	-0.03	-0.04	-0.46	-0.12	-0.18	-0.06	-0.03	-0.07	-0.03	-0.07		
200-300	0.8-1.0	2.38-0.10 ⁺	1.87	2.02	2.92	0.56	-0.01	0.06	0.02	-0.08	0.04	-0.10	-0.09	-0.01	0.14	0.06	-0.07	-0.14	-0.01	-0.03	-0.04	-0.45	-0.12	-0.18	-0.06	-0.03	-0.07	-0.03	-0.07		
200-300	1.0-1.2	2.36-0.10 ⁺	2.09	1.95	2.56	0.56	-0.01	0.06	0.02	-0.08	0.04	-0.10	-0.09	-0.01	0.14	0.06	-0.07	-0.14	-0.01	-0.03	-0.04	-0.44	-0.12	-0.18	-0.06	-0.03	-0.07	-0.03	-0.07		
200-300	1.2-1.4	2.36-0.10 ⁺	2.09	1.95	2.56	0.56	-0.01	0.06	0.02	-0.08	0.04	-0.10	-0.09	-0.01	0.14	0.06	-0.07	-0.14	-0.01	-0.03	-0.04	-0.43	-0.12	-0.18	-0.06	-0.03	-0.07	-0.03	-0.07		
200-300	1.4-1.6	2.36-0.10 ⁺	2.09	1.95	2.56	0.56	-0.01	0.06	0.02	-0.08	0.04	-0.10	-0.09	-0.01	0.14	0.06	-0.07	-0.14	-0.01	-0.03	-0.04	-0.42	-0.12	-0.18	-0.06	-0.03	-0.07	-0.03	-0.07		
200-300	1.6-1.8	2.36-0.10 ⁺	2.09	1.95	2.56	0.56	-0.01	0.06	0.02	-0.08	0.04	-0.10	-0.09	-0.01	0.14	0.06	-0.07	-0.14	-0.01	-0.03	-0.04	-0.41	-0.12	-0.18	-0.06	-0.03	-0.07	-0.03	-0.07		
200-300	1.8-2.0	2.36-0.10 ⁺	2.09	1.95	2.56	0.56	-0.01	0.06	0.02	-0.08	0.04	-0.10	-0.09	-0.01	0.14	0.06	-0.07	-0.14	-0.01	-0.03	-0.04	-0.40	-0.12	-0.18	-0.06	-0.03	-0.07	-0.03	-0.07		
200-300	2.0-2.2	2.36-0.10 ⁺	2.09	1.95	2.56	0.56	-0.01	0.06	0.02	-0.08	0.04	-0.10	-0.09	-0.01	0.14	0.06	-0.07	-0.14	-0.01	-0.03	-0.04	-0.39	-0.12	-0.18	-0.06	-0.03	-0.07	-0.03	-0.07		
200-300	2.2-2.4	2.36-0.10 ⁺	2.09	1.95	2.56	0.56	-0.01	0.06	0.02	-0.08	0.04	-0.10	-0.09	-0.01	0.14	0.06	-0.07	-0.14	-0.01	-0.03	-0.04	-0.38	-0.12	-0.18	-0.06	-0.03	-0.07	-0.03	-0.07		
200-300	2.4-2.6	2.36-0.10 ⁺	2.09	1.95	2.56	0.56	-0.01	0.06	0.02	-0.08	0.04	-0.10	-0.09	-0.01	0.14	0.06	-0.07	-0.14	-0.01	-0.03	-0.04	-0.37	-0.12	-0.18	-0.06	-0.03	-0.07	-0.03	-0.07		
200-300	2.6-2.8	2.36-0.10 ⁺	2.09	1.95	2.56	0.56	-0.01	0.06	0.02	-0.08	0.04	-0.10	-0.09	-0.01	0.14	0.06	-0.07	-0.14	-0.01	-0.03	-0.04	-0.36	-0.12	-0.18	-0.06	-0.03	-0.07	-0.03	-0.07		
200-300	2.8-3.0	2.36-0.10 ⁺	2.09	1.95	2.56	0.56	-0.01	0.06	0.02	-0.08	0.04	-0.10	-0.09	-0.01	0.14	0.06	-0.07	-0.14	-0.01	-0.03	-0.04	-0.35	-0.12	-0.18	-0.06	-0.03	-0.07	-0.03	-0.07		
200-300	3.0-3.2	2.36-0.10 ⁺	2.09	1.95	2.56	0.56	-0.01	0.06	0.02	-0.08	0.04	-0.10	-0.09	-0.01	0.14	0.06	-0.07	-0.14	-0.01	-0.03	-0.04	-0.34	-0.12	-0.18	-0.06	-0.03	-0.07	-0.03	-0.07		
200-300	3.2-3.4	2.36-0.10 ⁺	2.09	1.95	2.56	0.56	-0.01	0.0																							

Table 3: The combined Born-level double-differential cross section $\frac{d^2\sigma}{dm_{\text{miss}} dy_{\ell\ell}}$. The measurements are listed together with the statistical (δ^{stat}), systematic (δ^{sys}) and total (δ^{tot}) uncertainties. In addition the contributions from the individual correlated (δ_{cor}^1 - δ_{cor}^{35}) and uncorrelated (δ^{unc}) systematic error sources are also provided. The luminosity uncertainty of 1.9% is not shown and not included in the overall systematic and total uncertainties.

Table 4: The combined Born-level double-differential cross section $\frac{d^2\sigma}{dm_{eff} d\Delta m_{eff}}$. The measurements are listed together with the statistical (δ^{stat}), systematic (δ^{sys}) and total (δ^{tot}) uncertainties. In addition the contributions from the individual correlated ($\delta_{cor}^l - \delta_{cor}^{35}$) and uncorrelated (δ^{unc}) systematic error sources are also provided. The luminosity uncertainty of 1.9% is not shown and not included in the overall systematic and total uncertainties.

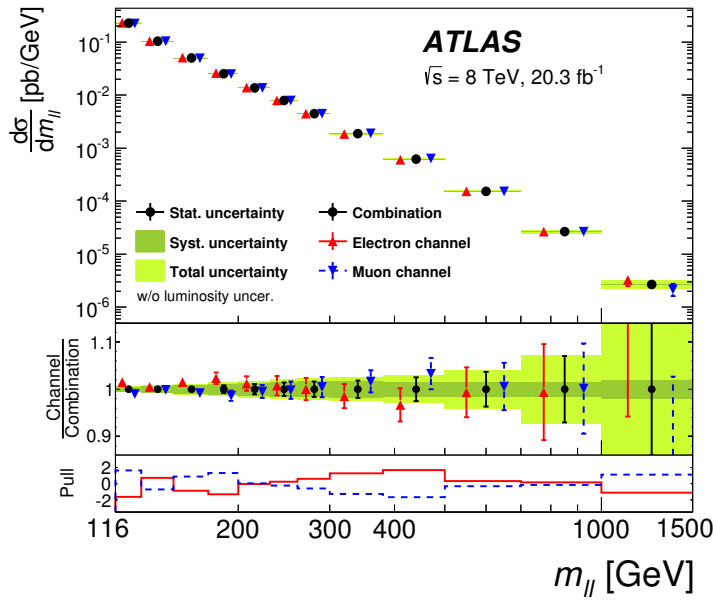


Figure 6: Comparison of the electron (red points), muon (blue points) and combined (black points) single-differential fiducial Born-level cross sections as a function of invariant mass $m_{\ell\ell}$. The error bars represent the statistical uncertainty. The inner shaded band represents the systematic uncertainty on the combined cross sections, and the outer shaded band represents the total measurement uncertainty (excluding the luminosity uncertainty). The central panel shows the ratio of each measurement channel to the combined data, and the lower panel shows the pull of the electron (red) and muon (blue) channel measurements with respect to the combined data.

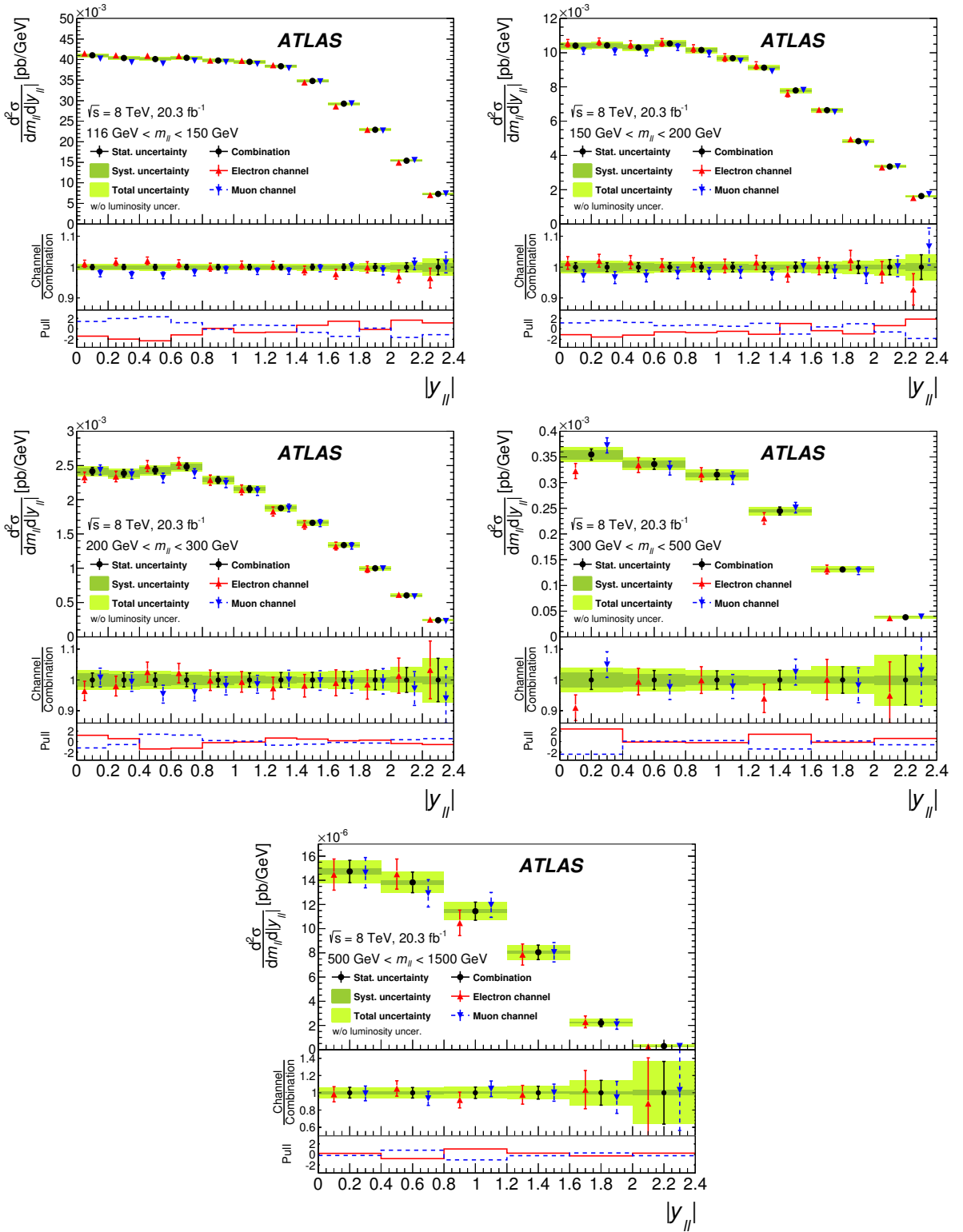


Figure 7: Comparison of the electron (red points), muon (blue points) and combined (black points) fiducial Born-level cross sections, differential in invariant mass $m_{\ell\ell}$ and absolute dilepton rapidity $|y_{\ell\ell}|$. The error bars represent the statistical uncertainty. The inner shaded band represents the systematic uncertainty on the combined cross sections, and the outer shaded band represents the total measurement uncertainty (excluding the luminosity uncertainty). The central panel shows the ratio of each measurement channel to the combined data, and the lower panel shows the pull of the electron (red) and muon (blue) channel measurements with respect to the combined data.

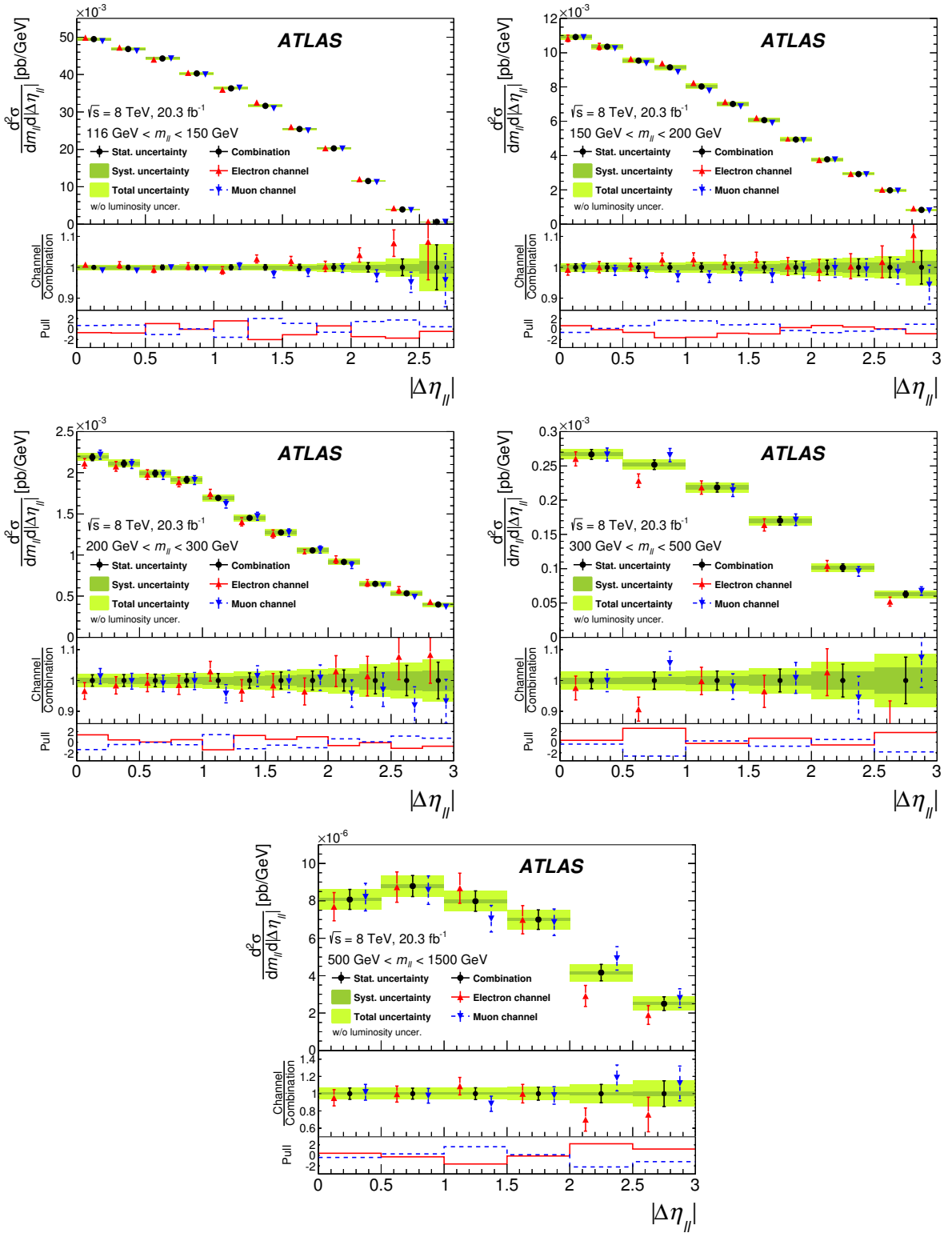


Figure 8: Comparison of the electron (red points), muon (blue points) and combined (black points) fiducial Born-level cross sections, differential in invariant mass $m_{\ell\ell}$ and absolute dilepton pseudorapidity separation $|\Delta\eta_{\ell\ell}|$. The error bars represent the statistical uncertainty. The inner shaded band represents the systematic uncertainty on the combined cross sections, and the outer shaded band represents the total measurement uncertainty (excluding the luminosity uncertainty). The central panel shows the ratio of each measurement channel to the combined data, and the lower panel shows the pull of the electron (red) and muon (blue) channel measurements with respect to the combined data.

9 Comparison to theoretical predictions

The combined fiducial cross sections at Born-level are compared to NNLO pQCD calculations using various PDFs. The calculations use the FEWZ 3.1 framework (see section 3), and include NLO EW corrections in the G_μ [82] electroweak scheme. The dynamic scale $m_{\ell\ell}$ is used in the calculation, and the renormalisation and factorisation scales are set to $\mu_R = \mu_F = m_{\ell\ell}$. The calculation includes the contribution of the non-resonant PI process, $\gamma\gamma \rightarrow \ell\ell$. This contribution is estimated at leading order (LO) using the photon PDF from the NNPDF2.3qed PDF set [22].

Theoretical predictions using the MMHT14 NNLO PDF set [20] are compared to the combined double-differential fiducial cross sections at Born-level as a function of $m_{\ell\ell}$ and either $|y_{\ell\ell}|$ or $|\Delta\eta_{\ell\ell}|$ in figure 9. The single-differential cross section as a function of $m_{\ell\ell}$ is shown in figure 10. The uncertainty bands assigned to the calculations show the combined 68% confidence level (CL) PDF and α_S variation, the renormalisation and factorisation scale uncertainties and the PI uncertainty. The α_S uncertainty is determined by varying α_S by 0.001 with respect to its default value of 0.118. The scale uncertainties are defined by the envelope of variations in which the scales are changed by factors of two subject to the constraint $0.5 \leq \mu_R/\mu_F \leq 2$. The relative uncertainty on the PI contribution represents the region covering 68% of the NNPDF2.3qed MC replicas,² corresponding to rather large values of 62%–92% depending on the bin.

Figures 11 and 12 show the ratio of theoretical predictions for the double-differential cross sections to the combined measurements. The corresponding ratios for the single-differential cross section are shown in the middle and lower panels of figure 10. The PI contribution reaches up to 15% in certain regions of phase space, as can be seen in the middle panels of figure 10 and the left panels of figures 11 and 12 where a comparison is shown between the ratios for the default calculation and a calculation neglecting the PI contribution. In the regions where the PI contribution is large the PI uncertainty dominates the total uncertainty band, otherwise the PDF uncertainty is dominant. Thus it can be inferred from, e.g., the middle panel of figure 10, that the PDF (PI) uncertainty dominates the uncertainty band at small (large) $m_{\ell\ell}$. The uncertainties are similar at about $m_{\ell\ell} \simeq 200$ GeV.

The uncertainties on the theoretical calculation are in general larger than those on the measurement for most of the phase space, indicating that the data presented here have the potential to constrain the theoretical predictions. The calculation including the PI contribution is in general in agreement with the data. However, it seems to undershoot the data at small $m_{\ell\ell}$ as can be seen in all three figures.

The change in the theoretical prediction when replacing the MMHT PDF by other NNLO PDFs such as HERAPDF2.0 [83], CT14 [18], ABM12 [84] or NNPDF3.0 [19] is shown in the lower panels of figure 10 and the right panels of figures 11 and 12. For ease of visibility, no separate uncertainty bands are shown for each individual PDF. However, they have been calculated and found to be smaller (ABM12), larger (CT14, NNPDF3.0) or even much larger (HERAPDF2.0) than the ones from MMHT14 when scaled to the 68% CL. The calculations using the various PDFs generally agree with the data, with the one using NNPDF3.0 showing the least agreement at low $m_{\ell\ell}$. In particular at low $m_{\ell\ell}$, the differences between the predictions in all three figures are larger than the total uncertainty of the measurement, indicating the sensitivity of the data to the PDFs, and the potential to constrain them.

² The NNPDF Collaboration provides a large number of MC replicas in order to represent the PDF, where the central PDF is given by the mean of all replicas and the uncertainty is defined as the region covering 68% of all MC replicas.

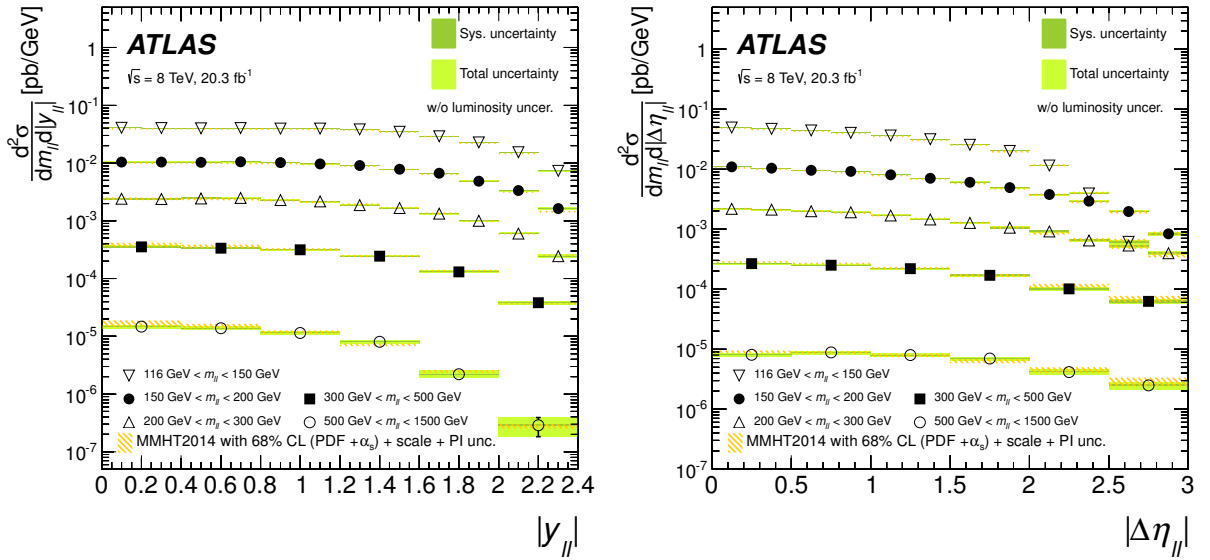


Figure 9: The combined double-differential cross sections as a function of invariant mass $m_{\ell\ell}$ and absolute dilepton rapidity $|y_{\ell\ell}|$ (left panel) and as a function of $m_{\ell\ell}$ and absolute dilepton pseudorapidity separation $|\Delta\eta_{\ell\ell}|$ (right panel) at the Born-level within the fiducial region with statistical, systematic and total uncertainties, excluding the 1.9% uncertainty on the luminosity. Data are compared to combined NNLO pQCD and NLO EW calculations using the MMHT2014 PDF, where the uncertainty band displays the combined 68% confidence level (CL) PDF and α_S variation, the renormalisation and factorisation scale uncertainties and the PI uncertainty.

	$m_{\ell\ell}$	$ y_{\ell\ell} $	$ \Delta\eta_{\ell\ell} $
MMHT2014	18.2/12	59.3/48	62.8/47
CT14	16.0/12	51.0/48	61.3/47
NNPDF3.0	20.0/12	57.6/48	62.1/47
HERAPDF2.0	15.1/12	55.5/48	60.8/47
ABM12	14.1/12	57.9/48	53.5/47

Table 5: The χ^2/dof values for the compatibility of data and theory after the minimisation procedure.

In order to quantitatively assess the compatibility between data and theory, a χ^2 minimisation procedure as implemented in the xFitter package [85] is used. All correlated and uncorrelated experimental uncertainties (see tables 2, 3 and 4), the luminosity uncertainty and the theoretical uncertainties are included in the χ^2 function. The correlated theoretical uncertainties include the uncertainties on the respective PDF, the PI contribution, α_S , and the scale. The PDF uncertainties for all the PDF sets except for the photon PDF are further decomposed into the full set of eigenvectors, where in the case of NNPDF3.0 the replica representation is transformed into an eigenvector representation. Uncorrelated theoretical uncertainties arising from the statistical precision of the calculations are also taken into account but are at the level of 0.1% for the calculation of the DY and 0.2% for the PI cross sections. All correlated uncertainties are included as nuisance parameters. After minimisation, the central values of the nuisance parameters may be shifted from unity and their uncertainties may be reduced. A sizeable shift and reduction in uncertainty indicates that the data can constrain the respective nuisance parameter.

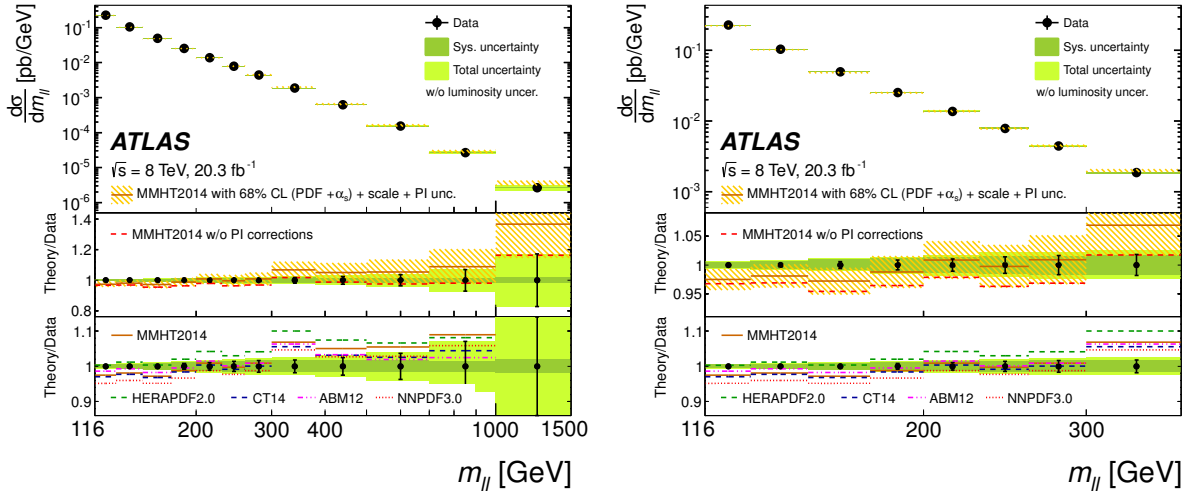


Figure 10: The combined single-differential cross section as a function of invariant mass $m_{\ell\ell}$ at the Born-level within the fiducial region with statistical, systematic and total uncertainties, excluding the 1.9% uncertainty on the luminosity. Data are compared to combined NNLO pQCD and NLO EW calculations using the MMHT2014 PDF, where the uncertainty band displays the combined 68% confidence level (CL) PDF and α_S variation, the renormalisation and factorisation scale uncertainties and the PI uncertainty. The two ratio panels show the ratio of the calculation, both with and without the PI contribution with respect to data (middle panel), as well as the ratio for calculations using different PDFs (bottom panel). On the right, the results are shown for a restricted range of $m_{\ell\ell}$.

The χ^2 minimisation is performed separately for all five PDF sets and for all three distributions shown in figures 10, 11 and 12. The χ^2 values after minimisation are given in table 5. They indicate general compatibility between the data and the theory, mainly due to the fact that the theoretical uncertainties for all PDF sets except for ABM12 are larger than the ones for MMHT14 shown in the figures. The overall best agreement with the data is found for the calculations using ABM12, especially when taking into account their smaller PDF uncertainties.

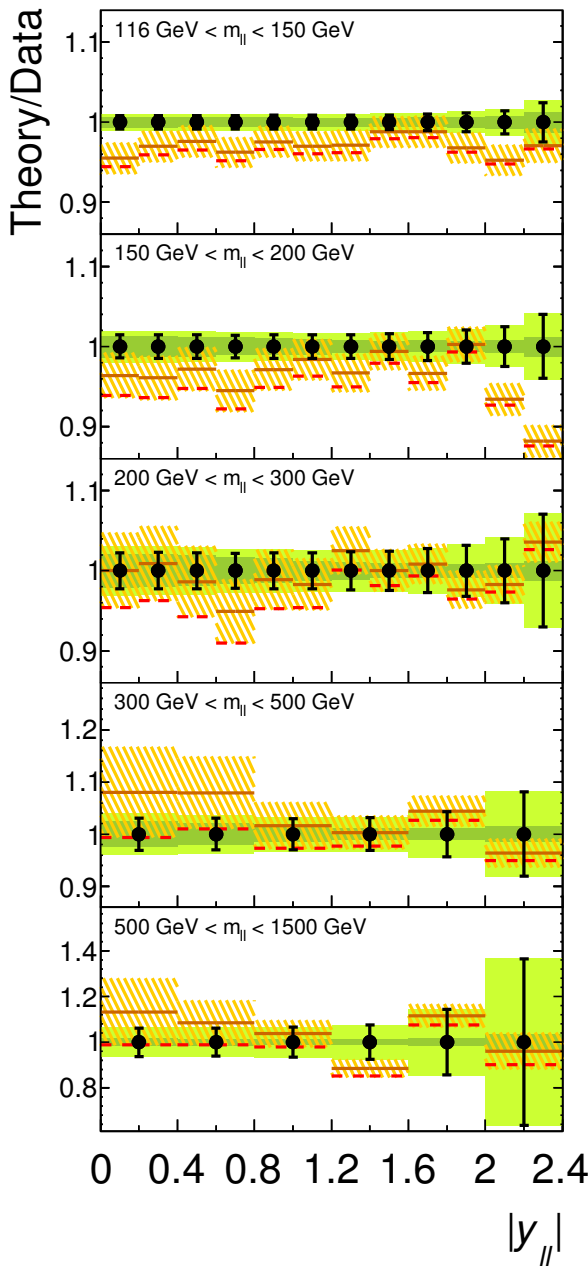
The impact of this data on existing PDF sets can be inferred using Bayesian reweighting [86], which has been further developed and validated by the NNPDF collaboration in the context of their MC replicas [87, 88]. Each replica is used together with this data set in the χ^2 minimisation described above, and a weight is assigned based on the resulting χ^2 . Replicas not describing the data well get a smaller weight assigned, and a new PDF is derived by including the weights in the calculation of the central value and the PDF uncertainty, i.e., without performing a new global PDF fit.

Bayesian reweighting is used for the 100 MC replicas representing the NNPDF2.3qed photon PDF obtained in NNLO fits. The results of the reweighting are shown in figure 13. The solid yellow area represents the 68% confidence level interval of the NNPDF2.3qed photon PDF at $Q^2 = 2 \text{ GeV}^2$ and at $Q^2 = 10^4 \text{ GeV}^2$, which are also displayed in ref. [22]. In addition, the MRST2004qed photon PDF [21] using two different quark mass schemes (see section 7) and the recent CT14qed photon PDF [89] are displayed, which exhibit a different PDF evolution compared to NNPDF2.3qed as can be seen when comparing the two plots at the input scale and at $Q^2 = 10^4 \text{ GeV}^2$. The shaded area indicates the new PDF after inclusion of this data by means of Bayesian reweighting, where the χ^2 minimisations are performed for the double-differential cross section as a function of $m_{\ell\ell}$ and $|y_{\ell\ell}|$ using the prediction based on the

ATLAS

$\sqrt{s} = 8 \text{ TeV}, 20.3 \text{ fb}^{-1}$

MMHT2014 with 68% CL
 $(\text{PDF} + \alpha_s) + \text{scale} + \text{PI unc.}$
 MMHT2014 w/o PI corrections



HERAPDF2.0 CT14 ABM12 NNPDF3.0	Data Sys. uncertainty Total uncertainty w/o luminosity uncer.
---	--

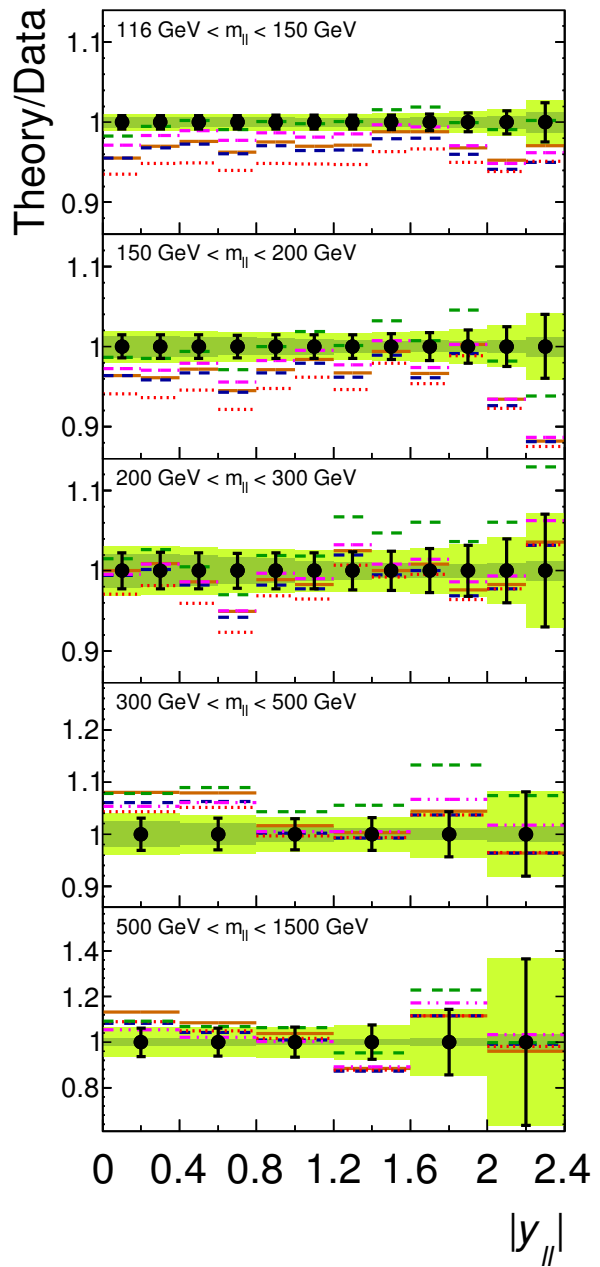


Figure 11: The ratio of theoretical NNLO pQCD and NLO EW calculations to the combined double-differential cross section as a function of invariant mass $m_{\ell\ell}$ and absolute dilepton rapidity $|y_{\ell\ell}|$ at the Born-level within the fiducial region with statistical, systematic and total uncertainties, excluding the 1.9% uncertainty on the luminosity. The calculations are shown for the MMHT14 PDF with and without the PI contribution on the left side and for MMHT14, HERAPDF2.0, CT10, ABM12 and NNPDF3.0 on the right side. The uncertainty band on the left side displays the combined 68% confidence level (CL) PDF and α_S variation, the renormalisation and factorisation scale uncertainties and the PI uncertainty.

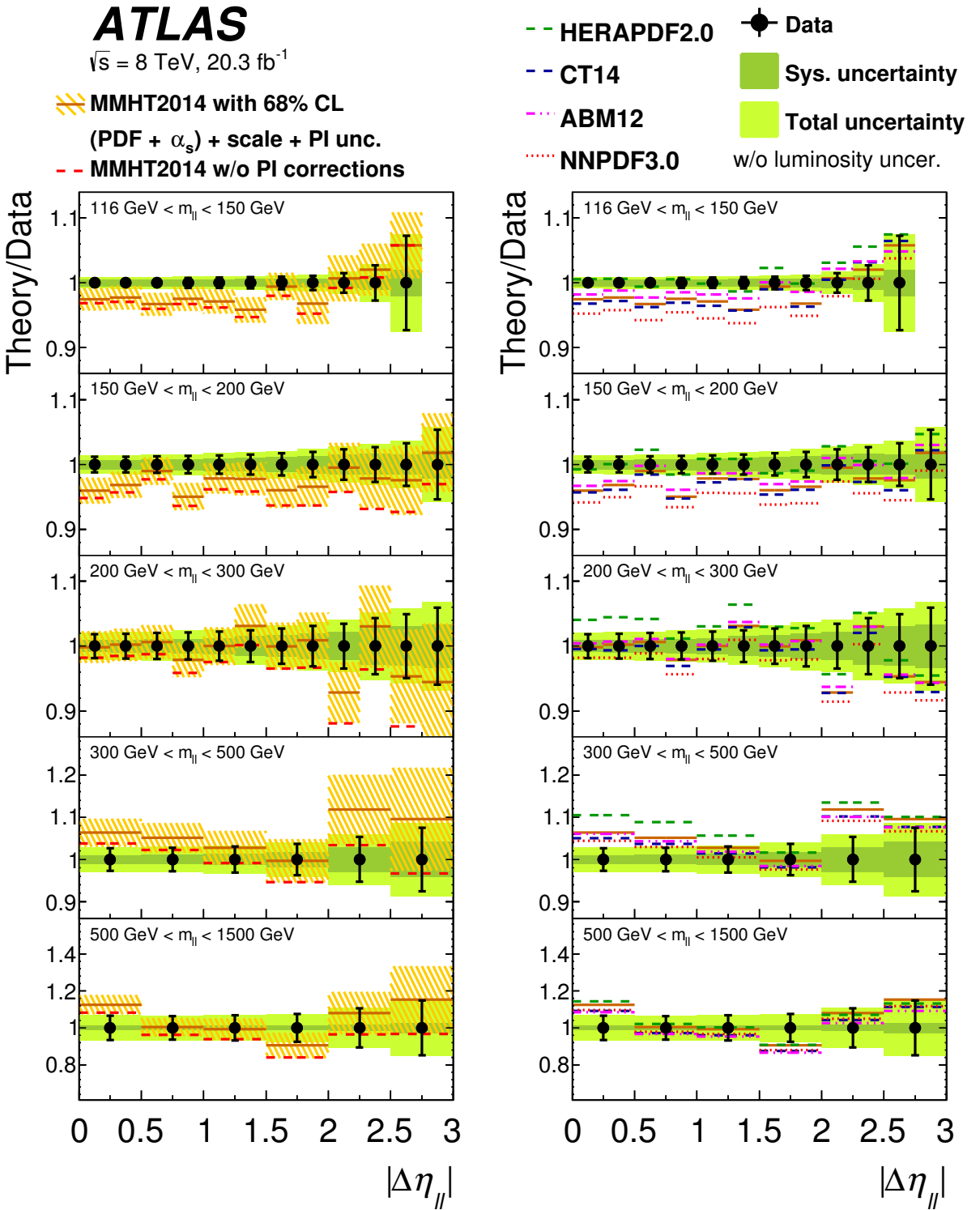


Figure 12: The ratio of theoretical NNLO pQCD and NLO EW calculations to the combined double-differential cross section as a function of invariant mass $m_{\ell\ell}$ and absolute dilepton pseudorapidity separation $|\Delta\eta_{\ell\ell}|$ at Born-level within the fiducial region with statistical, systematic and total uncertainties, excluding the 1.9% uncertainty on the luminosity. The calculations are shown for the MMHT14 PDF with and without the PI contribution on the left side and for MMHT14, HERAPDF2.0, CT10, ABM12 and NNPDF3.0 on the right side. The uncertainty band on the left side displays the combined 68% confidence level (CL) PDF and α_s variation, the renormalisation and factorisation scale uncertainties and the PI uncertainty.

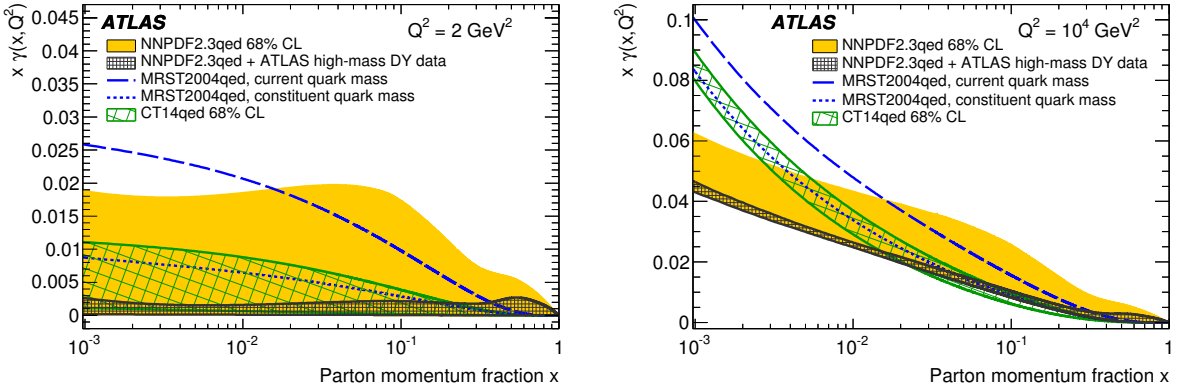


Figure 13: The 68% confidence level interval of the NNPDF2.3qed NNLO photon PDF as a function of momentum fraction x at the input scale $Q_0^2 = 2 \text{ GeV}^2$ (left panel) and $Q^2 = 10^4 \text{ GeV}^2$ (right panel) before (yellow solid area) [22] and after (grey shaded area) inclusion of the double-differential cross section measurement as a function of invariant mass $m_{\ell\ell}$ and absolute dilepton rapidity $|y_{\ell\ell}|$. Also shown is the MRST2004qed photon PDF in a current quark (blue dashed line) and a constituent quark (blue dotted line) mass scheme [21], and the 68% CL band (green shaded area) for the CT14qed photon PDF [89].

MMHT14 PDF. The reduction of uncertainties is rather large and confirms the strong sensitivity of this data to the photon PDF. Using the double-differential cross section as a function of $m_{\ell\ell}$ and $|\Delta\eta_{\ell\ell}|$ instead, a slightly smaller impact is found. This can be explained by the fact that the contributions from the PI process are largest in the regions of small $|y_{\ell\ell}|$ and large $|\Delta\eta_{\ell\ell}|$, where the uncertainties of the measurement are smallest for $|y_{\ell\ell}|$ but largest for $|\Delta\eta_{\ell\ell}|$.

Inspection of the optimised experimental nuisance parameters of those minimisations with the best χ^2 values shows that the largest pulls and uncertainty reductions are found for the luminosity. Larger values for the data luminosity by about 1.1 and 1.2 standard deviations are favoured for the minimisations in $|y_{\ell\ell}|$ and $|\Delta\eta_{\ell\ell}|$ respectively, leading to smaller values for the experimental cross section. For the MMHT14 PDF, the largest pulls and reduction of uncertainty by about 25% is found for an eigenvector (“eigenvector 21”) particularly sensitive to the sea and strange sea quark distribution, where previous ATLAS data on on-shell W and Z production [6] is already the most constraining data set in one eigenvector direction [20].

10 Conclusion

The double-differential fiducial cross sections $d^2\sigma/dm_{\ell\ell}d|y_{\ell\ell}|$ and $d^2\sigma/dm_{\ell\ell}d|\Delta\eta_{\ell\ell}|$ for the Drell–Yan and photon induced production of dileptons in the invariant mass range $116 < m_{\ell\ell} < 1500 \text{ GeV}$ are measured, as well as the single-differential fiducial cross section $d\sigma/dm_{\ell\ell}$. The measurements are performed in the electron and muon channels using 20.3 fb^{-1} of integrated luminosity collected by the ATLAS detector at the LHC in pp collisions at $\sqrt{s} = 8 \text{ TeV}$. The two measurements are combined taking into account the systematic uncertainty correlations. The combined cross sections achieve an experimental precision of better than 1% at low $m_{\ell\ell}$, excluding the overall uncertainty in the luminosity measurement of 1.9%.

The fiducial cross sections are compared to fixed order theoretical predictions at NNLO accuracy using

a selection of recent PDF sets. The calculations are performed using renormalisation and factorisation scales equal to $m_{\ell\ell}$, and are corrected for additional higher-order electroweak radiative effects. Theoretical uncertainties arising from the PDFs, the choice of scale and a variation of α_S are calculated and are found to be larger than the measurement uncertainties, indicating the data has the potential to constrain PDFs. This is confirmed by a χ^2 minimisation procedure comparing data to theoretical predictions, which in combination with a Bayesian reweighting method shows a dramatic reduction of the uncertainties on the photon PDF.

Acknowledgements

We thank CERN for the very successful operation of the LHC, as well as the support staff from our institutions without whom ATLAS could not be operated efficiently.

We acknowledge the support of ANPCyT, Argentina; YerPhI, Armenia; ARC, Australia; BMWFW and FWF, Austria; ANAS, Azerbaijan; SSTC, Belarus; CNPq and FAPESP, Brazil; NSERC, NRC and CFI, Canada; CERN; CONICYT, Chile; CAS, MOST and NSFC, China; COLCIENCIAS, Colombia; MSMT CR, MPO CR and VSC CR, Czech Republic; DNRF and DNSRC, Denmark; IN2P3-CNRS, CEA-DSM/IRFU, France; GNSF, Georgia; BMBF, HGF, and MPG, Germany; GSRT, Greece; RGC, Hong Kong SAR, China; ISF, I-CORE and Benoziyo Center, Israel; INFN, Italy; MEXT and JSPS, Japan; CNRST, Morocco; FOM and NWO, Netherlands; RCN, Norway; MNiSW and NCN, Poland; FCT, Portugal; MNE/IFA, Romania; MES of Russia and NRC KI, Russian Federation; JINR; MESTD, Serbia; MSSR, Slovakia; ARRS and MIZŠ, Slovenia; DST/NRF, South Africa; MINECO, Spain; SRC and Wallenberg Foundation, Sweden; SERI, SNSF and Cantons of Bern and Geneva, Switzerland; MOST, Taiwan; TAEK, Turkey; STFC, United Kingdom; DOE and NSF, United States of America. In addition, individual groups and members have received support from BCKDF, the Canada Council, CANARIE, CRC, Compute Canada, FQRNT, and the Ontario Innovation Trust, Canada; EPLANET, ERC, FP7, Horizon 2020 and Marie Skłodowska-Curie Actions, European Union; Investissements d’Avenir Labex and Idex, ANR, Région Auvergne and Fondation Partager le Savoir, France; DFG and AvH Foundation, Germany; Herakleitos, Thales and Aristeia programmes co-financed by EU-ESF and the Greek NSRF; BSF, GIF and Minerva, Israel; BRF, Norway; Generalitat de Catalunya, Generalitat Valenciana, Spain; the Royal Society and Leverhulme Trust, United Kingdom.

The crucial computing support from all WLCG partners is acknowledged gratefully, in particular from CERN and the ATLAS Tier-1 facilities at TRIUMF (Canada), NDGF (Denmark, Norway, Sweden), CC-IN2P3 (France), KIT/GridKA (Germany), INFN-CNAF (Italy), NL-T1 (Netherlands), PIC (Spain), ASGC (Taiwan), RAL (UK) and BNL (USA) and in the Tier-2 facilities worldwide.

Appendix

m_{ee} [GeV]	$\frac{d\sigma}{dm_{ee}}$ [pb/GeV]	δ^{stat} [%]	δ^{sys} [%]	δ^{tot} [%]	$\delta_{\text{cor}}^{\text{trig}}$ [%]	$\delta_{\text{unc}}^{\text{trig}}$ [%]	$\delta_{\text{cor}}^{\text{reco}}$ [%]	$\delta_{\text{cor}}^{\text{id}}$ [%]	$\delta_{\text{cor}}^{\text{iso}}$ [%]	$\delta_{\text{unc}}^{\text{iso}}$ [%]	$\delta_{\text{cor}}^{\text{Eres}}$ [%]	$\delta_{\text{cor}}^{\text{Escal}}$ [%]	$\delta_{\text{cor}}^{\text{mult.}}$ [%]	$\delta_{\text{unc}}^{\text{mult.}}$ [%]	$\delta_{\text{cor}}^{\text{top}}$ [%]	$\delta_{\text{cor}}^{\text{diboson}}$ [%]	$\delta_{\text{unc}}^{\text{bgMC}}$ [%]	$\delta_{\text{unc}}^{\text{MC}}$ [%]	k_{dressed}
116–130	2.31×10^{-1}	0.5	0.8	1.0	-0.1	0.0	0.0	-0.3	0.0	0.0	0.1	0.5	-0.5	0.1	-0.3	-0.1	0.0	0.1	1.047
130–150	1.05×10^{-1}	0.7	1.0	1.2	-0.1	0.0	-0.1	-0.4	0.0	0.1	0.1	0.4	-0.7	0.2	-0.5	-0.2	0.1	0.1	1.046
150–175	5.06×10^{-2}	0.8	1.3	1.6	0.0	0.1	-0.1	-0.5	0.0	0.1	0.1	0.4	-0.8	0.3	-0.7	-0.2	0.1	0.1	1.047
175–200	2.60×10^{-2}	1.2	1.6	2.0	-0.1	0.1	-0.1	-0.6	0.0	0.1	0.0	0.5	-0.9	0.3	-0.9	-0.3	0.2	0.1	1.052
200–230	1.39×10^{-2}	1.5	2.0	2.5	-0.1	0.1	-0.1	-0.7	0.0	0.2	0.1	0.7	-1.2	0.4	-1.1	-0.4	0.2	0.2	1.053
230–260	7.95×10^{-3}	2.0	2.2	3.0	-0.1	0.1	-0.2	-0.7	-0.1	0.2	0.1	1.0	-1.1	0.4	-1.3	-0.4	0.3	0.2	1.056
260–300	4.43×10^{-3}	2.4	2.3	3.3	-0.1	0.1	-0.2	-0.7	-0.1	0.2	0.1	0.9	-1.3	0.5	-1.3	-0.6	0.4	0.2	1.058
300–380	1.84×10^{-3}	2.6	2.5	3.6	-0.1	0.2	-0.2	-0.8	-0.1	0.3	0.1	1.3	-1.1	0.4	-1.4	-0.6	0.4	0.2	1.063
380–500	5.99×10^{-4}	3.6	2.7	4.5	-0.1	0.2	-0.2	-0.8	-0.2	0.5	0.1	1.6	-1.4	0.5	-1.1	-0.6	0.5	0.2	1.067
500–700	1.52×10^{-4}	5.3	2.6	6.0	-0.1	0.2	-0.2	-0.8	-0.2	0.7	0.1	2.0	-0.7	0.5	-0.7	-0.6	0.5	0.3	1.075
700–1000	2.64×10^{-5}	10.2	3.3	10.7	-0.2	0.4	-0.2	-0.8	-0.3	1.4	0.1	2.3	-0.6	0.8	-0.4	-0.6	0.7	0.4	1.085
1000–1500	3.23×10^{-6}	22.5	5.8	23.2	-0.7	0.9	-0.2	-0.8	-0.3	3.5	0.0	2.8	-1.9	1.6	-0.3	-0.6	2.1	0.2	1.100

Table 6: The electron channel Born-level single-differential cross section $\frac{d\sigma}{dm_{ee}}$. The measurements are listed together with the statistical (δ^{stat}), systematic (δ^{sys}) and total (δ^{tot}) uncertainties. In addition the contributions from the individual correlated (cor) and uncorrelated (unc) systematic error sources are also provided consisting of the trigger efficiency (δ^{trig}), electron reconstruction efficiency (δ^{reco}), electron identification efficiency (δ^{id}), the isolation efficiency (δ^{iso}), the electron energy resolution (δ^{Eres}), the electron energy scale (δ^{Escal}), the multijet and W +jets background ($\delta^{\text{mult.}}$), the top and diboson background normalisation ($\delta^{\text{top}}, \delta^{\text{diboson}}$), the top and diboson background MC statistical uncertainty (δ^{bgMC}), and the signal MC statistical uncertainty (δ^{MC}). The ratio of the dressed-level to Born-level predictions (k_{dressed}) is also provided. The luminosity uncertainty of 1.9% is not shown and not included in the overall systematic and total uncertainties.

m_{ee} [GeV]	$ y_{ee} $	$\frac{d^2\sigma}{dm_{ee}dy_{ee}}$ [pb/GeV]	δ^{stat} [%]	δ^{sys} [%]	δ^{tot} [%]	$\delta_{\text{cor}}^{\text{trig}}$ [%]	$\delta_{\text{unc}}^{\text{trig}}$ [%]	$\delta_{\text{cor}}^{\text{reco}}$ [%]	$\delta_{\text{cor}}^{\text{id}}$ [%]	$\delta_{\text{cor}}^{\text{iso}}$ [%]	$\delta_{\text{cor}}^{\text{iso unc}}$ [%]	$\delta_{\text{cor}}^{\text{Eres}}$ [%]	$\delta_{\text{cor}}^{\text{Escal}}$ [%]	$\delta_{\text{cor}}^{\text{mult unc}}$ [%]	$\delta_{\text{cor}}^{\text{mult top}}$ [%]	$\delta_{\text{cor}}^{\text{diboson}}$ [%]	$\delta_{\text{cor}}^{\text{bgMC}}$ [%]	$\delta_{\text{cor}}^{\text{MC}}$ [%]	k_{dressed}	
116–150	0.0–0.2	4.15×10^{-2}	1.1	0.8	1.4	-0.1	0.0	-0.1	-0.3	0.0	0.0	0.1	0.2	-0.3	0.1	-0.5	-0.1	0.1	0.2	1.048
116–150	0.2–0.4	4.11×10^{-2}	1.2	0.8	1.4	-0.1	0.0	-0.1	-0.3	0.0	0.0	0.1	0.3	-0.3	0.1	-0.5	-0.1	0.1	0.2	1.048
116–150	0.4–0.6	4.09×10^{-2}	1.2	0.9	1.5	-0.1	0.0	-0.1	-0.3	0.0	0.0	0.3	0.3	-0.4	0.1	-0.5	-0.1	0.1	0.3	1.047
116–150	0.6–0.8	4.09×10^{-2}	1.2	0.9	1.5	-0.1	0.0	-0.1	-0.3	0.0	0.0	0.2	0.4	-0.3	0.1	-0.4	-0.1	0.1	0.3	1.048
116–150	0.8–1.0	3.97×10^{-2}	1.3	0.9	1.6	-0.1	0.0	-0.1	-0.3	0.0	0.0	0.2	0.5	-0.3	0.2	-0.4	-0.1	0.1	0.3	1.047
116–150	1.0–1.2	3.97×10^{-2}	1.3	1.0	1.6	-0.1	0.0	-0.1	-0.3	0.0	0.0	0.1	0.6	-0.5	0.2	-0.3	-0.1	0.1	0.3	1.047
116–150	1.2–1.4	3.86×10^{-2}	1.3	1.2	1.8	-0.1	0.0	-0.1	-0.3	0.0	0.0	0.3	0.7	-0.6	0.2	-0.3	-0.1	0.1	0.3	1.046
116–150	1.4–1.6	3.44×10^{-2}	1.4	1.3	1.9	-0.1	0.0	-0.1	-0.4	0.0	0.0	0.2	0.8	-0.7	0.2	-0.2	-0.1	0.1	0.3	1.046
116–150	1.6–1.8	2.86×10^{-2}	1.6	1.5	2.2	-0.1	0.0	-0.1	-0.5	0.0	0.0	0.2	1.0	-0.9	0.3	-0.2	-0.1	0.1	0.4	1.044
116–150	1.8–2.0	2.29×10^{-2}	1.8	1.6	2.4	-0.1	0.0	-0.1	-0.6	0.0	0.1	0.3	1.1	-0.9	0.3	-0.1	-0.1	0.1	0.4	1.043
116–150	2.0–2.2	1.49×10^{-2}	2.1	2.0	2.9	-0.1	0.0	-0.1	-0.6	0.0	0.1	0.4	0.8	-1.5	0.4	-0.1	-0.1	0.1	0.5	1.044
116–150	2.2–2.4	7.05×10^{-3}	3.3	3.1	4.5	0.0	0.0	-0.2	-0.7	0.0	0.1	0.4	1.2	-2.5	0.6	-0.1	0.2	0.8	1.045	
150–200	0.0–0.2	1.06×10^{-2}	2.0	1.5	2.5	-0.1	0.1	-0.1	-0.5	0.0	0.1	0.1	0.2	-0.6	0.2	-1.2	-0.3	0.3	0.2	1.052
150–200	0.2–0.4	1.06×10^{-2}	2.0	1.5	2.6	-0.1	0.1	-0.1	-0.5	0.0	0.1	0.1	0.3	-0.6	0.3	-1.1	-0.3	0.3	0.2	1.050
150–200	0.4–0.6	1.05×10^{-2}	2.1	1.5	2.6	-0.1	0.1	-0.1	-0.5	0.0	0.1	0.1	0.2	-0.6	0.3	-1.1	-0.4	0.3	0.3	1.052
150–200	0.6–0.8	1.06×10^{-2}	2.1	1.5	2.6	-0.1	0.1	-0.1	-0.5	0.0	0.1	0.2	0.5	-0.7	0.3	-1.0	-0.3	0.3	0.3	1.053
150–200	0.8–1.0	1.02×10^{-2}	2.1	1.5	2.6	-0.1	0.1	-0.1	-0.5	0.0	0.1	0.1	0.4	-0.8	0.4	-0.8	-0.3	0.3	0.3	1.050
150–200	1.0–1.2	9.71×10^{-3}	2.2	1.7	2.8	-0.1	0.1	-0.1	-0.5	0.0	0.1	0.2	0.6	-1.1	0.4	-0.7	-0.3	0.3	0.3	1.050
150–200	1.2–1.4	9.25×10^{-3}	2.3	1.5	2.7	-0.1	0.1	-0.1	-0.5	0.0	0.1	0.1	0.7	-0.8	0.3	-0.6	-0.3	0.3	0.3	1.048
150–200	1.4–1.6	7.60×10^{-3}	2.5	1.8	3.1	0.0	0.1	-0.1	-0.6	0.0	0.1	0.1	1.0	-1.0	0.4	-0.5	-0.3	0.3	0.3	1.046
150–200	1.6–1.8	6.66×10^{-3}	2.8	1.9	3.3	0.0	0.1	-0.2	-0.7	0.0	0.1	0.2	1.2	-1.1	0.4	-0.3	-0.2	0.3	0.4	1.043
150–200	1.8–2.0	4.94×10^{-3}	3.1	1.7	3.6	0.0	0.1	-0.2	-0.8	0.0	0.1	0.3	0.8	-1.0	0.4	-0.2	-0.2	0.3	0.5	1.043
150–200	2.0–2.2	3.30×10^{-3}	3.5	1.9	4.0	0.0	0.1	-0.4	-0.8	0.0	0.1	0.2	0.5	-1.4	0.4	-0.1	-0.1	0.3	0.5	1.038
150–200	2.2–2.4	1.52×10^{-3}	5.5	3.2	6.3	-0.1	0.1	-0.6	-0.9	0.0	0.1	0.2	1.3	-2.4	0.8	-0.1	-0.1	0.3	0.8	1.038
200–300	0.0–0.2	2.33×10^{-3}	3.2	2.5	4.1	-0.1	0.1	-0.2	-0.7	-0.1	0.2	0.1	0.5	-0.9	0.5	-1.9	-0.5	0.6	0.3	1.063
200–300	0.2–0.4	2.34×10^{-3}	3.2	2.4	4.0	-0.1	0.1	-0.2	-0.7	-0.1	0.2	0.2	0.4	-0.9	0.5	-1.8	-0.5	0.6	0.3	1.063
200–300	0.4–0.6	2.49×10^{-3}	3.2	2.4	4.0	-0.1	0.1	-0.2	-0.7	-0.1	0.2	0.1	0.5	-1.3	0.6	-1.6	-0.6	0.6	0.3	1.063
200–300	0.6–0.8	2.54×10^{-3}	3.1	2.3	3.9	-0.1	0.1	-0.1	-0.7	-0.1	0.2	0.1	0.8	-1.2	0.6	-1.4	-0.5	0.5	0.3	1.060
200–300	0.8–1.0	2.29×10^{-3}	3.3	2.3	4.0	-0.1	0.1	-0.1	-0.7	-0.1	0.2	0.2	1.0	-1.1	0.6	-1.3	-0.5	0.5	0.3	1.056
200–300	1.0–1.2	2.14×10^{-3}	3.4	2.4	4.1	-0.1	0.1	-0.2	-0.7	-0.1	0.2	0.2	1.3	-1.3	0.5	-1.0	-0.5	0.5	0.4	1.053
200–300	1.2–1.4	1.83×10^{-3}	3.6	2.4	4.4	-0.1	0.1	-0.2	-0.7	-0.1	0.2	0.1	1.4	-1.4	0.5	-0.8	-0.4	0.5	0.4	1.049
200–300	1.4–1.6	1.63×10^{-3}	3.7	2.1	4.3	-0.1	0.1	-0.2	-0.8	-0.1	0.2	0.1	1.2	-1.2	0.4	-0.6	-0.3	0.5	0.4	1.044
200–300	1.6–1.8	1.32×10^{-3}	4.2	2.3	4.8	-0.1	0.1	-0.3	-0.8	-0.1	0.2	0.3	1.5	-1.2	0.4	-0.4	-0.3	0.5	0.5	1.041
200–300	1.8–2.0	9.87×10^{-4}	4.8	2.4	5.4	-0.1	0.1	-0.4	-0.9	-0.1	0.2	0.3	1.5	-1.2	0.5	-0.2	-0.2	0.5	0.6	1.044
200–300	2.0–2.2	6.13×10^{-4}	5.6	2.3	6.1	-0.1	0.1	-0.6	-1.0	-0.1	0.2	0.3	0.7	-1.6	0.5	-0.1	-0.1	0.4	0.6	1.044
200–300	2.2–2.4	2.51×10^{-4}	9.1	3.2	9.6	-0.1	0.2	-0.9	-1.1	-0.1	0.2	0.7	1.4	-1.8	1.1	-0.1	-0.1	0.5	1.1	1.042
300–500	0.0–0.4	3.23×10^{-4}	4.6	3.3	5.7	-0.1	0.2	-0.2	-0.8	-0.1	0.4	0.1	0.9	-1.8	0.6	-2.2	-0.8	0.8	0.3	1.080
300–500	0.4–0.8	3.34×10^{-4}	4.3	2.8	5.1	-0.1	0.2	-0.2	-0.8	-0.1	0.4	0.1	1.4	-1.1	0.6	-1.6	-0.7	0.7	0.3	1.072
300–500	0.8–1.2	3.16×10^{-4}	4.3	2.8	5.2	-0.1	0.2	-0.2	-0.8	-0.1	0.4	0.2	2.0	-0.9	0.5	-1.1	-0.6	0.7	0.3	1.058
300–500	1.2–1.6	2.30×10^{-4}	4.9	2.9	5.7	-0.1	0.2	-0.2	-0.8	-0.1	0.4	0.1	2.0	-1.6	0.5	-0.6	-0.4	0.6	0.4	1.053
300–500	1.6–2.0	1.31×10^{-4}	6.5	3.2	7.3	-0.1	0.2	-0.4	-0.9	-0.2	0.4	0.2	2.8	-0.3	0.4	-0.2	-0.2	0.5	0.6	1.047
300–500	2.0–2.4	3.62×10^{-5}	11.5	3.5	12.0	-0.1	0.2	-0.6	-1.0	-0.2	0.4	0.4	2.5	-1.3	1.0	0.0	-0.1	0.8	0.9	1.046
500–1500	0.0–0.4	1.45×10^{-5}	8.9	2.8	9.4	-0.2	0.3	-0.2	-0.8	-0.2	1.0	0.1	1.5	-0.7	0.8	-1.0	-0.7	1.0	0.3	1.096
500–1500	0.4–0.8	1.45×10^{-5}	8.5	2.9	9.0	-0.2	0.3	-0.2	-0.8	-0.2	1.0	0.1	2.1	-0.3	0.6	-0.6	-0.6	0.7	0.5	1.083
500–1500	0.8–1.2	1.05×10^{-5}	10.0	3.5	10.6	-0.1	0.3	-0.2	-0.8	-0.2	0.9	0.1	2.7	-1.1	0.8	-0.5	-0.5	0.9	0.5	1.067
500–1500	1.2–1.6	7.86×10^{-6}	11.1	3.6	11.7	-0.1	0.2	-0.2	-0.8	-0.2	0.9	0.1	3.2	-0.3	0.7	-0.1	-0.2	0.4	0.4	1.055
500–1500	1.6–2.0	2.29×10^{-6}	21.4	4.3	21.8	-0.1	0.2	-0.4	-0.9	-0.3	0.8	0.3	3.9	-0.4	0.7	-0.1	-0.2	0.7	0.9	1.056
500–1500	2.0–2.4	2.51×10^{-7}	60.4	7.8	60.9	-0.1	0.2	-0.6	-1.0	-0.3	0.8	1.1	5.7	-2.7	2.7	-0.1	-0.1	2.3	2.4	1.067

Table 7: The electron channel Born-level double-differential cross section $\frac{d^2\sigma}{dm_{ee}dy_{ee}}$. The measurements are listed together with the statistical (δ^{stat}), systematic (δ^{sys}) and total (δ^{tot}) uncertainties. In addition the contributions from the individual correlated (cor) and uncorrelated (unc) systematic error sources are also provided consisting of the trigger efficiency (δ^{trig}), electron reconstruction efficiency (δ^{reco}), electron identification efficiency (δ^{id}), the isolation efficiency (δ^{iso}), the electron energy resolution (δ^{Eres}), the electron energy scale (δ^{Escal}), the multijet and $W+jets$ background ($\delta^{\text{mult.}}$), the top and diboson background normalisation ($\delta^{\text{top}}, \delta^{\text{diboson}}$), the top and diboson background MC statistical uncertainty (δ^{bgMC}), and the signal MC statistical uncertainty (δ^{MC}). The ratio of the dressed-level to Born-level predictions (k_{dressed}) is also provided. The luminosity uncertainty of 1.9% is not shown and not included in the overall systematic and total uncertainties.

m_{ee} [GeV]	$ \Delta\eta_{ee} $	$\frac{d^2\sigma}{dm_{ee}d \Delta\eta_{ee} }$ [pb/GeV]	δ^{stat} [%]	δ^{sys} [%]	δ^{tot} [%]	$\delta_{\text{cor}}^{\text{trig}}$ [%]	$\delta_{\text{unc}}^{\text{trig}}$ [%]	$\delta_{\text{cor}}^{\text{reco}}$ [%]	$\delta_{\text{cor}}^{\text{id}}$ [%]	$\delta_{\text{cor}}^{\text{iso}}$ [%]	$\delta_{\text{unc}}^{\text{iso}}$ [%]	$\delta_{\text{cor}}^{\text{Eres}}$ [%]	$\delta_{\text{cor}}^{\text{Escal}}$ [%]	$\delta_{\text{cor}}^{\text{mult.}}$ [%]	$\delta_{\text{unc}}^{\text{mult.}}$ [%]	$\delta_{\text{cor}}^{\text{top}}$ [%]	$\delta_{\text{cor}}^{\text{diboson}}$ [%]	$\delta_{\text{unc}}^{\text{bgMC}}$ [%]	$\delta_{\text{unc}}^{\text{MC}}$ [%]	k_{dressed}
116–150	0.00–0.25	4.99×10^{-2}	1.0	1.0	1.4	0.0	0.1	-0.1	-0.4	0.0	0.1	0.2	0.6	-0.5	0.1	-0.3	-0.1	0.1	0.2	1.043
116–150	0.25–0.50	4.72×10^{-2}	1.0	1.1	1.5	-0.1	0.0	-0.1	-0.4	0.0	0.1	0.2	0.7	-0.5	0.1	-0.3	-0.1	0.1	0.2	1.044
116–150	0.50–0.75	4.40×10^{-2}	1.1	1.0	1.5	-0.1	0.0	-0.1	-0.4	0.0	0.1	0.1	0.7	-0.5	0.1	-0.3	-0.1	0.1	0.2	1.044
116–150	0.75–1.00	4.05×10^{-2}	1.1	0.9	1.4	-0.1	0.0	-0.1	-0.3	0.0	0.0	0.1	0.5	-0.4	0.1	-0.3	-0.1	0.1	0.3	1.045
116–150	1.00–1.25	3.59×10^{-2}	1.2	0.9	1.5	-0.1	0.0	-0.1	-0.3	0.0	0.0	0.2	0.5	-0.5	0.2	-0.4	-0.1	0.1	0.3	1.048
116–150	1.25–1.50	3.25×10^{-2}	1.3	0.9	1.5	-0.1	0.0	0.0	-0.3	0.0	0.0	0.1	0.4	-0.5	0.2	-0.4	-0.1	0.1	0.3	1.050
116–150	1.50–1.75	2.60×10^{-2}	1.4	1.0	1.8	-0.1	0.0	0.0	-0.2	0.0	0.0	0.2	0.4	-0.6	0.2	-0.4	-0.2	0.1	0.3	1.050
116–150	1.75–2.00	2.03×10^{-2}	1.7	1.1	2.0	-0.1	0.0	0.0	-0.3	0.0	0.0	0.1	0.5	-0.7	0.3	-0.4	-0.2	0.2	0.4	1.055
116–150	2.00–2.25	1.20×10^{-2}	2.2	1.4	2.6	-0.1	0.0	0.0	-0.3	0.0	0.0	0.2	0.5	-0.9	0.5	-0.5	-0.3	0.3	0.4	1.055
116–150	2.25–2.50	4.25×10^{-3}	4.0	2.2	4.5	-0.1	0.0	0.0	-0.3	0.0	0.0	0.2	0.6	-1.4	0.9	-0.8	-0.3	0.5	0.6	1.047
116–150	2.50–2.75	6.70×10^{-4}	11.4	5.3	12.5	-0.1	0.0	-0.1	-0.4	0.0	0.0	0.4	0.5	-3.6	2.4	-1.4	-0.8	1.8	1.7	1.044
150–200	0.00–0.25	1.08×10^{-2}	1.7	1.3	2.2	-0.1	0.1	-0.1	-0.7	0.0	0.1	0.1	0.7	-0.7	0.2	-0.6	-0.1	0.2	0.2	1.042
150–200	0.25–0.50	1.04×10^{-2}	1.8	1.3	2.2	-0.1	0.1	-0.1	-0.6	0.0	0.1	0.1	0.7	-0.6	0.2	-0.6	-0.2	0.2	0.2	1.042
150–200	0.50–0.75	9.63×10^{-3}	1.9	1.3	2.3	0.0	0.1	-0.1	-0.6	0.0	0.1	0.1	0.6	-0.7	0.2	-0.7	-0.2	0.2	0.2	1.043
150–200	0.75–1.00	9.38×10^{-3}	2.0	1.3	2.4	0.0	0.1	-0.1	-0.6	0.0	0.1	0.1	0.6	-0.6	0.2	-0.7	-0.2	0.2	0.3	1.044
150–200	1.00–1.25	8.24×10^{-3}	2.0	1.4	2.5	0.0	0.1	-0.1	-0.5	0.0	0.1	0.1	0.5	-0.7	0.2	-0.8	-0.2	0.3	0.3	1.046
150–200	1.25–1.50	7.14×10^{-3}	2.2	1.4	2.7	0.0	0.1	-0.1	-0.5	0.0	0.1	0.1	0.4	-0.8	0.3	-0.9	-0.3	0.3	0.3	1.049
150–200	1.50–1.75	6.21×10^{-3}	2.5	1.5	2.9	-0.1	0.0	-0.1	-0.4	0.0	0.1	0.1	0.3	-0.9	0.3	-1.0	-0.3	0.3	0.3	1.054
150–200	1.75–2.00	4.95×10^{-3}	2.9	1.9	3.4	-0.1	0.0	-0.1	-0.3	0.0	0.0	0.1	0.3	-1.2	0.5	-1.1	-0.5	0.5	0.4	1.058
150–200	2.00–2.25	3.74×10^{-3}	3.5	2.1	4.1	-0.1	0.0	-0.1	-0.3	0.0	0.0	0.2	0.3	-1.3	0.7	-1.3	-0.6	0.6	0.4	1.064
150–200	2.25–2.50	2.94×10^{-3}	4.0	2.5	4.8	-0.1	0.0	0.0	-0.3	0.0	0.0	0.1	0.3	-1.7	1.0	-1.2	-0.6	0.6	0.5	1.071
150–200	2.50–2.75	2.01×10^{-3}	5.1	2.9	5.9	-0.1	0.0	0.0	-0.3	0.0	0.0	0.1	0.4	-1.8	1.6	-1.2	-0.7	0.8	0.7	1.073
150–200	2.75–3.00	9.24×10^{-4}	8.0	4.9	9.4	-0.1	0.0	0.0	-0.4	0.0	0.0	0.6	0.7	-3.4	2.7	-1.4	-0.8	1.2	1.0	1.070
200–300	0.00–0.25	2.11×10^{-3}	2.8	1.8	3.3	-0.1	0.2	-0.2	-0.8	-0.1	0.2	0.1	1.1	-0.7	0.2	-0.7	-0.2	0.3	0.3	1.043
200–300	0.25–0.50	2.08×10^{-3}	2.9	1.9	3.4	-0.1	0.2	-0.2	-0.8	-0.1	0.2	0.1	1.2	-0.7	0.2	-0.8	-0.2	0.4	0.3	1.044
200–300	0.50–0.75	1.98×10^{-3}	3.0	1.9	3.6	-0.1	0.1	-0.2	-0.8	-0.1	0.2	0.1	1.1	-0.8	0.2	-0.9	-0.2	0.4	0.3	1.044
200–300	0.75–1.00	1.89×10^{-3}	3.1	1.9	3.6	-0.1	0.1	-0.2	-0.8	-0.1	0.2	0.1	1.0	-0.9	0.2	-0.9	-0.3	0.4	0.3	1.047
200–300	1.00–1.25	1.74×10^{-3}	3.1	1.8	3.6	-0.1	0.1	-0.2	-0.8	-0.1	0.2	0.1	0.8	-0.8	0.2	-1.0	-0.3	0.4	0.3	1.048
200–300	1.25–1.50	1.40×10^{-3}	3.6	2.2	4.2	-0.1	0.1	-0.2	-0.7	-0.1	0.2	0.1	0.7	-1.2	0.3	-1.3	-0.4	0.6	0.3	1.049
200–300	1.50–1.75	1.25×10^{-3}	3.9	2.2	4.5	-0.1	0.1	-0.1	-0.7	0.0	0.1	0.1	0.6	-1.1	0.4	-1.4	-0.4	0.6	0.4	1.057
200–300	1.75–2.00	1.02×10^{-3}	4.6	2.5	5.2	0.0	0.1	-0.1	-0.6	0.0	0.1	0.1	0.5	-1.2	0.5	-1.8	-0.6	0.8	0.4	1.060
200–300	2.00–2.25	9.44×10^{-4}	4.9	2.8	5.6	0.0	0.1	-0.1	-0.5	0.0	0.1	0.1	0.4	-1.5	0.7	-1.8	-0.7	0.9	0.5	1.068
200–300	2.25–2.50	6.59×10^{-4}	6.3	3.8	7.4	0.0	0.1	-0.1	-0.5	0.0	0.1	0.1	0.4	-2.2	1.2	-2.3	-1.1	1.3	0.6	1.078
200–300	2.50–2.75	5.75×10^{-4}	7.0	3.6	7.8	-0.1	0.0	-0.1	-0.4	0.0	0.1	0.2	0.4	-1.9	1.4	-2.1	-1.2	1.4	0.7	1.087
200–300	2.75–3.00	4.31×10^{-4}	8.5	5.2	10.0	-0.1	0.0	-0.1	-0.3	0.0	0.0	0.4	0.5	-3.5	2.4	-2.2	-1.5	1.7	1.0	1.110
300–500	0.00–0.50	2.60×10^{-4}	3.9	2.4	4.6	-0.1	0.2	-0.2	-0.8	-0.2	0.5	0.1	1.8	-0.7	0.2	-0.6	-0.2	0.5	0.3	1.048
300–500	0.50–1.00	2.28×10^{-4}	4.3	2.3	4.9	-0.1	0.2	-0.2	-0.8	-0.2	0.4	0.1	1.6	-0.9	0.2	-0.8	-0.3	0.6	0.3	1.048
300–500	1.00–1.50	2.18×10^{-4}	4.4	2.3	5.0	-0.1	0.2	-0.2	-0.8	-0.1	0.4	0.1	1.4	-0.9	0.3	-1.0	-0.4	0.7	0.3	1.057
300–500	1.50–2.00	1.64×10^{-4}	5.4	2.7	6.1	-0.1	0.2	-0.2	-0.8	-0.1	0.3	0.1	1.2	-1.4	0.4	-1.5	-0.5	0.9	0.4	1.064
300–500	2.00–2.50	1.04×10^{-4}	7.4	3.5	8.2	-0.1	0.1	-0.2	-0.8	-0.1	0.2	0.2	0.8	-1.7	0.8	-2.3	-0.8	1.4	0.6	1.082
300–500	2.50–3.00	5.21×10^{-5}	12.7	6.5	14.3	-0.1	0.1	-0.2	-0.7	-0.1	0.2	0.1	1.0	-3.2	2.3	-4.1	-2.2	2.9	0.8	1.107
500–1500	0.00–0.50	7.69×10^{-6}	9.8	3.1	10.3	-0.2	0.3	-0.2	-0.8	-0.3	1.3	0.1	2.4	-0.6	0.6	-0.2	-0.3	0.7	0.3	1.054
500–1500	0.50–1.00	8.74×10^{-6}	9.3	2.9	9.7	-0.2	0.3	-0.2	-0.8	-0.3	1.2	0.1	2.3	-0.3	0.4	-0.3	-0.3	0.8	0.3	1.058
500–1500	1.00–1.50	8.68×10^{-6}	9.3	2.7	9.7	-0.1	0.3	-0.2	-0.8	-0.2	1.0	0.0	2.2	-0.1	0.4	-0.4	-0.3	0.6	0.4	1.063
500–1500	1.50–2.00	6.99×10^{-6}	10.8	2.7	11.1	-0.1	0.2	-0.2	-0.8	-0.2	0.7	0.1	1.9	-1.1	0.6	-0.5	-0.5	0.7	0.4	1.078
500–1500	2.00–2.50	2.92×10^{-6}	19.2	4.1	19.6	-0.1	0.2	-0.2	-0.8	-0.2	0.5	0.2	1.7	-0.5	1.7	-1.6	-1.2	2.6	0.5	1.095
500–1500	2.50–3.00	1.90×10^{-6}	26.3	6.0	27.0	-0.1	0.2	-0.3	-0.8	-0.1	0.4	0.1	1.6	-0.9	3.0	-2.6	-1.9	3.9	1.2	1.120

Table 8: The electron channel Born-level double-differential cross section $\frac{d^2\sigma}{dm_{ee}d|\Delta\eta_{ee}|}$. The measurements are listed together with the statistical (δ^{stat}), systematic (δ^{sys}) and total (δ^{tot}) uncertainties. In addition the contributions from the individual correlated (cor) and uncorrelated (unc) systematic error sources are also provided consisting of the trigger efficiency (δ^{trig}), electron reconstruction efficiency (δ^{reco}), electron identification efficiency (δ^{id}), the isolation efficiency (δ^{iso}), the electron energy resolution (δ^{Eres}), the electron energy scale (δ^{Escal}), the multijet and $W+jets$ background ($\delta^{\text{mult.}}$), the top and diboson background normalisation ($\delta^{\text{top}}, \delta^{\text{diboson}}$), the top and diboson background MC statistical uncertainty (δ^{bgMC}), and the signal MC statistical uncertainty (δ^{MC}). The ratio of the dressed-level to Born-level predictions (k_{dressed}) is also provided. The luminosity uncertainty of 1.9% is not shown and not included in the overall systematic and total uncertainties.

$m_{\mu\mu}$ [GeV]	$\frac{d\sigma}{dm_{\mu\mu}}$ [pb/GeV]	δ^{stat} [%]	δ^{sys} [%]	δ^{tot} [%]	$\delta_{\text{cor}}^{\text{trig}}$ [%]	$\delta_{\text{cor}}^{\text{reco}}$ [%]	$\delta_{\text{cor}}^{\text{MSres}}$ [%]	$\delta_{\text{cor}}^{\text{IDres}}$ [%]	$\delta_{\text{cor}}^{\text{pT}}$ [%]	$\delta_{\text{cor}}^{\text{iso}}$ [%]	$\delta_{\text{cor}}^{\text{top}}$ [%]	$\delta_{\text{cor}}^{\text{diboson}}$ [%]	$\delta_{\text{cor}}^{\text{bgMC}}$ [%]	$\delta_{\text{cor}}^{\text{mult.}}$ [%]	$\delta_{\text{unc}}^{\text{mult.}}$ [%]	$\delta_{\text{unc}}^{\text{MC}}$ [%]	k_{dressed}
116 – 130	2.25×10^{-1}	0.5	0.6	0.8	-0.1	-0.4	-0.1	-0.1	-0.4	-0.1	-0.3	-0.1	0.0	0.0	0.1	0.1	1.055
130 – 150	1.04×10^{-1}	0.6	0.7	0.9	-0.1	-0.4	-0.1	0.0	-0.3	-0.1	-0.5	-0.1	0.1	0.0	0.1	0.1	1.047
150 – 175	4.94×10^{-2}	0.8	0.9	1.2	-0.1	-0.4	0.0	0.0	-0.2	-0.1	-0.7	-0.2	0.1	-0.1	0.1	0.1	1.043
175 – 200	2.51×10^{-2}	1.1	1.2	1.6	-0.1	-0.5	0.0	0.0	-0.2	-0.1	-1.0	-0.3	0.1	-0.1	0.2	0.1	1.040
200 – 230	1.37×10^{-2}	1.4	1.5	2.0	-0.1	-0.5	0.0	-0.1	-0.2	-0.1	-1.2	-0.4	0.2	-0.1	0.3	0.2	1.037
230 – 260	7.87×10^{-3}	1.8	1.6	2.5	-0.1	-0.5	0.0	0.1	-0.3	-0.1	-1.3	-0.4	0.3	-0.1	0.5	0.2	1.036
260 – 300	4.45×10^{-3}	2.1	1.7	2.7	-0.1	-0.6	0.0	-0.1	-0.2	-0.2	-1.4	-0.5	0.3	-0.1	0.5	0.2	1.037
300 – 380	1.90×10^{-3}	2.3	1.9	3.0	-0.1	-0.6	0.1	0.0	-0.3	-0.2	-1.4	-0.6	0.4	-0.2	0.7	0.2	1.035
380 – 500	6.40×10^{-4}	3.2	1.8	3.7	-0.1	-0.7	-0.1	-0.1	-0.2	-0.3	-1.2	-0.5	0.5	-0.1	0.8	0.2	1.037
500 – 700	1.54×10^{-4}	5.0	2.0	5.4	-0.1	-0.8	-0.1	0.0	-0.2	-0.4	-0.9	-0.5	0.6	-1.3	0.0	0.2	1.036
700 – 1000	2.66×10^{-5}	9.6	2.1	9.8	-0.1	-0.8	-0.5	-0.1	-0.4	-0.5	-0.5	-0.5	0.8	-1.3	0.0	0.4	1.040
1000 – 1500	2.17×10^{-6}	26.0	2.7	26.2	-0.1	-1.1	-0.1	-1.0	-0.3	-0.6	-0.4	-0.6	1.5	-1.4	0.0	0.4	1.043

Table 9: The muon channel Born-level single-differential cross section $\frac{d\sigma}{dm_{\mu\mu}}$. The measurements are listed together with the statistical (δ^{stat}), systematic (δ^{sys}) and total (δ^{tot}) uncertainties. In addition the contributions from the individual correlated (cor) and uncorrelated (unc) systematic error sources are also provided consisting of the trigger efficiency (δ^{trig}), muon reconstruction efficiency (δ^{reco}), the MS resolution (δ^{MSres}), the ID resolution (δ^{IDres}), the muon transverse momentum scale (δ^{pT}), the isolation efficiency (δ^{iso}), the top and diboson background normalisation ($\delta^{\text{top}}, \delta^{\text{diboson}}$), the top and diboson background MC statistical uncertainty (δ^{bgMC}), the multijet background ($\delta^{\text{mult.}}$) and the signal MC statistical uncertainty (δ^{MC}). The ratio of the dressed-level to Born-level predictions (k_{dressed}) is also provided. The luminosity uncertainty of 1.9% is not shown and not included in the overall systematic and total uncertainties.

$m_{\mu\mu}$ [GeV]	$ y_{\mu\mu} $	$\frac{d^2\sigma}{dm_{\mu\mu}dy_{\mu\mu}} [pb/GeV]$	δ^{stat} [%]	δ^{sys} [%]	δ^{tot} [%]	δ_{cor}^{trig} [%]	δ_{cor}^{reco} [%]	δ_{cor}^{MSres} [%]	δ_{cor}^{IDres} [%]	δ_{cor}^{pT} [%]	δ_{unc}^{iso} [%]	δ_{cor}^{top} [%]	$\delta_{cor}^{diboson}$ [%]	δ_{unc}^{bgMC} [%]	$\delta_{cor}^{mult.unc.}$ [%]	$\delta_{unc}^{mult.unc.}$ [%]	δ_{unc}^{MC} [%]	$k_{dressed}$
116 – 150	0.0 – 0.2	4.02×10^{-2}	1.1	0.8	1.4	-0.1	-0.4	-0.1	-0.1	-0.2	-0.1	-0.5	-0.1	0.1	-0.1	0.1	0.2	1.054
116 – 150	0.2 – 0.4	3.94×10^{-2}	1.1	0.8	1.4	-0.1	-0.4	-0.1	0.0	-0.3	-0.1	-0.5	-0.1	0.1	-0.1	0.1	0.2	1.052
116 – 150	0.4 – 0.6	3.90×10^{-2}	1.1	0.7	1.4	-0.1	-0.4	0.0	0.0	-0.3	-0.1	-0.5	-0.1	0.1	-0.1	0.1	0.2	1.054
116 – 150	0.6 – 0.8	3.97×10^{-2}	1.1	0.7	1.3	-0.1	-0.4	-0.2	0.0	-0.2	-0.1	-0.5	-0.1	0.1	0.0	0.1	0.2	1.054
116 – 150	0.8 – 1.0	3.94×10^{-2}	1.1	0.7	1.3	-0.1	-0.4	-0.1	-0.1	-0.3	-0.1	-0.4	-0.1	0.1	0.0	0.1	0.2	1.054
116 – 150	1.0 – 1.2	3.89×10^{-2}	1.1	0.7	1.3	-0.1	-0.3	-0.1	0.0	-0.3	-0.1	-0.3	-0.1	0.1	0.0	0.1	0.2	1.054
116 – 150	1.2 – 1.4	3.79×10^{-2}	1.1	0.7	1.3	-0.1	-0.4	-0.1	0.0	-0.4	-0.1	-0.2	-0.1	0.1	0.0	0.0	0.2	1.053
116 – 150	1.4 – 1.6	3.47×10^{-2}	1.1	0.7	1.3	-0.1	-0.4	0.1	-0.1	-0.4	-0.1	-0.2	-0.1	0.1	0.0	0.0	0.3	1.050
116 – 150	1.6 – 1.8	2.93×10^{-2}	1.3	0.7	1.4	-0.1	-0.4	0.0	-0.1	-0.4	-0.1	-0.1	-0.1	0.1	0.0	0.0	0.3	1.050
116 – 150	1.8 – 2.0	2.27×10^{-2}	1.5	0.8	1.7	-0.1	-0.5	0.1	-0.1	-0.5	-0.1	-0.1	-0.1	0.1	0.0	0.0	0.4	1.049
116 – 150	2.0 – 2.2	1.56×10^{-2}	1.9	1.0	2.1	-0.1	-0.6	-0.4	0.1	-0.5	-0.1	-0.1	-0.1	0.1	0.0	0.0	0.5	1.047
116 – 150	2.2 – 2.4	7.42×10^{-3}	3.3	1.7	3.7	-0.1	-0.7	-0.7	0.2	-0.9	-0.1	0.0	-0.1	0.2	0.0	0.0	1.0	1.045
150 – 200	0.0 – 0.2	1.01×10^{-2}	2.0	1.5	2.5	-0.1	-0.4	0.1	0.0	-0.2	-0.1	-1.3	-0.3	0.3	-0.1	0.2	0.2	1.045
150 – 200	0.2 – 0.4	1.01×10^{-2}	2.0	1.5	2.5	-0.1	-0.4	0.0	-0.1	-0.2	-0.1	-1.2	-0.3	0.3	-0.1	0.2	0.2	1.043
150 – 200	0.4 – 0.6	1.00×10^{-2}	2.0	1.4	2.4	-0.1	-0.4	-0.1	-0.1	-0.2	-0.1	-1.2	-0.3	0.3	-0.1	0.2	0.2	1.043
150 – 200	0.6 – 0.8	1.03×10^{-2}	1.9	1.2	2.3	-0.1	-0.4	-0.1	0.1	-0.2	-0.1	-1.0	-0.3	0.3	-0.1	0.1	0.2	1.044
150 – 200	0.8 – 1.0	9.95×10^{-3}	1.9	1.1	2.2	-0.1	-0.4	0.1	0.0	-0.1	-0.1	-0.9	-0.3	0.3	-0.1	0.1	0.2	1.044
150 – 200	1.0 – 1.2	9.52×10^{-3}	1.9	1.0	2.2	-0.1	-0.4	0.0	0.0	-0.2	-0.1	-0.7	-0.2	0.2	-0.1	0.1	0.2	1.041
150 – 200	1.2 – 1.4	8.91×10^{-3}	1.9	0.9	2.1	-0.1	-0.4	-0.1	0.0	-0.2	-0.1	-0.6	-0.3	0.2	-0.1	0.1	0.2	1.043
150 – 200	1.4 – 1.6	7.82×10^{-3}	2.1	0.8	2.2	-0.1	-0.5	0.1	-0.1	-0.3	-0.1	-0.4	-0.2	0.2	-0.1	0.0	0.3	1.040
150 – 200	1.6 – 1.8	6.54×10^{-3}	2.2	0.8	2.4	-0.1	-0.5	0.1	0.1	-0.3	-0.1	-0.3	-0.1	0.2	0.0	0.0	0.3	1.037
150 – 200	1.8 – 2.0	4.71×10^{-3}	2.7	0.8	2.8	-0.1	-0.6	-0.1	0.0	-0.3	-0.1	-0.2	-0.1	0.2	0.0	0.0	0.4	1.038
150 – 200	2.0 – 2.2	3.36×10^{-3}	3.3	1.0	3.5	-0.1	-0.6	-0.1	-0.1	-0.3	-0.1	-0.1	-0.1	0.2	0.0	0.0	0.5	1.041
150 – 200	2.2 – 2.4	1.74×10^{-3}	5.6	1.5	5.8	-0.1	-0.7	-0.2	0.3	-0.6	-0.1	-0.1	-0.1	0.3	0.0	0.0	1.1	1.038
200 – 300	0.0 – 0.2	2.43×10^{-3}	3.0	2.4	3.9	-0.1	-0.5	-0.2	-0.1	-0.2	-0.1	-2.1	-0.5	0.5	-0.2	0.5	0.2	1.038
200 – 300	0.2 – 0.4	2.37×10^{-3}	3.1	2.3	3.8	-0.1	-0.5	-0.1	-0.1	-0.2	-0.1	-2.0	-0.5	0.6	-0.2	0.4	0.2	1.040
200 – 300	0.4 – 0.6	2.32×10^{-3}	3.0	2.2	3.7	-0.1	-0.5	0.1	0.0	-0.2	-0.1	-1.9	-0.6	0.6	-0.2	0.4	0.3	1.037
200 – 300	0.6 – 0.8	2.38×10^{-3}	2.9	1.9	3.5	-0.1	-0.5	0.1	0.0	-0.2	-0.1	-1.6	-0.5	0.5	-0.1	0.3	0.3	1.037
200 – 300	0.8 – 1.0	2.24×10^{-3}	3.0	1.6	3.4	-0.1	-0.5	0.0	-0.1	-0.3	-0.1	-1.3	-0.4	0.5	-0.1	0.2	0.3	1.035
200 – 300	1.0 – 1.2	2.13×10^{-3}	3.0	1.3	3.2	-0.1	-0.5	0.0	-0.1	-0.2	-0.1	-1.0	-0.4	0.4	-0.1	0.1	0.3	1.037
200 – 300	1.2 – 1.4	1.88×10^{-3}	3.0	1.2	3.3	-0.1	-0.5	0.2	-0.1	-0.2	-0.1	-0.8	-0.3	0.4	-0.1	0.1	0.3	1.033
200 – 300	1.4 – 1.6	1.66×10^{-3}	3.2	1.0	3.3	-0.1	-0.5	-0.1	0.0	-0.2	-0.1	-0.5	-0.2	0.4	-0.1	0.0	0.3	1.034
200 – 300	1.6 – 1.8	1.33×10^{-3}	3.5	0.9	3.7	-0.1	-0.6	0.0	-0.1	-0.2	-0.1	-0.3	-0.2	0.4	0.0	0.0	0.4	1.035
200 – 300	1.8 – 2.0	9.97×10^{-4}	4.1	1.0	4.3	-0.1	-0.7	0.1	-0.1	-0.3	-0.1	-0.2	-0.2	0.4	0.0	0.0	0.5	1.036
200 – 300	2.0 – 2.2	5.87×10^{-4}	5.7	1.2	5.8	-0.1	-0.7	-0.1	-0.2	-0.5	-0.1	-0.1	-0.1	0.4	0.0	0.0	0.7	1.037
200 – 300	2.2 – 2.4	2.29×10^{-4}	10.9	2.1	11.1	-0.1	-0.9	-0.3	-0.3	-0.5	-0.1	-0.1	-0.1	0.8	0.0	0.0	1.6	1.040
300 – 500	0.0 – 0.4	3.72×10^{-4}	4.0	2.9	4.9	-0.1	-0.6	0.2	0.1	-0.2	-0.2	-2.2	-0.8	0.7	-0.5	1.2	0.2	1.036
300 – 500	0.4 – 0.8	3.28×10^{-4}	4.1	2.5	4.8	-0.1	-0.6	-0.2	-0.1	-0.3	-0.2	-1.9	-0.7	0.8	-0.4	0.7	0.2	1.036
300 – 500	0.8 – 1.2	3.09×10^{-4}	4.0	1.6	4.2	-0.1	-0.6	0.1	-0.1	-0.3	-0.2	-1.1	-0.5	0.6	-0.1	0.2	0.2	1.034
300 – 500	1.2 – 1.6	2.51×10^{-4}	4.1	1.1	4.2	-0.1	-0.6	0.0	0.1	-0.3	-0.2	-0.5	-0.3	0.5	-0.1	0.0	0.3	1.035
300 – 500	1.6 – 2.0	1.29×10^{-4}	5.7	1.2	5.8	-0.1	-0.8	-0.2	-0.1	-0.3	-0.2	-0.2	-0.3	0.6	0.0	0.0	0.4	1.040
300 – 500	2.0 – 2.4	3.93×10^{-5}	11.2	1.9	11.4	-0.1	-1.0	-0.3	-0.1	-0.5	-0.2	-0.1	-0.1	0.7	0.0	0.0	1.3	1.037
500 – 1500	0.0 – 0.4	1.46×10^{-5}	8.6	2.3	8.9	-0.1	-0.7	-0.1	0.1	-0.2	-0.4	-1.4	-0.8	1.1	-0.7	0.0	0.3	1.036
500 – 1500	0.4 – 0.8	1.29×10^{-5}	8.7	1.9	8.9	-0.1	-0.7	-0.2	-0.2	-0.2	-0.4	-1.0	-0.6	1.0	-0.4	0.0	0.3	1.036
500 – 1500	0.8 – 1.2	1.20×10^{-5}	8.5	1.4	8.6	-0.1	-0.8	-0.3	-0.2	-0.3	-0.4	-0.5	-0.3	0.7	-0.1	0.0	0.3	1.038
500 – 1500	1.2 – 1.6	8.06×10^{-6}	10.0	1.3	10.0	-0.1	-0.8	0.1	-0.1	-0.3	-0.4	-0.1	-0.2	0.6	0.0	0.0	0.4	1.038
500 – 1500	1.6 – 2.0	2.09×10^{-6}	19.5	2.1	19.6	-0.1	-1.1	-0.9	-0.5	-0.2	-0.4	-0.1	-0.1	0.5	0.0	0.0	1.3	1.042
500 – 1500	2.0 – 2.4	2.96×10^{-7}	45.3	12.1	46.9	-0.1	-2.0	-1.9	-2.7	-0.5	-0.4	0.0	-0.1	0.6	0.0	0.0	11.4	1.053

Table 10: The muon channel Born-level double-differential cross section $\frac{d^2\sigma}{dm_{\mu\mu}dy_{\mu\mu}}$. The measurements are listed together with the statistical (δ^{stat}), systematic (δ^{sys}) and total (δ^{tot}) uncertainties. In addition the contributions from the individual correlated (cor) and uncorrelated (unc) systematic error sources are also provided consisting of the trigger efficiency (δ^{trig}), muon reconstruction efficiency (δ^{reco}), the MS resolution (δ^{MSres}), the ID resolution (δ^{IDres}), the muon transverse momentum scale (δ^{pT}), the isolation efficiency (δ^{iso}), the top and diboson background normalisation (δ^{top} , $\delta^{diboson}$), the top and diboson background MC statistical uncertainty (δ^{bgMC}), the multijet background ($\delta^{mult.unc.}$) and the signal MC statistical uncertainty (δ^{MC}). The ratio of the dressed-level to Born-level predictions ($k_{dressed}$) is also provided. The luminosity uncertainty of 1.9% is not shown and not included in the overall systematic and total uncertainties.

$m_{\mu\mu}$ [GeV]	$ \Delta\eta_{\mu\mu} $	$\frac{d^2\sigma}{dm_{\mu\mu}d \Delta\eta_{\mu\mu} }$ [pb/GeV]	δ^{stat} [%]	δ^{sys} [%]	δ^{tot} [%]	$\delta_{\text{cor}}^{\text{trig}}$ [%]	$\delta_{\text{cor}}^{\text{reco}}$ [%]	$\delta_{\text{cor}}^{\text{MSres}}$ [%]	$\delta_{\text{cor}}^{\text{IDres}}$ [%]	$\delta_{\text{cor}}^{\text{pt}}$ [%]	$\delta_{\text{unc}}^{\text{iso}}$ [%]	$\delta_{\text{cor}}^{\text{top}}$ [%]	$\delta_{\text{cor}}^{\text{diboson}}$ [%]	$\delta_{\text{cor}}^{\text{bgMC}}$ [%]	$\delta_{\text{cor}}^{\text{mult.}}$ [%]	$\delta_{\text{unc}}^{\text{multi.}}$ [%]	$\delta_{\text{unc}}^{\text{MC}}$ [%]	k_{dressed}
116 – 150	0.00 – 0.25	4.89×10^{-2}	0.9	0.6	1.1	-0.1	-0.4	-0.1	-0.1	-0.3	-0.1	-0.3	-0.1	0.1	0.0	0.0	0.2	1.046
116 – 150	0.25 – 0.50	4.63×10^{-2}	0.9	0.6	1.1	-0.1	-0.4	-0.1	-0.1	-0.3	-0.1	-0.3	-0.1	0.1	0.0	0.0	0.2	1.047
116 – 150	0.50 – 0.75	4.43×10^{-2}	0.9	0.7	1.1	-0.1	-0.4	-0.1	0.0	-0.3	-0.1	-0.3	-0.1	0.1	0.0	0.0	0.2	1.047
116 – 150	0.75 – 1.00	4.00×10^{-2}	1.0	0.7	1.2	-0.1	-0.4	-0.1	-0.1	-0.4	-0.1	-0.3	-0.1	0.1	0.0	0.0	0.2	1.048
116 – 150	1.00 – 1.25	3.65×10^{-2}	1.0	0.7	1.2	-0.1	-0.4	-0.1	0.0	-0.3	-0.1	-0.3	-0.1	0.1	0.0	0.0	0.2	1.052
116 – 150	1.25 – 1.50	3.09×10^{-2}	1.1	0.7	1.3	-0.1	-0.4	0.0	-0.1	-0.3	-0.1	-0.4	-0.1	0.1	0.0	0.1	0.3	1.053
116 – 150	1.50 – 1.75	2.50×10^{-2}	1.3	0.8	1.5	-0.1	-0.4	-0.1	0.0	-0.4	-0.1	-0.4	-0.1	0.1	-0.1	0.1	0.3	1.057
116 – 150	1.75 – 2.00	2.02×10^{-2}	1.4	0.8	1.6	-0.1	-0.4	-0.1	-0.1	-0.4	-0.1	-0.4	-0.1	0.1	-0.1	0.1	0.3	1.067
116 – 150	2.00 – 2.25	1.12×10^{-2}	1.9	1.0	2.2	-0.1	-0.4	-0.1	-0.2	-0.4	-0.1	-0.6	-0.2	0.2	-0.1	0.2	0.4	1.079
116 – 150	2.25 – 2.50	3.75×10^{-3}	3.5	1.3	3.7	-0.1	-0.4	-0.1	-0.1	-0.2	-0.1	-0.9	-0.3	0.5	-0.3	0.2	0.6	1.088
116 – 150	2.50 – 2.75	5.93×10^{-4}	9.0	2.8	9.4	-0.1	-0.4	-0.4	-0.3	-0.2	-0.1	-1.6	-0.7	1.5	-0.3	0.4	1.3	1.099
150 – 200	0.00 – 0.25	1.09×10^{-2}	1.6	0.8	1.8	-0.1	-0.5	0.1	-0.1	-0.2	-0.1	-0.5	-0.1	0.2	0.0	0.0	0.2	1.037
150 – 200	0.25 – 0.50	1.03×10^{-2}	1.6	0.8	1.8	-0.1	-0.5	0.0	0.0	-0.2	-0.1	-0.6	-0.1	0.2	0.0	0.0	0.2	1.037
150 – 200	0.50 – 0.75	9.38×10^{-3}	1.7	0.9	1.9	-0.1	-0.4	0.0	0.0	-0.2	-0.1	-0.6	-0.2	0.2	0.0	0.0	0.2	1.037
150 – 200	0.75 – 1.00	8.88×10^{-3}	1.8	0.9	2.0	-0.1	-0.4	-0.1	0.0	-0.2	-0.1	-0.7	-0.2	0.2	-0.1	0.1	0.2	1.038
150 – 200	1.00 – 1.25	7.79×10^{-3}	1.9	1.1	2.2	-0.1	-0.4	0.0	0.0	-0.2	-0.1	-0.8	-0.2	0.2	-0.1	0.1	0.2	1.040
150 – 200	1.25 – 1.50	6.86×10^{-3}	2.1	1.2	2.4	-0.1	-0.5	0.0	-0.1	-0.2	-0.1	-0.9	-0.3	0.3	-0.1	0.1	0.3	1.041
150 – 200	1.50 – 1.75	5.90×10^{-3}	2.3	1.3	2.6	-0.1	-0.5	0.0	0.0	-0.2	-0.1	-1.0	-0.3	0.3	-0.1	0.1	0.3	1.043
150 – 200	1.75 – 2.00	4.89×10^{-3}	2.6	1.5	3.0	-0.1	-0.5	0.0	0.1	-0.2	-0.1	-1.2	-0.4	0.4	-0.1	0.2	0.3	1.046
150 – 200	2.00 – 2.25	3.77×10^{-3}	3.0	1.7	3.4	-0.1	-0.5	0.0	-0.1	-0.3	-0.1	-1.3	-0.4	0.5	-0.2	0.3	0.4	1.050
150 – 200	2.25 – 2.50	2.91×10^{-3}	3.4	1.8	3.8	-0.1	-0.5	0.1	0.1	-0.2	-0.1	-1.3	-0.6	0.6	-0.3	0.4	0.4	1.057
150 – 200	2.50 – 2.75	1.95×10^{-3}	4.0	1.8	4.4	-0.1	-0.4	0.1	0.0	-0.2	-0.1	-1.3	-0.6	0.7	-0.3	0.5	0.5	1.064
150 – 200	2.75 – 3.00	7.89×10^{-4}	6.7	2.8	7.2	-0.1	-0.5	-0.1	0.0	-0.3	-0.1	-1.7	-1.1	1.3	-0.4	0.8	0.9	1.086
200 – 300	0.00 – 0.25	2.22×10^{-3}	2.5	1.0	2.7	-0.1	-0.5	-0.1	-0.1	-0.2	-0.1	-0.6	-0.1	0.3	0.0	0.0	0.2	1.032
200 – 300	0.25 – 0.50	2.11×10^{-3}	2.6	1.0	2.7	-0.1	-0.5	0.0	0.0	-0.2	-0.1	-0.7	-0.1	0.3	0.0	0.0	0.2	1.033
200 – 300	0.50 – 0.75	1.97×10^{-3}	2.7	1.1	2.9	-0.1	-0.5	0.0	-0.1	-0.2	-0.1	-0.8	-0.2	0.3	-0.1	0.1	0.2	1.033
200 – 300	0.75 – 1.00	1.91×10^{-3}	2.8	1.2	3.0	-0.1	-0.5	0.1	-0.1	-0.2	-0.1	-0.9	-0.2	0.4	-0.1	0.1	0.3	1.036
200 – 300	1.00 – 1.25	1.62×10^{-3}	3.1	1.4	3.4	-0.1	-0.5	0.0	0.0	-0.2	-0.1	-1.1	-0.3	0.5	0.0	0.1	0.3	1.035
200 – 300	1.25 – 1.50	1.47×10^{-3}	3.3	1.6	3.7	-0.1	-0.5	-0.1	0.1	-0.2	-0.1	-1.3	-0.3	0.5	-0.1	0.1	0.3	1.035
200 – 300	1.50 – 1.75	1.27×10^{-3}	3.6	1.9	4.1	-0.1	-0.6	0.0	-0.1	-0.1	-0.1	-1.6	-0.5	0.6	-0.2	0.2	0.3	1.036
200 – 300	1.75 – 2.00	1.07×10^{-3}	4.1	2.3	4.7	-0.1	-0.6	-0.2	-0.1	-0.2	-0.1	-1.9	-0.7	0.8	-0.1	0.2	0.3	1.038
200 – 300	2.00 – 2.25	8.77×10^{-4}	4.6	2.5	5.3	-0.1	-0.6	-0.1	-0.1	-0.2	-0.1	-2.1	-0.7	0.8	-0.2	0.4	0.4	1.038
200 – 300	2.25 – 2.50	6.30×10^{-4}	5.6	3.3	6.5	-0.2	-0.6	-0.1	0.1	-0.3	-0.1	-2.7	-0.9	1.1	-0.5	0.6	0.4	1.041
200 – 300	2.50 – 2.75	4.91×10^{-4}	6.5	3.8	7.6	-0.2	-0.6	-0.1	-0.1	-0.3	-0.1	-2.9	-1.4	1.5	-0.6	0.9	0.4	1.046
200 – 300	2.75 – 3.00	3.71×10^{-4}	7.6	4.1	8.6	-0.1	-0.6	-0.1	0.1	-0.3	-0.1	-3.0	-1.4	1.7	-0.6	1.3	0.5	1.054
300 – 500	0.00 – 0.50	2.67×10^{-4}	3.6	1.1	3.7	-0.1	-0.6	-0.1	0.1	-0.2	-0.2	-0.6	-0.2	0.4	-0.2	0.1	0.2	1.034
300 – 500	0.50 – 1.00	2.66×10^{-4}	3.6	1.1	3.8	-0.1	-0.6	-0.1	0.0	-0.2	-0.2	-0.6	-0.2	0.4	0.0	0.0	0.2	1.033
300 – 500	1.00 – 1.50	2.14×10^{-4}	4.2	1.4	4.5	-0.1	-0.6	0.0	0.0	-0.2	-0.2	-1.0	-0.3	0.6	-0.1	0.1	0.3	1.035
300 – 500	1.50 – 2.00	1.71×10^{-4}	5.0	2.1	5.4	-0.1	-0.6	0.3	0.1	-0.3	-0.2	-1.6	-0.5	0.8	-0.3	0.2	0.3	1.036
300 – 500	2.00 – 2.50	9.59×10^{-5}	7.3	3.6	8.2	-0.2	-0.7	-0.1	0.0	-0.3	-0.2	-2.8	-1.1	1.5	-0.6	0.8	0.4	1.038
300 – 500	2.50 – 3.00	6.75×10^{-5}	9.0	4.6	10.1	-0.2	-0.7	0.1	-0.1	-0.5	-0.2	-3.5	-1.3	2.0	-0.7	1.5	0.4	1.041
500 – 1500	0.00 – 0.50	8.20×10^{-6}	9.0	1.2	9.1	-0.1	-0.8	-0.3	-0.1	-0.2	-0.5	-0.3	-0.2	0.5	-0.1	0.0	0.4	1.035
500 – 1500	0.50 – 1.00	8.57×10^{-6}	8.8	1.2	8.9	-0.1	-0.8	0.0	-0.2	-0.2	-0.5	-0.3	-0.2	0.5	0.0	0.0	0.4	1.035
500 – 1500	1.00 – 1.50	7.05×10^{-6}	10.0	1.5	10.1	-0.1	-0.8	-0.1	-0.1	-0.2	-0.4	-0.5	-0.3	0.9	-0.1	0.0	0.3	1.036
500 – 1500	1.50 – 2.00	6.85×10^{-6}	10.4	1.6	10.5	-0.1	-0.7	-0.3	0.0	-0.3	-0.4	-0.7	-0.3	1.0	-0.1	0.0	0.4	1.037
500 – 1500	2.00 – 2.50	4.92×10^{-6}	12.7	2.3	12.9	-0.1	-0.8	-0.2	-0.2	-0.2	-0.3	-1.0	-0.6	1.6	-0.3	0.0	0.5	1.042
500 – 1500	2.50 – 3.00	2.80×10^{-6}	17.9	3.7	18.3	-0.1	-0.8	-0.3	0.2	-0.4	-0.3	-1.9	-1.1	2.5	-0.8	0.0	0.7	1.040

Table 11: the muon channel Born-level double-differential cross section $\frac{d^2\sigma}{dm_{\mu\mu}d|\Delta\eta_{\mu\mu}|}$. The measurements are listed together with the statistical (δ^{stat}), systematic (δ^{sys}) and total (δ^{tot}) uncertainties. In addition the contributions from the individual correlated (cor) and uncorrelated (unc) systematic error sources are also provided consisting of the trigger efficiency (δ^{trig}), muon reconstruction efficiency (δ^{reco}), the MS resolution (δ^{MSres}), the ID resolution (δ^{IDres}), the muon transverse momentum scale (δ^{pt}), the isolation efficiency (δ^{iso}), the top and diboson background normalisation ($\delta^{\text{top}}, \delta^{\text{diboson}}$), the top and diboson background MC statistical uncertainty (δ^{bgMC}), the multijet background ($\delta^{\text{mult.}}$) and the signal MC statistical uncertainty (δ^{MC}). The ratio of the dressed-level to Born-level predictions (k_{dressed}) is also provided. The luminosity uncertainty of 1.9% is not shown and not included in the overall systematic and total uncertainties.

References

- [1] S. D. Drell and T.-M. Yan,
Massive Lepton-Pair Production in Hadron-Hadron Collisions at High Energies,
Phys. Rev. Lett. **25** (1970) 316.
- [2] R. Hamberg, W. L. van Neerven and T. Matsuura,
A Complete calculation of the order α_s^2 correction to the Drell–Yan K factor,
Nucl. Phys. B **359** (1991) 343.
- [3] S. Catani et al., *Vector boson production at hadron colliders: a fully exclusive QCD calculation at next-to-next-to-leading order*, *Phys. Rev. Lett.* **103** (2009) 082001, arXiv:[0903.2120 \[hep-ph\]](#).
- [4] S. Catani and M. Grazzini, *Next-to-next-to-leading order subtraction formalism in hadron collisions and its application to Higgs boson production at the LHC*,
Phys. Rev. Lett. **98** (2007) 222002, arXiv:[hep-ph/0703012 \[hep-ph\]](#).
- [5] Y. Li and F. Petriello, *Combining QCD and electroweak corrections to dilepton production in the framework of the FEWZ simulation code*, *Phys. Rev. D* **86** (2012) 094034, arXiv:[1208.5967 \[hep-ph\]](#).
- [6] ATLAS Collaboration, *Measurement of the inclusive W^\pm and Z/γ^* cross sections in the e and μ decay channels in pp collisions at $\sqrt{s} = 7$ TeV with the ATLAS detector*,
Phys. Rev. D **85** (2012) 072004, arXiv:[1109.5141 \[hep-ex\]](#).
- [7] ATLAS Collaboration, *Measurement of the high-mass Drell-Yan differential cross-section in pp collisions at $\sqrt{s} = 7$ TeV with the ATLAS detector*, *Phys. Lett. B* **725** (2013) 223, arXiv:[1305.4192 \[hep-ex\]](#).
- [8] ATLAS Collaboration, *Measurement of the low-mass Drell-Yan differential cross section at $\sqrt{s} = 7$ TeV using the ATLAS detector*, *JHEP* **1406** (2014) 112, arXiv:[1404.1212 \[hep-ex\]](#).
- [9] CMS Collaboration, *Measurement of the inclusive W and Z production cross sections in pp collisions at $\sqrt{s} = 7$ TeV with the CMS experiment*, *JHEP* **1110** (2011) 132, arXiv:[1107.4789 \[hep-ex\]](#).
- [10] CMS Collaboration, *Measurement of the Drell-Yan Cross Section in pp Collisions at $\sqrt{s} = 7$ TeV*, *JHEP* **1110** (2011) 007, arXiv:[1108.0566 \[hep-ex\]](#).
- [11] CMS Collaboration, *Measurement of the differential and double-differential Drell-Yan cross sections in proton–proton collisions at $\sqrt{s} = 7$ TeV*, *JHEP* **1312** (2013) 030, arXiv:[1310.7291 \[hep-ex\]](#).
- [12] CMS Collaboration, *Measurements of differential and double-differential Drell-Yan cross sections in proton–proton collisions at 8 TeV*, *Eur. Phys. J. C* **75** (2015) 147, arXiv:[1412.1115 \[hep-ex\]](#).
- [13] LHCb Collaboration, R. Aaij et al.,
Inclusive W and Z production in the forward region at $\sqrt{s} = 7$ TeV, *JHEP* **1206** (2012) 058, arXiv:[1204.1620 \[hep-ex\]](#).
- [14] LHCb Collaboration, R. Aaij et al.,
Measurement of the cross-section for $Z \rightarrow e^+ e^-$ production in pp collisions at $\sqrt{s} = 7$ TeV, *JHEP* **1302** (2013) 106, arXiv:[1212.4620 \[hep-ex\]](#).
- [15] LHCb Collaboration, R. Aaij et al.,
Measurement of forward $Z \rightarrow e^+ e^-$ production at $\sqrt{s} = 8$ TeV, *JHEP* **1505** (2015) 109, arXiv:[1503.00963 \[hep-ex\]](#).

- [16] LHCb Collaboration, R. Aaij et al.,
Measurement of the forward Z boson production cross-section in pp collisions at $\sqrt{s} = 7$ TeV, **JHEP 1508** (2015) 039, arXiv:[1505.07024 \[hep-ex\]](#).
- [17] LHCb Collaboration, R. Aaij et al.,
Measurement of forward W and Z boson production in pp collisions at $\sqrt{s} = 8$ TeV, **JHEP 1601** (2016) 155, arXiv:[1511.08039 \[hep-ex\]](#).
- [18] S. Dulat et al., *The CT14 Global Analysis of Quantum Chromodynamics*, **Phys. Rev. D 93** (2015) 033006, arXiv:[1506.07443 \[hep-ph\]](#).
- [19] NNPDF Collaboration, R. D. Ball et al., *Parton distributions for the LHC Run II*, **JHEP 04** (2015) 040, arXiv:[1410.8849 \[hep-ph\]](#).
- [20] L. A. Harland-Lang et al., *Parton distributions in the LHC era: MMHT 2014 PDFs*, **Eur. Phys. J. C 75** (2015) 204, arXiv:[1412.3989 \[hep-ph\]](#).
- [21] A. D. Martin et al., *Parton distributions incorporating QED contributions*, **Eur. Phys. J. C 39** (2005) 155, arXiv:[hep-ph/0411040 \[hep-ph\]](#).
- [22] NNPDF Collaboration, R. D. Ball et al., *Parton distributions with QED corrections*, **Nucl. Phys. B 877** (2013) 290, arXiv:[1308.0598 \[hep-ph\]](#).
- [23] D. S. M. Alves et al., *Running Electroweak Couplings as a Probe of New Physics*, **JHEP 1502** (2015) 007, arXiv:[1410.6810 \[hep-ph\]](#).
- [24] CMS Collaboration, *Search for physics beyond the standard model in dilepton mass spectra in proton–proton collisions at $\sqrt{s} = 8$ TeV*, **JHEP 1504** (2015) 025, arXiv:[1412.6302 \[hep-ex\]](#).
- [25] ATLAS Collaboration, *Search for high-mass dilepton resonances in pp collisions at $\sqrt{s} = 8$ TeV with the ATLAS detector*, **Phys. Rev. D 90** (2014) 052005, arXiv:[1405.4123 \[hep-ex\]](#).
- [26] ATLAS Collaboration, *Search for contact interactions and large extra dimensions in the dilepton channel using proton–proton collisions at $\sqrt{s} = 8$ TeV with the ATLAS detector*, **Eur. Phys. J. C 74** (2014) 3134, arXiv:[1407.2410 \[hep-ex\]](#).
- [27] R. Boughezal, Y. Li and F. Petriello, *Disentangling radiative corrections using the high-mass Drell-Yan process at the LHC*, **Phys. Rev. D 89** (2014) 034030, arXiv:[1312.3972 \[hep-ph\]](#).
- [28] ATLAS Collaboration, *The ATLAS Experiment at the CERN Large Hadron Collider*, **JINST 3** (2008) S08003.
- [29] ATLAS Collaboration, *Performance of the ATLAS Trigger System in 2010*, **Eur. Phys. J. C 72** (2012) 1849, arXiv:[1110.1530 \[hep-ex\]](#).
- [30] P. Nason, *A New method for combining NLO QCD with shower Monte Carlo algorithms*, **JHEP 0411** (2004) 040, arXiv:[hep-ph/0409146 \[hep-ph\]](#).
- [31] S. Frixione, P. Nason and C. Oleari, *Matching NLO QCD computations with Parton Shower simulations: the POWHEG method*, **JHEP 0711** (2007) 070, arXiv:[0709.2092 \[hep-ph\]](#).
- [32] S. Alioli et al., *NLO vector-boson production matched with shower in POWHEG*, **JHEP 0807** (2008) 060, arXiv:[0805.4802 \[hep-ph\]](#).
- [33] S. Alioli, P. Nason, C. Oleari, and E. Re, *A general framework for implementing NLO calculations in shower Monte Carlo programs: the POWHEG BOX*, **JHEP 1006** (2010) 043, arXiv:[1002.2581 \[hep-ph\]](#).

- [34] H.-L. Lai et al., *New parton distributions for collider physics*, Phys. Rev. D **82** (2010) 074024, arXiv:[1007.2241 \[hep-ph\]](#).
- [35] T. Sjöstrand, S. Mrenna and P. Z. Skands, *A Brief Introduction to PYTHIA 8.1*, Comput. Phys. Commun. **178** (2008) 852, arXiv:[0710.3820 \[hep-ph\]](#).
- [36] S. Frixione and B. R. Webber, *Matching NLO QCD computations and parton shower simulations*, JHEP **0206** (2002) 029, arXiv:[hep-ph/0204244 \[hep-ph\]](#).
- [37] S. Frixione, P. Nason and B. R. Webber, *Matching NLO QCD and parton showers in heavy flavor production*, JHEP **0308** (2003) 007, arXiv:[hep-ph/0305252 \[hep-ph\]](#).
- [38] S. Frixione et al., *Single-top hadroproduction in association with a W boson*, JHEP **0807** (2008) 029, arXiv:[0805.3067 \[hep-ph\]](#).
- [39] M. Bahr et al., *Herwig++ Physics and Manual*, Eur. Phys. J. C **58** (2008) 639, arXiv:[0803.0883 \[hep-ph\]](#).
- [40] K. Melnikov and F. Petriello, *Electroweak gauge boson production at hadron colliders through $O(\alpha_s^2)$* , Phys. Rev. D **74** (2006) 114017, arXiv:[hep-ph/0609070 \[hep-ph\]](#).
- [41] R. Gavin et al., *FEWZ 2.0: A code for hadronic Z production at next-to-next-to-leading order*, Comput. Phys. Commun. **182** (2011) 2388, arXiv:[1011.3540 \[hep-ph\]](#).
- [42] A. D. Martin et al., *Parton distributions for the LHC*, Eur. Phys. J. C **63** (2009) 189, arXiv:[0901.0002 \[hep-ph\]](#).
- [43] D. Bardin et al., *SANC integrator in the progress: QCD and EW contributions*, JETP Lett. **96** (2012) 285, arXiv:[1207.4400 \[hep-ph\]](#).
- [44] S. G. Bondarenko and A. A. Sapronov, *NLO EW and QCD proton-proton cross section calculations with mcsanc-v1.01*, Comput. Phys. Commun. **184** (2013) 2343, arXiv:[1301.3687 \[hep-ph\]](#).
- [45] T. Sjöstrand, S. Mrenna and P. Z. Skands, *PYTHIA 6.4 Physics and Manual*, JHEP **0605** (2006) 026, arXiv:[hep-ph/0603175 \[hep-ph\]](#).
- [46] G. Corcella et al., *HERWIG 6: An Event generator for hadron emission reactions with interfering gluons (including supersymmetric processes)*, JHEP **0101** (2001) 010, arXiv:[hep-ph/0011363 \[hep-ph\]](#).
- [47] G. Corcella et al., *HERWIG 6.5 release note*, (2002), arXiv:[hep-ph/0210213 \[hep-ph\]](#).
- [48] M Cacciari et al., *Top-pair production at hadron colliders with next-to-next-to-leading logarithmic soft-gluon resummation*, Phys. Lett. B **710** (2012) 612, arXiv:[1111.5869 \[hep-ph\]](#).
- [49] P. Bärnreuther, M. Czakon and A. Mitov, *Percent level precision physics at the Tevatron: next-to-next-to-leading order QCD corrections to $q\bar{q} \rightarrow t\bar{t} + X$* , Phys. Rev. Lett. **109** (2012) 132001, arXiv:[1204.5201 \[hep-ph\]](#).
- [50] M. Czakon and A. Mitov, *NNLO corrections to top-pair production at hadron colliders: the all-fermionic scattering channels*, JHEP **1212** (2012) 054, arXiv:[1207.0236 \[hep-ph\]](#).
- [51] M. Czakon and A. Mitov, *NNLO corrections to top pair production at hadron colliders: the quark-gluon reaction*, JHEP **1301** (2013) 080, arXiv:[1210.6832 \[hep-ph\]](#).

- [52] M. Czakon, P. Fiedler and A. Mitov,
The total top quark pair production cross-section at hadron colliders through $O(\alpha_S^4)$,
Phys. Rev. Lett. **110** (2013) 252004, arXiv:1303.6254 [hep-ph].
- [53] M. Czakon and A. Mitov,
Top++: A Program for the Calculation of the Top-Pair Cross-Section at Hadron Colliders,
Comput. Phys. Commun. **185** (2014) 2930, arXiv:1112.5675 [hep-ph].
- [54] M. Botje et al., *The PDF4LHC Working Group Interim Recommendations*, (2011),
arXiv:1101.0538 [hep-ph].
- [55] A. D. Martin et al., *Uncertainties on α_S in global PDF analyses and implications for predicted hadronic cross sections*, *Eur. Phys. J. C* **64** (2009) 653, arXiv:0905.3531 [hep-ph].
- [56] J. Gao et al., *CT10 next-to-next-to-leading order global analysis of QCD*,
Phys. Rev. D **89** (2014) 033009, arXiv:1302.6246 [hep-ph].
- [57] NNPDF Collaboration, R. D. Ball et al., *Parton distributions with LHC data*,
Nucl. Phys. B **867** (2013) 244, arXiv:1207.1303 [hep-ph].
- [58] N. Kidonakis,
Two-loop soft anomalous dimensions for single top quark associated production with a W^- or H^- ,
Phys. Rev. D **82** (2010) 054018, arXiv:1005.4451 [hep-ph].
- [59] J. Pumplin et al.,
New generation of parton distributions with uncertainties from global QCD analysis,
JHEP **0207** (2002) 012, arXiv:hep-ph/0201195 [hep-ph].
- [60] J. M. Campbell and R. K. Ellis, *An Update on vector boson pair production at hadron colliders*,
Phys. Rev. D **60** (1999) 113006, arXiv:hep-ph/9905386 [hep-ph].
- [61] J. M. Campbell, R. K. Ellis and C. Williams, *Vector boson pair production at the LHC*,
JHEP **1107** (2011) 018, arXiv:1105.0020 [hep-ph].
- [62] ATLAS Collaboration,
Observation and measurement of Higgs boson decays to WW^ with the ATLAS detector*,
Phys. Rev. D **92** (2015) 012006, arXiv:1412.2641 [hep-ex].
- [63] ATLAS Collaboration,
Measurement of total and differential W^+W^- production cross sections in proton-proton collisions at $\sqrt{s} = 8$ TeV with the ATLAS detector and limits on anomalous triple-gauge-boson couplings,
(2016), arXiv:1603.01702 [hep-ex].
- [64] P. Golonka and Z. Was,
PHOTOS Monte Carlo: A Precision tool for QED corrections in Z and W decays,
Eur. Phys. J. C **45** (2006) 97, arXiv:hep-ph/0506026 [hep-ph].
- [65] ATLAS Collaboration, *The ATLAS Simulation Infrastructure*, *Eur. Phys. J. C* **70** (2010) 823,
arXiv:1005.4568 [hep-ex].
- [66] GEANT4 Collaboration, S. Agostinelli et al., *GEANT4: A simulation toolkit*,
Nucl. Instrum. Meth. A **506** (2003) 250.
- [67] ATLAS Collaboration, *Summary of ATLAS Pythia 8 tunes*, ATL-PHYS-PUB-2012-003, 2012,
URL: <http://cds.cern.ch/record/1474107>.
- [68] R. Corke and T. Sjöstrand, *Interleaved Parton Showers and Tuning Prospects*,
JHEP **1103** (2011) 032, arXiv:1011.1759 [hep-ph].

- [69] ATLAS Collaboration, *New ATLAS event generator tunes to 2010 data*, ATL-PHYS-PUB-2011-008, 2011, URL: <http://cds.cern.ch/record/1345343>.
- [70] ATLAS Collaboration, *Electron and photon energy calibration with the ATLAS detector using LHC Run 1 data*, Eur. Phys. J. C **74** (2014) 3071, arXiv:1407.5063 [hep-ex].
- [71] ATLAS Collaboration, *Electron reconstruction and identification efficiency measurements with the ATLAS detector using the 2011 LHC proton–proton collision data*, Eur. Phys. J. C **74** (2014) 2941, arXiv:1404.2240 [hep-ex].
- [72] ATLAS Collaboration, *Electron efficiency measurements with the ATLAS detector using the 2012 LHC proton–proton collision data*, ATLAS-CONF-2014-032, 2014, URL: <http://cdsweb.cern.ch/record/1706245>.
- [73] ATLAS Collaboration, *Measurement of the muon reconstruction performance of the ATLAS detector using 2011 and 2012 LHC proton–proton collision data*, Eur. Phys. J. C **74** (2014) 3130, arXiv:1407.3935 [hep-ex].
- [74] ATLAS Collaboration, *Performance of Missing Transverse Momentum Reconstruction in ATLAS studied in Proton–Proton Collisions recorded in 2012 at $\sqrt{s} = 8$ TeV*, ATLAS-CONF-2013-082, 2013, URL: <http://cdsweb.cern.ch/record/1570993>.
- [75] ATLAS Collaboration, *Performance of the ATLAS muon trigger in pp collisions at $\sqrt{s} = 8$ TeV*, Eur. Phys. J. C **75** (2015) 120, arXiv:1408.3179 [hep-ex].
- [76] ATLAS Collaboration, *Improved luminosity determination in pp collisions at $\sqrt{s} = 7$ TeV using the ATLAS detector at the LHC*, Eur. Phys. J. C **73** (2013) 2518, arXiv:1302.4393 [hep-ex].
- [77] G. D’Agostini, *A Multidimensional unfolding method based on Bayes’ theorem*, Nucl. Instrum. Meth. A **362** (1995) 487.
- [78] T. Adye, *Unfolding algorithms and tests using RooUnfold*, (2011) 313–318, arXiv:1105.1160 [physics.data-an].
- [79] A. Glazov, *Averaging of DIS cross section data*, AIP Conf. Proc. **792** (2005) 237.
- [80] H1 Collaboration, F. D. Aaron et al., *Measurement of the Inclusive ep Scattering Cross Section at Low Q^2 and x at HERA*, Eur. Phys. J. C **63** (2009) 625, arXiv:0904.0929 [hep-ex].
- [81] H1 and ZEUS Collaborations, F. D. Aaron et al., *Combined Measurement and QCD Analysis of the Inclusive $e^\pm p$ Scattering Cross Sections at HERA*, JHEP **1001** (2010) 109, arXiv:0911.0884 [hep-ex].
- [82] S. Dittmaier and M. Huber, *Radiative corrections to the neutral-current Drell-Yan process in the Standard Model and its minimal supersymmetric extension*, JHEP **1001** (2010) 060, arXiv:0911.2329 [hep-ph].
- [83] H1 and ZEUS Collaborations, H. Abramowicz et al., *Combination of measurements of inclusive deep inelastic $e^\pm p$ scattering cross sections and QCD analysis of HERA data*, Eur. Phys. J. C **75** (2015) 580, arXiv:1506.06042 [hep-ex].
- [84] S. Alekhin, J. Blumlein and S. Moch, *The ABM parton distributions tuned to LHC data*, Phys. Rev. D **89** (2014) 054028, arXiv:1310.3059 [hep-ph].
- [85] S. Alekhin et al., *HERAFitter Open source QCD fit project*, Eur. Phys. J. C **75** (2015) 304, arXiv:1410.4412 [hep-ph].

- [86] W. T. Giele and S. Keller,
Implications of hadron collider observables on parton distribution function uncertainties,
Phys. Rev. D **58** (1998) 094023, arXiv:[hep-ph/9803393 \[hep-ph\]](#).
- [87] NNPDF Collaboration, R. D. Ball et al., *Reweighting NNPDFs: the W lepton asymmetry*,
Nucl. Phys. B **849** (2011), [Erratum: Nucl. Phys.B855,927(2012)], arXiv:[1012.0836 \[hep-ph\]](#).
- [88] NNPDF Collaboration, R. D. Ball et al.,
Reweighting and Unweighting of Parton Distributions and the LHC W lepton asymmetry data,
Nucl. Phys. B **855** (2012), arXiv:[1108.1758 \[hep-ph\]](#).
- [89] C. Schmidt et al., *CT14QED PDFs from Isolated Photon Production in Deep Inelastic Scattering*,
(2015), arXiv:[1509.02905 \[hep-ph\]](#).

The ATLAS Collaboration

G. Aad⁸⁷, B. Abbott¹¹⁴, J. Abdallah⁶⁵, O. Abdinov¹², B. Abelsoos¹¹⁸, R. Aben¹⁰⁸, O.S. AbouZeid¹³⁸, N.L. Abraham¹⁵⁰, H. Abramowicz¹⁵⁴, H. Abreu¹⁵³, R. Abreu¹¹⁷, Y. Abulaiti^{147a,147b}, B.S. Acharya^{164a,164b,^a}, L. Adamczyk^{40a}, D.L. Adams²⁷, J. Adelman¹⁰⁹, S. Adomeit¹⁰¹, T. Adye¹³², A.A. Affolder⁷⁶, T. Agatonovic-Jovin¹⁴, J. Agricola⁵⁶, J.A. Aguilar-Saavedra^{127a,127f}, S.P. Ahlen²⁴, F. Ahmadov^{67,b}, G. Aielli^{134a,134b}, H. Akerstedt^{147a,147b}, T.P.A. Åkesson⁸³, A.V. Akimov⁹⁷, G.L. Alberghi^{22a,22b}, J. Albert¹⁶⁹, S. Albrand⁵⁷, M.J. Alconada Verzini⁷³, M. Alekса³², I.N. Aleksandrov⁶⁷, C. Alexa^{28b}, G. Alexander¹⁵⁴, T. Alexopoulos¹⁰, M. Alhroob¹¹⁴, M. Aliev^{75a,75b}, G. Alimonti^{93a}, J. Alison³³, S.P. Alkire³⁷, B.M.M. Allbrooke¹⁵⁰, B.W. Allen¹¹⁷, P.P. Allport¹⁹, A. Aloisio^{105a,105b}, A. Alonso³⁸, F. Alonso⁷³, C. Alpigiani¹³⁹, M. Alstaty⁸⁷, B. Alvarez Gonzalez³², D. Álvarez Piqueras¹⁶⁷, M.G. Alviggi^{105a,105b}, B.T. Amadio¹⁶, K. Amako⁶⁸, Y. Amaral Coutinho^{26a}, C. Amelung²⁵, D. Amidei⁹¹, S.P. Amor Dos Santos^{127a,127c}, A. Amorim^{127a,127b}, S. Amoroso³², G. Amundsen²⁵, C. Anastopoulos¹⁴⁰, L.S. Ansu⁵¹, N. Andari¹⁰⁹, T. Andeen¹¹, C.F. Anders^{60b}, G. Anders³², J.K. Anders⁷⁶, K.J. Anderson³³, A. Andreazza^{93a,93b}, V. Andrei^{60a}, S. Angelidakis⁹, I. Angelozzi¹⁰⁸, P. Anger⁴⁶, A. Angerami³⁷, F. Anghinolfi³², A.V. Anisenkov^{110,c}, N. Anjos¹³, A. Annovi^{125a,125b}, M. Antonelli⁴⁹, A. Antonov⁹⁹, F. Anulli^{133a}, M. Aoki⁶⁸, L. Aperio Bella¹⁹, G. Arabidze⁹², Y. Arai⁶⁸, J.P. Araque^{127a}, A.T.H. Arce⁴⁷, F.A. Arduh⁷³, J.-F. Arguin⁹⁶, S. Argyropoulos⁶⁵, M. Arik^{20a}, A.J. Armbruster¹⁴⁴, L.J. Armitage⁷⁸, O. Arnaez³², H. Arnold⁵⁰, M. Arratia³⁰, O. Arslan²³, A. Artamonov⁹⁸, G. Artoni¹²¹, S. Artz⁸⁵, S. Asai¹⁵⁶, N. Asbah⁴⁴, A. Ashkenazi¹⁵⁴, B. Åsman^{147a,147b}, L. Asquith¹⁵⁰, K. Assamagan²⁷, R. Astalos^{145a}, M. Atkinson¹⁶⁶, N.B. Atlay¹⁴², K. Augsten¹²⁹, G. Avolio³², B. Axen¹⁶, M.K. Ayoub¹¹⁸, G. Azuelos^{96,d}, M.A. Baak³², A.E. Baas^{60a}, M.J. Baca¹⁹, H. Bachacou¹³⁷, K. Bachas^{75a,75b}, M. Backes³², M. Backhaus³², P. Bagiacchi^{133a,133b}, P. Bagnaia^{133a,133b}, Y. Bai^{35a}, J.T. Barnes¹³², O.K. Baker¹⁷⁶, E.M. Baldin^{110,c}, P. Balek¹³⁰, T. Balestri¹⁴⁹, F. Balli¹³⁷, W.K. Balunas¹²³, E. Banas⁴¹, Sw. Banerjee^{173,e}, A.A.E. Bannoura¹⁷⁵, L. Barak³², E.L. Barberio⁹⁰, D. Barberis^{52a,52b}, M. Barbero⁸⁷, T. Barillari¹⁰², T. Barklow¹⁴⁴, N. Barlow³⁰, S.L. Barnes⁸⁶, B.M. Barnett¹³², R.M. Barnett¹⁶, Z. Barnovska⁵, A. Baroncelli^{135a}, G. Barone²⁵, A.J. Barr¹²¹, L. Barranco Navarro¹⁶⁷, F. Barreiro⁸⁴, J. Barreiro Guimarães da Costa^{35a}, R. Bartoldus¹⁴⁴, A.E. Barton⁷⁴, P. Bartos^{145a}, A. Basalaev¹²⁴, A. Bassalat¹¹⁸, R.L. Bates⁵⁵, S.J. Batista¹⁵⁹, J.R. Batley³⁰, M. Battaglia¹³⁸, M. Baucé^{133a,133b}, F. Bauer¹³⁷, H.S. Bawa^{144,f}, J.B. Beacham¹¹², M.D. Beattie⁷⁴, T. Beau⁸², P.H. Beauchemin¹⁶², P. Bechtle²³, H.P. Beck^{18,g}, K. Becker¹²¹, M. Becker⁸⁵, M. Beckingham¹⁷⁰, C. Becot¹¹¹, A.J. Beddall^{20e}, A. Beddall^{20b}, V.A. Bednyakov⁶⁷, M. Bedognetti¹⁰⁸, C.P. Bee¹⁴⁹, L.J. Beemster¹⁰⁸, T.A. Beermann³², M. Begel²⁷, J.K. Behr⁴⁴, C. Belanger-Champagne⁸⁹, A.S. Bell⁸⁰, G. Bella¹⁵⁴, L. Bellagamba^{22a}, A. Bellerive³¹, M. Bellomo⁸⁸, K. Belotskiy⁹⁹, O. Beltramello³², N.L. Belyaev⁹⁹, O. Benary¹⁵⁴, D. Benchekroun^{136a}, M. Bender¹⁰¹, K. Bendtz^{147a,147b}, N. Benekos¹⁰, Y. Benhammou¹⁵⁴, E. Benhar Noccioli¹⁷⁶, J. Benitez⁶⁵, D.P. Benjamin⁴⁷, J.R. Bensinger²⁵, S. Bentvelsen¹⁰⁸, L. Beresford¹²¹, M. Beretta⁴⁹, D. Berge¹⁰⁸, E. Bergeaas Kuutmann¹⁶⁵, N. Berger⁵, J. Beringer¹⁶, S. Berlendis⁵⁷, N.R. Bernard⁸⁸, C. Bernius¹¹¹, F.U. Bernlochner²³, T. Berry⁷⁹, P. Berta¹³⁰, C. Bertella⁸⁵, G. Bertoli^{147a,147b}, F. Bertolucci^{125a,125b}, I.A. Bertram⁷⁴, C. Bertsche⁴⁴, D. Bertsche¹¹⁴, G.J. Besjes³⁸, O. Bessidskaia Bylund^{147a,147b}, M. Bessner⁴⁴, N. Besson¹³⁷, C. Betancourt⁵⁰, S. Bethke¹⁰², A.J. Bevan⁷⁸, W. Bhimji¹⁶, R.M. Bianchi¹²⁶, L. Bianchini²⁵, M. Bianco³², O. Biebel¹⁰¹, D. Biedermann¹⁷, R. Bielski⁸⁶, N.V. Biesuz^{125a,125b}, M. Biglietti^{135a}, J. Bilbao De Mendizabal⁵¹, H. Bilonok⁴⁹, M. Bindi⁵⁶, S. Binet¹¹⁸, A. Bingul^{20b}, C. Bini^{133a,133b}, S. Biondi^{22a,22b}, D.M. Bjergaard⁴⁷, C.W. Black¹⁵¹, J.E. Black¹⁴⁴, K.M. Black²⁴, D. Blackburn¹³⁹, R.E. Blair⁶, J.-B. Blanchard¹³⁷, J.E. Blanco⁷⁹, T. Blazek^{145a}, I. Bloch⁴⁴, C. Blocker²⁵, W. Blum^{85,*}, U. Blumenschein⁵⁶, S. Blunier^{34a},

G.J. Bobbink¹⁰⁸, V.S. Bobrovnikov^{110,c}, S.S. Bocchetta⁸³, A. Bocci⁴⁷, C. Bock¹⁰¹, M. Boehler⁵⁰,
 D. Boerner¹⁷⁵, J.A. Bogaerts³², D. Bogavac¹⁴, A.G. Bogdanchikov¹¹⁰, C. Bohm^{147a}, V. Boisvert⁷⁹,
 P. Bokan¹⁴, T. Bold^{40a}, A.S. Boldyrev^{164a,164c}, M. Bomben⁸², M. Bona⁷⁸, M. Boonekamp¹³⁷,
 A. Borisov¹³¹, G. Borissov⁷⁴, J. Bortfeldt¹⁰¹, D. Bortoletto¹²¹, V. Bortolotto^{62a,62b,62c}, K. Bos¹⁰⁸,
 D. Boscherini^{22a}, M. Bosman¹³, J.D. Bossio Sola²⁹, J. Boudreau¹²⁶, J. Bouffard²,
 E.V. Bouhova-Thacker⁷⁴, D. Boumediene³⁶, C. Bourdarios¹¹⁸, S.K. Boutle⁵⁵, A. Boveia³², J. Boyd³²,
 I.R. Boyko⁶⁷, J. Bracinik¹⁹, A. Brandt⁸, G. Brandt⁵⁶, O. Brandt^{60a}, U. Bratzler¹⁵⁷, B. Brau⁸⁸,
 J.E. Brau¹¹⁷, H.M. Braun^{175,*}, W.D. Breaden Madden⁵⁵, K. Brendlinger¹²³, A.J. Brennan⁹⁰,
 L. Brenner¹⁰⁸, R. Brenner¹⁶⁵, S. Bressler¹⁷², T.M. Bristow⁴⁸, D. Britton⁵⁵, D. Britzger⁴⁴, F.M. Brochu³⁰,
 I. Brock²³, R. Brock⁹², G. Brooijmans³⁷, T. Brooks⁷⁹, W.K. Brooks^{34b}, J. Brosamer¹⁶, E. Brost¹¹⁷,
 J.H. Broughton¹⁹, P.A. Bruckman de Renstrom⁴¹, D. Bruncko^{145b}, R. Bruneliere⁵⁰, A. Bruni^{22a},
 G. Bruni^{22a}, BH Brunt³⁰, M. Bruschi^{22a}, N. Bruscino²³, P. Bryant³³, L. Bryngemark⁸³, T. Buanes¹⁵,
 Q. Buat¹⁴³, P. Buchholz¹⁴², A.G. Buckley⁵⁵, I.A. Budagov⁶⁷, F. Buehrer⁵⁰, M.K. Bugge¹²⁰,
 O. Bulekov⁹⁹, D. Bullock⁸, H. Burckhart³², S. Burdin⁷⁶, C.D. Burgard⁵⁰, B. Burghgrave¹⁰⁹, K. Burka⁴¹,
 S. Burke¹³², I. Burmeister⁴⁵, E. Busato³⁶, D. Büscher⁵⁰, V. Büscher⁸⁵, P. Bussey⁵⁵, J.M. Butler²⁴,
 C.M. Buttar⁵⁵, J.M. Butterworth⁸⁰, P. Butti¹⁰⁸, W. Buttlinger²⁷, A. Buzatu⁵⁵, A.R. Buzykaev^{110,c},
 S. Cabrera Urbán¹⁶⁷, D. Caforio¹²⁹, V.M. Cairo^{39a,39b}, O. Cakir^{4a}, N. Calace⁵¹, P. Calafuria¹⁶,
 A. Calandri⁸⁷, G. Calderini⁸², P. Calfayan¹⁰¹, L.P. Caloba^{26a}, D. Calvet³⁶, S. Calvet³⁶, T.P. Calvet⁸⁷,
 R. Camacho Toro³³, S. Camarda³², P. Camarri^{134a,134b}, D. Cameron¹²⁰, R. Caminal Armadans¹⁶⁶,
 C. Camincher⁵⁷, S. Campana³², M. Campanelli⁸⁰, A. Camplani^{93a,93b}, A. Campoverde¹⁴⁹,
 V. Canale^{105a,105b}, A. Canepa^{160a}, M. Cano Bret^{35e}, J. Cantero¹¹⁵, R. Cantrill^{127a}, T. Cao⁴²,
 M.D.M. Capeans Garrido³², I. Caprini^{28b}, M. Caprini^{28b}, M. Capua^{39a,39b}, R. Caputo⁸⁵, R.M. Carbone³⁷,
 R. Cardarelli^{134a}, F. Cardillo⁵⁰, I. Carli¹³⁰, T. Carli³², G. Carlino^{105a}, L. Carminati^{93a,93b}, S. Caron¹⁰⁷,
 E. Carquin^{34b}, G.D. Carrillo-Montoya³², J.R. Carter³⁰, J. Carvalho^{127a,127c}, D. Casadei¹⁹,
 M.P. Casado^{13,h}, M. Casolino¹³, D.W. Casper¹⁶³, E. Castaneda-Miranda^{146a}, R. Castelijn¹⁰⁸,
 A. Castelli¹⁰⁸, V. Castillo Gimenez¹⁶⁷, N.F. Castro^{127a,i}, A. Catinaccio³², J.R. Catmore¹²⁰, A. Cattai³²,
 J. Caudron⁸⁵, V. Cavalieri¹⁶⁶, E. Cavallaro¹³, D. Cavalli^{93a}, M. Cavalli-Sforza¹³, V. Cavasinni^{125a,125b},
 F. Ceradini^{135a,135b}, L. Cerdá Alberich¹⁶⁷, B.C. Cerio⁴⁷, A.S. Cerqueira^{26b}, A. Cerri¹⁵⁰, L. Cerrito⁷⁸,
 F. Cerutti¹⁶, M. Cerv³², A. Cervelli¹⁸, S.A. Cetin^{20d}, A. Chafaq^{136a}, D. Chakraborty¹⁰⁹, S.K. Chan⁵⁹,
 Y.L. Chan^{62a}, P. Chang¹⁶⁶, J.D. Chapman³⁰, D.G. Charlton¹⁹, A. Chatterjee⁵¹, C.C. Chau¹⁵⁹,
 C.A. Chavez Barajas¹⁵⁰, S. Che¹¹², S. Cheatham⁷⁴, A. Chegwidden⁹², S. Chekanov⁶,
 S.V. Chekulaev^{160a}, G.A. Chelkov^{67,j}, M.A. Chelstowska⁹¹, C. Chen⁶⁶, H. Chen²⁷, K. Chen¹⁴⁹,
 S. Chen^{35c}, S. Chen¹⁵⁶, X. Chen^{35f}, Y. Chen⁶⁹, H.C. Cheng⁹¹, H.J. Cheng^{35a}, Y. Cheng³³,
 A. Cheplakov⁶⁷, E. Cheremushkina¹³¹, R. Cherkaoui El Moursli^{136e}, V. Chernyatin^{27,*}, E. Cheu⁷,
 L. Chevalier¹³⁷, V. Chiarella⁴⁹, G. Chiarelli^{125a,125b}, G. Chiodini^{75a}, A.S. Chisholm¹⁹, A. Chitan^{28b},
 M.V. Chizhov⁶⁷, K. Choi⁶³, A.R. Chomont³⁶, S. Chouridou⁹, B.K.B. Chow¹⁰¹, V. Christodoulou⁸⁰,
 D. Chromek-Burckhardt³², J. Chudoba¹²⁸, A.J. Chuinard⁸⁹, J.J. Chwastowski⁴¹, L. Chytka¹¹⁶,
 G. Ciapetti^{133a,133b}, A.K. Ciftci^{4a}, D. Cinca⁵⁵, V. Cindro⁷⁷, I.A. Cioara²³, A. Ciocio¹⁶, F. Cirotto^{105a,105b},
 Z.H. Citron¹⁷², M. Citterio^{93a}, M. Ciubancan^{28b}, A. Clark⁵¹, B.L. Clark⁵⁹, M.R. Clark³⁷, P.J. Clark⁴⁸,
 R.N. Clarke¹⁶, C. Clement^{147a,147b}, Y. Coadou⁸⁷, M. Cobal^{164a,164c}, A. Coccaro⁵¹, J. Cochran⁶⁶,
 L. Coffey²⁵, L. Colasurdo¹⁰⁷, B. Cole³⁷, A.P. Colijn¹⁰⁸, J. Collot⁵⁷, T. Colombo³², G. Compostella¹⁰²,
 P. Conde Muiño^{127a,127b}, E. Coniavitis⁵⁰, S.H. Connell^{146b}, I.A. Connolly⁷⁹, V. Consorti⁵⁰,
 S. Constantinescu^{28b}, G. Conti³², F. Conventi^{105a,k}, M. Cooke¹⁶, B.D. Cooper⁸⁰, A.M. Cooper-Sarkar¹²¹,
 K.J.R. Cormier¹⁵⁹, T. Cornelissen¹⁷⁵, M. Corradi^{133a,133b}, F. Corriveau^{89,l}, A. Corso-Radu¹⁶³,
 A. Cortes-Gonzalez¹³, G. Cortiana¹⁰², G. Costa^{93a}, M.J. Costa¹⁶⁷, D. Costanzo¹⁴⁰, G. Cottin³⁰,
 G. Cowan⁷⁹, B.E. Cox⁸⁶, K. Cranmer¹¹¹, S.J. Crawley⁵⁵, G. Cree³¹, S. Crépé-Renaudin⁵⁷, F. Crescioli⁸²,
 W.A. Cribbs^{147a,147b}, M. Crispin Ortuzar¹²¹, M. Cristinziani²³, V. Croft¹⁰⁷, G. Crosetti^{39a,39b},

T. Cuhadar Donszelmann¹⁴⁰, J. Cummings¹⁷⁶, M. Curatolo⁴⁹, J. Cúth⁸⁵, C. Cuthbert¹⁵¹, H. Czirr¹⁴²,
 P. Czodrowski³, G. D'amen^{22a,22b}, S. D'Auria⁵⁵, M. D'Onofrio⁷⁶,
 M.J. Da Cunha Sargedas De Sousa^{127a,127b}, C. Da Via⁸⁶, W. Dabrowski^{40a}, T. Dado^{145a}, T. Dai⁹¹,
 O. Dale¹⁵, F. Dallaire⁹⁶, C. Dallapiccola⁸⁸, M. Dam³⁸, J.R. Dandoy³³, N.P. Dang⁵⁰, A.C. Daniells¹⁹,
 N.S. Dann⁸⁶, M. Danninger¹⁶⁸, M. Dano Hoffmann¹³⁷, V. Dao⁵⁰, G. Darbo^{52a}, S. Darmora⁸,
 J. Dassoulas³, A. Dattagupta⁶³, W. Davey²³, C. David¹⁶⁹, T. Davidek¹³⁰, M. Davies¹⁵⁴, P. Davison⁸⁰,
 E. Dawe⁹⁰, I. Dawson¹⁴⁰, R.K. Daya-Ishmukhametova⁸⁸, K. De⁸, R. de Asmundis^{105a},
 A. De Benedetti¹¹⁴, S. De Castro^{22a,22b}, S. De Cecco⁸², N. De Groot¹⁰⁷, P. de Jong¹⁰⁸, H. De la Torre⁸⁴,
 F. De Lorenzi⁶⁶, A. De Maria⁵⁶, D. De Pedis^{133a}, A. De Salvo^{133a}, U. De Sanctis¹⁵⁰, A. De Santo¹⁵⁰,
 J.B. De Vivie De Regie¹¹⁸, W.J. Dearnaley⁷⁴, R. Debbe²⁷, C. Debenedetti¹³⁸, D.V. Dedovich⁶⁷,
 N. Dehghanian³, I. Deigaard¹⁰⁸, M. Del Gaudio^{39a,39b}, J. Del Peso⁸⁴, T. Del Prete^{125a,125b},
 D. Delgove¹¹⁸, F. Deliot¹³⁷, C.M. Delitzsch⁵¹, M. Deliyergiyev⁷⁷, A. Dell'Acqua³², L. Dell'Asta²⁴,
 M. Dell'Orso^{125a,125b}, M. Della Pietra^{105a,k}, D. della Volpe⁵¹, M. Delmastro⁵, P.A. Delsart⁵⁷,
 C. Deluca¹⁰⁸, D.A. DeMarco¹⁵⁹, S. Demers¹⁷⁶, M. Demichev⁶⁷, A. Demilly⁸², S.P. Denisov¹³¹,
 D. Denysiuk¹³⁷, D. Derendarz⁴¹, J.E. Derkaoui^{136d}, F. Derue⁸², P. Dervan⁷⁶, K. Desch²³, C. Deterre⁴⁴,
 K. Dette⁴⁵, P.O. Deviveiros³², A. Dewhurst¹³², S. Dhaliwal²⁵, A. Di Ciacio^{134a,134b}, L. Di Ciacio⁵,
 W.K. Di Clemente¹²³, C. Di Donato^{133a,133b}, A. Di Girolamo³², B. Di Girolamo³², B. Di Micco^{135a,135b},
 R. Di Nardo³², A. Di Simone⁵⁰, R. Di Sipio¹⁵⁹, D. Di Valentino³¹, C. Diaconu⁸⁷, M. Diamond¹⁵⁹,
 F.A. Dias⁴⁸, M.A. Diaz^{34a}, E.B. Diehl⁹¹, J. Dietrich¹⁷, S. Diglio⁸⁷, A. Dimitrieva¹⁴, J. Dingfelder²³,
 P. Dita^{28b}, S. Dita^{28b}, F. Dittus³², F. Djama⁸⁷, T. Djobava^{53b}, J.I. Djuvsland^{60a}, M.A.B. do Vale^{26c},
 D. Dobos³², M. Dobre^{28b}, C. Doglioni⁸³, T. Dohmae¹⁵⁶, J. Dolejsi¹³⁰, Z. Dolezal¹³⁰,
 B.A. Dolgoshein^{99,*}, M. Donadelli^{26d}, S. Donati^{125a,125b}, P. Dondero^{122a,122b}, J. Donini³⁶, J. Dopke¹³²,
 A. Doria^{105a}, M.T. Dova⁷³, A.T. Doyle⁵⁵, E. Drechsler⁵⁶, M. Dris¹⁰, Y. Du^{35d}, J. Duarte-Campderros¹⁵⁴,
 E. Duchovni¹⁷², G. Duckeck¹⁰¹, O.A. Ducu^{96,m}, D. Duda¹⁰⁸, A. Dudarev³², E.M. Duffield¹⁶,
 L. Duflot¹¹⁸, L. Duguid⁷⁹, M. Dührssen³², M. Dumancic¹⁷², M. Dunford^{60a}, H. Duran Yildiz^{4a},
 M. Düren⁵⁴, A. Durglishvili^{53b}, D. Duschinger⁴⁶, B. Dutta⁴⁴, M. Dyndal⁴⁴, C. Eckardt⁴⁴, K.M. Ecker¹⁰²,
 R.C. Edgar⁹¹, N.C. Edwards⁴⁸, T. Eifert³², G. Eigen¹⁵, K. Einsweiler¹⁶, T. Ekelof¹⁶⁵, M. El Kacimi^{136c},
 V. Ellajosyula⁸⁷, M. Ellert¹⁶⁵, S. Elles⁵, F. Ellinghaus¹⁷⁵, A.A. Elliott¹⁶⁹, N. Ellis³², J. Elmsheuser²⁷,
 M. Elsing³², D. Emeliyanov¹³², Y. Enari¹⁵⁶, O.C. Endner⁸⁵, M. Endo¹¹⁹, J.S. Ennis¹⁷⁰, J. Erdmann⁴⁵,
 A. Ereditato¹⁸, G. Ernis¹⁷⁵, J. Ernst², M. Ernst²⁷, S. Errede¹⁶⁶, E. Ertel⁸⁵, M. Escalier¹¹⁸, H. Esch⁴⁵,
 C. Escobar¹²⁶, B. Esposito⁴⁹, A.I. Etienvre¹³⁷, E. Etzion¹⁵⁴, H. Evans⁶³, A. Ezhilov¹²⁴, F. Fabbri^{22a,22b},
 L. Fabbri^{22a,22b}, G. Facini³³, R.M. Fakhrutdinov¹³¹, S. Falciano^{133a}, R.J. Falla⁸⁰, J. Faltova¹³⁰,
 Y. Fang^{35a}, M. Fanti^{93a,93b}, A. Farbin⁸, A. Farilla^{135a}, C. Farina¹²⁶, T. Farooque¹³, S. Farrell¹⁶,
 S.M. Farrington¹⁷⁰, P. Farthouat³², F. Fassi^{136e}, P. Fassnacht³², D. Fassouliotis⁹, M. Fucci Giannelli⁷⁹,
 A. Favareto^{52a,52b}, W.J. Fawcett¹²¹, L. Fayard¹¹⁸, O.L. Fedin^{124,n}, W. Fedorko¹⁶⁸, S. Feigl¹²⁰,
 L. Feligioni⁸⁷, C. Feng^{35d}, E.J. Feng³², H. Feng⁹¹, A.B. Fenyuk¹³¹, L. Feremenga⁸,
 P. Fernandez Martinez¹⁶⁷, S. Fernandez Perez¹³, J. Ferrando⁵⁵, A. Ferrari¹⁶⁵, P. Ferrari¹⁰⁸, R. Ferrari^{122a},
 D.E. Ferreira de Lima^{60b}, A. Ferrer¹⁶⁷, D. Ferrere⁵¹, C. Ferretti⁹¹, A. Ferretto Parodi^{52a,52b}, F. Fiedler⁸⁵,
 A. Filipčič⁷⁷, M. Filipuzzi⁴⁴, F. Filthaut¹⁰⁷, M. Fincke-Keeler¹⁶⁹, K.D. Finelli¹⁵¹,
 M.C.N. Fiolhais^{127a,127c}, L. Fiorini¹⁶⁷, A. Firan⁴², A. Fischer², C. Fischer¹³, J. Fischer¹⁷⁵, W.C. Fisher⁹²,
 N. Flaschel⁴⁴, I. Fleck¹⁴², P. Fleischmann⁹¹, G.T. Fletcher¹⁴⁰, R.R.M. Fletcher¹²³, T. Flick¹⁷⁵,
 A. Floderus⁸³, L.R. Flores Castillo^{62a}, M.J. Flowerdew¹⁰², G.T. Forcolin⁸⁶, A. Formica¹³⁷, A. Forti⁸⁶,
 A.G. Foster¹⁹, D. Fournier¹¹⁸, H. Fox⁷⁴, S. Fracchia¹³, P. Francavilla⁸², M. Franchini^{22a,22b},
 D. Francis³², L. Franconi¹²⁰, M. Franklin⁵⁹, M. Frate¹⁶³, M. Fraternali^{122a,122b}, D. Freeborn⁸⁰,
 S.M. Fressard-Batraneanu³², F. Friedrich⁴⁶, D. Froidevaux³², J.A. Frost¹²¹, C. Fukunaga¹⁵⁷,
 E. Fullana Torregrossa⁸⁵, T. Fusayasu¹⁰³, J. Fuster¹⁶⁷, C. Gabaldon⁵⁷, O. Gabizon¹⁷⁵, A. Gabrielli^{22a,22b},
 A. Gabrielli¹⁶, G.P. Gach^{40a}, S. Gadatsch³², S. Gadomski⁵¹, G. Gagliardi^{52a,52b}, L.G. Gagnon⁹⁶,

P. Gagnon⁶³, C. Galea¹⁰⁷, B. Galhardo^{127a,127c}, E.J. Gallas¹²¹, B.J. Gallop¹³², P. Gallus¹²⁹, G. Galster³⁸, K.K. Gan¹¹², J. Gao^{35b,87}, Y. Gao⁴⁸, Y.S. Gao^{144,f}, F.M. Garay Walls⁴⁸, C. García¹⁶⁷, J.E. García Navarro¹⁶⁷, M. Garcia-Sciveres¹⁶, R.W. Gardner³³, N. Garelli¹⁴⁴, V. Garonne¹²⁰, A. Gascon Bravo⁴⁴, C. Gatti⁴⁹, A. Gaudiello^{52a,52b}, G. Gaudio^{122a}, B. Gaur¹⁴², L. Gauthier⁹⁶, I.L. Gavrilenko⁹⁷, C. Gay¹⁶⁸, G. Gaycken²³, E.N. Gazis¹⁰, Z. Gecse¹⁶⁸, C.N.P. Gee¹³², Ch. Geich-Gimbel²³, M. Geisen⁸⁵, M.P. Geisler^{60a}, C. Gemme^{52a}, M.H. Genest⁵⁷, C. Geng^{35b,o}, S. Gentile^{133a,133b}, S. George⁷⁹, D. Gerbaudo¹³, A. Gershon¹⁵⁴, S. Ghasemi¹⁴², H. Ghazlane^{136b}, M. Ghneimat²³, B. Giacobbe^{22a}, S. Giagu^{133a,133b}, P. Giannetti^{125a,125b}, B. Gibbard²⁷, S.M. Gibson⁷⁹, M. Gignac¹⁶⁸, M. Gilchriese¹⁶, T.P.S. Gillam³⁰, D. Gillberg³¹, G. Gilles¹⁷⁵, D.M. Gingrich^{3,d}, N. Giokaris⁹, M.P. Giordani^{164a,164c}, F.M. Giorgi^{22a}, F.M. Giorgi¹⁷, P.F. Giraud¹³⁷, P. Giromini⁵⁹, D. Giugni^{93a}, F. Giuli¹²¹, C. Giuliani¹⁰², M. Giulini^{60b}, B.K. Gjelsten¹²⁰, S. Gkaitatzis¹⁵⁵, I. Gkialas¹⁵⁵, E.L. Gkougkousis¹¹⁸, L.K. Gladilin¹⁰⁰, C. Glasman⁸⁴, J. Glatzer³², P.C.F. Glaysher⁴⁸, A. Glazov⁴⁴, M. Goblirsch-Kolb¹⁰², J. Godlewski⁴¹, S. Goldfarb⁹¹, T. Golling⁵¹, D. Golubkov¹³¹, A. Gomes^{127a,127b,127d}, R. Gonçalo^{127a}, J. Goncalves Pinto Firmino Da Costa¹³⁷, L. Gonella¹⁹, A. Gongadze⁶⁷, S. González de la Hoz¹⁶⁷, G. Gonzalez Parra¹³, S. Gonzalez-Sevilla⁵¹, L. Goossens³², P.A. Gorbounov⁹⁸, H.A. Gordon²⁷, I. Gorelov¹⁰⁶, B. Gorini³², E. Gorini^{75a,75b}, A. Gorišek⁷⁷, E. Gornicki⁴¹, A.T. Goshaw⁴⁷, C. Gössling⁴⁵, M.I. Gostkin⁶⁷, C.R. Goudet¹¹⁸, D. Goujdami^{136c}, A.G. Goussiou¹³⁹, N. Govender^{146b,p}, E. Gozani¹⁵³, L. Graber⁵⁶, I. Grabowska-Bold^{40a}, P.O.J. Gradin⁵⁷, P. Grafström^{22a,22b}, J. Gramling⁵¹, E. Gramstad¹²⁰, S. Grancagnolo¹⁷, V. Gratchev¹²⁴, P.M. Gravila^{28e}, H.M. Gray³², E. Graziani^{135a}, Z.D. Greenwood^{81,q}, C. Grefe²³, K. Gregersen⁸⁰, I.M. Gregor⁴⁴, P. Grenier¹⁴⁴, K. Grevtsov⁵, J. Griffiths⁸, A.A. Grillo¹³⁸, K. Grimm⁷⁴, S. Grinstein^{13,r}, Ph. Gris³⁶, J.-F. Grivaz¹¹⁸, S. Groh⁸⁵, J.P. Grohs⁴⁶, E. Gross¹⁷², J. Grosse-Knetter⁵⁶, G.C. Grossi⁸¹, Z.J. Grout¹⁵⁰, L. Guan⁹¹, W. Guan¹⁷³, J. Guenther¹²⁹, F. Guescini⁵¹, D. Guest¹⁶³, O. Gueta¹⁵⁴, E. Guido^{52a,52b}, T. Guillemin⁵, S. Guindon², U. Gul⁵⁵, C. Gumpert³², J. Guo^{35e}, Y. Guo^{35b,o}, S. Gupta¹²¹, G. Gustavino^{133a,133b}, P. Gutierrez¹¹⁴, N.G. Gutierrez Ortiz⁸⁰, C. Gutschow⁴⁶, C. Guyot¹³⁷, C. Gwenlan¹²¹, C.B. Gwilliam⁷⁶, A. Haas¹¹¹, C. Haber¹⁶, H.K. Hadavand⁸, N. Haddad^{136e}, A. Hadef⁸⁷, P. Haefner²³, S. Hageböck²³, Z. Hajduk⁴¹, H. Hakobyan^{177,*}, M. Haleem⁴⁴, J. Haley¹¹⁵, G. Halladjian⁹², G.D. Hallewell⁸⁷, K. Hamacher¹⁷⁵, P. Hamal¹¹⁶, K. Hamano¹⁶⁹, A. Hamilton^{146a}, G.N. Hamity¹⁴⁰, P.G. Hamnett⁴⁴, L. Han^{35b}, K. Hanagaki^{68,s}, K. Hanawa¹⁵⁶, M. Hance¹³⁸, B. Haney¹²³, P. Hanke^{60a}, R. Hanna¹³⁷, J.B. Hansen³⁸, J.D. Hansen³⁸, M.C. Hansen²³, P.H. Hansen³⁸, K. Hara¹⁶¹, A.S. Hard¹⁷³, T. Harenberg¹⁷⁵, F. Hariri¹¹⁸, S. Harkusha⁹⁴, R.D. Harrington⁴⁸, P.F. Harrison¹⁷⁰, F. Hartjes¹⁰⁸, N.M. Hartmann¹⁰¹, M. Hasegawa⁶⁹, Y. Hasegawa¹⁴¹, A. Hasib¹¹⁴, S. Hassani¹³⁷, S. Haug¹⁸, R. Hauser⁹², L. Hauswald⁴⁶, M. Havranek¹²⁸, C.M. Hawkes¹⁹, R.J. Hawkings³², D. Hayden⁹², C.P. Hays¹²¹, J.M. Hays⁷⁸, H.S. Hayward⁷⁶, S.J. Haywood¹³², S.J. Head¹⁹, T. Heck⁸⁵, V. Hedberg⁸³, L. Heelan⁸, S. Heim¹²³, T. Heim¹⁶, B. Heinemann¹⁶, J.J. Heinrich¹⁰¹, L. Heinrich¹¹¹, C. Heinz⁵⁴, J. Hejbal¹²⁸, L. Helary²⁴, S. Hellman^{147a,147b}, C. Helsens³², J. Henderson¹²¹, R.C.W. Henderson⁷⁴, Y. Heng¹⁷³, S. Henkelmann¹⁶⁸, A.M. Henriques Correia³², S. Henrot-Versille¹¹⁸, G.H. Herbert¹⁷, Y. Hernández Jiménez¹⁶⁷, G. Herten⁵⁰, R. Hertenberger¹⁰¹, L. Hervas³², G.G. Hesketh⁸⁰, N.P. Hessey¹⁰⁸, J.W. Hetherly⁴², R. Hickling⁷⁸, E. Higón-Rodriguez¹⁶⁷, E. Hill¹⁶⁹, J.C. Hill³⁰, K.H. Hiller⁴⁴, S.J. Hillier¹⁹, I. Hinchliffe¹⁶, E. Hines¹²³, R.R. Hinman¹⁶, M. Hirose¹⁵⁸, D. Hirschbuehl¹⁷⁵, J. Hobbs¹⁴⁹, N. Hod^{160a}, M.C. Hodgkinson¹⁴⁰, P. Hodgson¹⁴⁰, A. Hoecker³², M.R. Hoeferkamp¹⁰⁶, F. Hoenig¹⁰¹, D. Hohn²³, T.R. Holmes¹⁶, M. Homann⁴⁵, T.M. Hong¹²⁶, B.H. Hooberman¹⁶⁶, W.H. Hopkins¹¹⁷, Y. Horii¹⁰⁴, A.J. Horton¹⁴³, J.-Y. Hostachy⁵⁷, S. Hou¹⁵², A. Hoummada^{136a}, J. Howarth⁴⁴, M. Hrabovsky¹¹⁶, I. Hristova¹⁷, J. Hrvnac¹¹⁸, T. Hrynev'ova⁵, A. Hrynevich⁹⁵, C. Hsu^{146c}, P.J. Hsu^{152,t}, S.-C. Hsu¹³⁹, D. Hu³⁷, Q. Hu^{35b}, Y. Huang⁴⁴, Z. Hubacek¹²⁹, F. Hubaut⁸⁷, F. Huegging²³, T.B. Huffman¹²¹, E.W. Hughes³⁷, G. Hughes⁷⁴, M. Huhtinen³², T.A. Hülsing⁸⁵, P. Huo¹⁴⁹, N. Huseynov^{67,b}, J. Huston⁹², J. Huth⁵⁹, G. Iacobucci⁵¹, G. Iakovidis²⁷,

I. Ibragimov¹⁴², L. Iconomidou-Fayard¹¹⁸, E. Ideal¹⁷⁶, Z. Idrissi^{136e}, P. Iengo³², O. Igonkina^{108,u},
 T. Iizawa¹⁷¹, Y. Ikegami⁶⁸, M. Ikeno⁶⁸, Y. Ilchenko^{11,v}, D. Iliadis¹⁵⁵, N. Ilie¹⁴⁴, T. Ince¹⁰²,
 G. Introzzi^{122a,122b}, P. Ioannou^{9,*}, M. Iodice^{135a}, K. Iordanidou³⁷, V. Ippolito⁵⁹, M. Ishino⁷⁰,
 M. Ishitsuka¹⁵⁸, R. Ishmukhametov¹¹², C. Issever¹²¹, S. Istin^{20a}, F. Ito¹⁶¹, J.M. Iturbe Ponce⁸⁶,
 R. Iuppa^{134a,134b}, W. Iwanski⁴¹, H. Iwasaki⁶⁸, J.M. Izen⁴³, V. Izzo^{105a}, S. Jabbar³, B. Jackson¹²³,
 M. Jackson⁷⁶, P. Jackson¹, V. Jain², K.B. Jakobi⁸⁵, K. Jakobs⁵⁰, S. Jakobsen³², T. Jakoubek¹²⁸,
 D.O. Jamin¹¹⁵, D.K. Jana⁸¹, E. Jansen⁸⁰, R. Jansky⁶⁴, J. Janssen²³, M. Janus⁵⁶, G. Jarlskog⁸³,
 N. Javadov^{67,b}, T. Javurek⁵⁰, F. Jeanneau¹³⁷, L. Jeanty¹⁶, J. Jejelava^{53a,w}, G.-Y. Jeng¹⁵¹, D. Jennens⁹⁰,
 P. Jenni^{50,x}, J. Jentzsch⁴⁵, C. Jeske¹⁷⁰, S. Jézéquel⁵, H. Ji¹⁷³, J. Jia¹⁴⁹, H. Jiang⁶⁶, Y. Jiang^{35b},
 S. Jiggins⁸⁰, J. Jimenez Pena¹⁶⁷, S. Jin^{35a}, A. Jinaru^{28b}, O. Jinnouchi¹⁵⁸, P. Johansson¹⁴⁰, K.A. Johns⁷,
 W.J. Johnson¹³⁹, K. Jon-And^{147a,147b}, G. Jones¹⁷⁰, R.W.L. Jones⁷⁴, S. Jones⁷, T.J. Jones⁷⁶,
 J. Jongmanns^{60a}, P.M. Jorge^{127a,127b}, J. Jovicevic^{160a}, X. Ju¹⁷³, A. Juste Rozas^{13,r}, M.K. Köhler¹⁷²,
 A. Kaczmarcka⁴¹, M. Kado¹¹⁸, H. Kagan¹¹², M. Kagan¹⁴⁴, S.J. Kahn⁸⁷, E. Kajomovitz⁴⁷,
 C.W. Kalderon¹²¹, A. Kaluza⁸⁵, S. Kama⁴², A. Kamenshchikov¹³¹, N. Kanaya¹⁵⁶, S. Kaneti³⁰,
 L. Kanjur⁷⁷, V.A. Kantserov⁹⁹, J. Kanzaki⁶⁸, B. Kaplan¹¹¹, L.S. Kaplan¹⁷³, A. Kapliy³³, D. Kar^{146c},
 K. Karakostas¹⁰, A. Karamaoun³, N. Karastathis¹⁰, M.J. Kareem⁵⁶, E. Karentzos¹⁰, M. Karnevskiy⁸⁵,
 S.N. Karpov⁶⁷, Z.M. Karpova⁶⁷, K. Karthik¹¹¹, V. Kartvelishvili⁷⁴, A.N. Karyukhin¹³¹, K. Kasahara¹⁶¹,
 L. Kashif¹⁷³, R.D. Kass¹¹², A. Kastanas¹⁵, Y. Kataoka¹⁵⁶, C. Kato¹⁵⁶, A. Katre⁵¹, J. Katzy⁴⁴,
 K. Kawagoe⁷², T. Kawamoto¹⁵⁶, G. Kawamura⁵⁶, S. Kazama¹⁵⁶, V.F. Kazanin^{110,c}, R. Keeler¹⁶⁹,
 R. Kehoe⁴², J.S. Keller⁴⁴, J.J. Kempster⁷⁹, K. Kentaro¹⁰⁴, H. Keoshkerian¹⁵⁹, O. Kepka¹²⁸,
 B.P. Kerševan⁷⁷, S. Kersten¹⁷⁵, R.A. Keyes⁸⁹, F. Khalil-zada¹², A. Khanov¹¹⁵, A.G. Kharlamov^{110,c},
 T.J. Khoo⁵¹, V. Khovanskij⁹⁸, E. Khramov⁶⁷, J. Khubua^{53b,y}, S. Kido⁶⁹, H.Y. Kim⁸, S.H. Kim¹⁶¹,
 Y.K. Kim³³, N. Kimura¹⁵⁵, O.M. Kind¹⁷, B.T. King⁷⁶, M. King¹⁶⁷, S.B. King¹⁶⁸, J. Kirk¹³²,
 A.E. Kiryunin¹⁰², T. Kishimoto⁶⁹, D. Kisielewska^{40a}, F. Kiss⁵⁰, K. Kiuchi¹⁶¹, O. Kivernyk¹³⁷,
 E. Kladiva^{145b}, M.H. Klein³⁷, M. Klein⁷⁶, U. Klein⁷⁶, K. Kleinknecht⁸⁵, P. Klimek^{147a,147b},
 A. Klimentov²⁷, R. Klingenberg⁴⁵, J.A. Klinger¹⁴⁰, T. Klioutchnikova³², E.-E. Kluge^{60a}, P. Kluit¹⁰⁸,
 S. Kluth¹⁰², J. Knapik⁴¹, E. Kneringer⁶⁴, E.B.F.G. Knoops⁸⁷, A. Knue⁵⁵, A. Kobayashi¹⁵⁶,
 D. Kobayashi¹⁵⁸, T. Kobayashi¹⁵⁶, M. Kobel⁴⁶, M. Kocian¹⁴⁴, P. Kodys¹³⁰, T. Koffman³¹, E. Koffeman¹⁰⁸,
 T. Koi¹⁴⁴, H. Kolanoski¹⁷, M. Kolb^{60b}, I. Koletsou⁵, A.A. Komar^{97,*}, Y. Komori¹⁵⁶, T. Kondo⁶⁸,
 N. Kondrashova⁴⁴, K. Köneke⁵⁰, A.C. König¹⁰⁷, T. Kono^{68,z}, R. Konoplich^{111,aa}, N. Konstantinidis⁸⁰,
 R. Kopeliansky⁶³, S. Koperny^{40a}, L. Köpke⁸⁵, A.K. Kopp⁵⁰, K. Korcyl⁴¹, K. Kordas¹⁵⁵, A. Korn⁸⁰,
 A.A. Korol^{110,c}, I. Korolkov¹³, E.V. Korolkova¹⁴⁰, O. Kortner¹⁰², S. Kortner¹⁰², T. Kosek¹³⁰,
 V.V. Kostyukhin²³, A. Kotwal⁴⁷, A. Kourkoumeli-Charalampidi¹⁵⁵, C. Kourkoumelis⁹, V. Kouskoura²⁷,
 A.B. Kowalewska⁴¹, R. Kowalewski¹⁶⁹, T.Z. Kowalski^{40a}, C. Kozakai¹⁵⁶, W. Kozanecki¹³⁷,
 A.S. Kozhin¹³¹, V.A. Kramarenko¹⁰⁰, G. Kramberger⁷⁷, D. Krasnopol'tsev⁹⁹, M.W. Krasny⁸²,
 A. Krasznahorkay³², J.K. Kraus²³, A. Kravchenko²⁷, M. Kretz^{60c}, J. Kretzscher⁷⁶, K. Kreutzfeldt⁵⁴,
 P. Krieger¹⁵⁹, K. Krizka³³, K. Kroeninger⁴⁵, H. Kroha¹⁰², J. Kroll¹²³, J. Kroeseberg²³, J. Krstic¹⁴,
 U. Kruchonak⁶⁷, H. Krüger²³, N. Krumnack⁶⁶, A. Kruse¹⁷³, M.C. Kruse⁴⁷, M. Kruskal²⁴, T. Kubota⁹⁰,
 H. Kucuk⁸⁰, S. Kuday^{4b}, J.T. Kuechler¹⁷⁵, S. Kuehn⁵⁰, A. Kugel^{60c}, F. Kuger¹⁷⁴, A. Kuhl¹³⁸, T. Kuhl⁴⁴,
 V. Kukhtin⁶⁷, R. Kukla¹³⁷, Y. Kulchitsky⁹⁴, S. Kuleshov^{34b}, M. Kuna^{133a,133b}, T. Kunigo⁷⁰, A. Kupco¹²⁸,
 H. Kurashige⁶⁹, Y.A. Kurochkin⁹⁴, V. Kus¹²⁸, E.S. Kuwertz¹⁶⁹, M. Kuze¹⁵⁸, J. Kvita¹¹⁶, T. Kwan¹⁶⁹,
 D. Kyriazopoulos¹⁴⁰, A. La Rosa¹⁰², J.L. La Rosa Navarro^{26d}, L. La Rotonda^{39a,39b}, C. Lacasta¹⁶⁷,
 F. Lacava^{133a,133b}, J. Lacey³¹, H. Lacker¹⁷, D. Lacour⁸², V.R. Lacuesta¹⁶⁷, E. Ladygin⁶⁷, R. Lafaye⁵,
 B. Laforge⁸², T. Lagouri¹⁷⁶, S. Lai⁵⁶, S. Lammers⁶³, W. Lampl⁷, E. Lançon¹³⁷, U. Landgraf⁵⁰,
 M.P.J. Landon⁷⁸, V.S. Lang^{60a}, J.C. Lange¹³, A.J. Lankford¹⁶³, F. Lanni²⁷, K. Lantzsch²³, A. Lanza^{122a},
 S. Laplace⁸², C. Lapoire³², J.F. Laporte¹³⁷, T. Lari^{93a}, F. Lasagni Manghi^{22a,22b}, M. Lassnig³²,
 P. Laurelli⁴⁹, W. Lavrijssen¹⁶, A.T. Law¹³⁸, P. Laycock⁷⁶, T. Lazovich⁵⁹, M. Lazzaroni^{93a,93b}, B. Le⁹⁰,

O. Le Dertz⁸², E. Le Guiriec⁸⁷, E.P. Le Quilleuc¹³⁷, M. LeBlanc¹⁶⁹, T. LeCompte⁶,
 F. Ledroit-Guillon⁵⁷, C.A. Lee²⁷, S.C. Lee¹⁵², L. Lee¹, G. Lefebvre⁸², M. Lefebvre¹⁶⁹, F. Legger¹⁰¹,
 C. Leggett¹⁶, A. Lehan⁷⁶, G. Lehmann Miotto³², X. Lei⁷, W.A. Leight³¹, A. Leisos^{155,ab},
 A.G. Leister¹⁷⁶, M.A.L. Leite^{26d}, R. Leitner¹³⁰, D. Lellouch¹⁷², B. Lemmer⁵⁶, K.J.C. Leney⁸⁰,
 T. Lenz²³, B. Lenzi³², R. Leone⁷, S. Leone^{125a,125b}, C. Leonidopoulos⁴⁸, S. Leontsinis¹⁰, G. Lerner¹⁵⁰,
 C. Leroy⁹⁶, A.A.J. Lesage¹³⁷, C.G. Lester³⁰, M. Levchenko¹²⁴, J. Levêque⁵, D. Levin⁹¹,
 L.J. Levinson¹⁷², M. Levy¹⁹, D. Lewis⁷⁸, A.M. Leyko²³, M. Leyton⁴³, B. Li^{35b,o}, H. Li¹⁴⁹, H.L. Li³³,
 L. Li⁴⁷, L. Li^{35e}, Q. Li^{35a}, S. Li⁴⁷, X. Li⁸⁶, Y. Li¹⁴², Z. Liang^{35a}, B. Liberti^{134a}, A. Liblong¹⁵⁹,
 P. Lichard³², K. Lie¹⁶⁶, J. Liebal²³, W. Liebig¹⁵, A. Limosani¹⁵¹, S.C. Lin^{152,ac}, T.H. Lin⁸⁵,
 B.E. Lindquist¹⁴⁹, A.E. Lionti⁵¹, E. Lipeles¹²³, A. Lipniacka¹⁵, M. Lisovyi^{60b}, T.M. Liss¹⁶⁶,
 A. Lister¹⁶⁸, A.M. Litke¹³⁸, B. Liu^{152,ad}, D. Liu¹⁵², H. Liu⁹¹, H. Liu²⁷, J. Liu⁸⁷, J.B. Liu^{35b}, K. Liu⁸⁷,
 L. Liu¹⁶⁶, M. Liu⁴⁷, M. Liu^{35b}, Y.L. Liu^{35b}, M. Livan^{122a,122b}, A. Lleres⁵⁷,
 J. Llorente Merino^{35a}, S.L. Lloyd⁷⁸, F. Lo Sterzo¹⁵², E. Lobodzinska⁴⁴, P. Loch⁷, W.S. Lockman¹³⁸,
 F.K. Loebinger⁸⁶, A.E. Loevschall-Jensen³⁸, K.M. Loew²⁵, A. Loginov¹⁷⁶, T. Lohse¹⁷, K. Lohwasser⁴⁴,
 M. Lokajicek¹²⁸, B.A. Long²⁴, J.D. Long¹⁶⁶, R.E. Long⁷⁴, L. Longo^{75a,75b}, K.A.Looper¹¹²,
 L. Lopes^{127a}, D. Lopez Mateos⁵⁹, B. Lopez Paredes¹⁴⁰, I. Lopez Paz¹³, A. Lopez Solis⁸², J. Lorenz¹⁰¹,
 N. Lorenzo Martinez⁶³, M. Losada²¹, P.J. Lösel¹⁰¹, X. Lou^{35a}, A. Lounis¹¹⁸, J. Love⁶, P.A. Love⁷⁴,
 H. Lu^{62a}, N. Lu⁹¹, H.J. Lubatti¹³⁹, C. Luci^{133a,133b}, A. Lucotte⁵⁷, C. Luedtke⁵⁰, F. Luehring⁶³,
 W. Lukas⁶⁴, L. Luminari^{133a}, O. Lundberg^{147a,147b}, B. Lund-Jensen¹⁴⁸, P.M. Luzi⁸², D. Lynn²⁷,
 R. Lysak¹²⁸, E. Lytken⁸³, V. Lyubushkin⁶⁷, H. Ma²⁷, L.L. Ma^{35d}, Y. Ma^{35d}, G. Maccarrone⁴⁹,
 A. Macchiolo¹⁰², C.M. Macdonald¹⁴⁰, B. Maček⁷⁷, J. Machado Miguens^{123,127b}, D. Madaffari⁸⁷,
 R. Madar³⁶, H.J. Maddocks¹⁶⁵, W.F. Mader⁴⁶, A. Madsen⁴⁴, J. Maeda⁶⁹, S. Maeland¹⁵, T. Maeno²⁷,
 A. Maevskiy¹⁰⁰, E. Magradze⁵⁶, J. Mahlstedt¹⁰⁸, C. Maiani¹¹⁸, C. Maidantchik^{26a}, A.A. Maier¹⁰²,
 T. Maier¹⁰¹, A. Maio^{127a,127b,127d}, S. Majewski¹¹⁷, Y. Makida⁶⁸, N. Makovec¹¹⁸, B. Malaescu⁸²,
 Pa. Malecki⁴¹, V.P. Maleev¹²⁴, F. Malek⁵⁷, U. Mallik⁶⁵, D. Malon⁶, C. Malone¹⁴⁴, S. Maltezos¹⁰,
 S. Malyukov³², J. Mamuzic¹⁶⁷, G. Mancini⁴⁹, B. Mandelli³², L. Mandelli^{93a}, I. Mandić⁷⁷,
 J. Maneira^{127a,127b}, L. Manhaes de Andrade Filho^{26b}, J. Manjarres Ramos^{160b}, A. Mann¹⁰¹,
 A. Manousos³², B. Mansoulie¹³⁷, J.D. Mansour^{35a}, R. Mantifel⁸⁹, M. Mantoani⁵⁶, S. Manzoni^{93a,93b},
 L. Mapelli³², G. Marceca²⁹, L. March⁵¹, G. Marchiori⁸², M. Marcisovsky¹²⁸, M. Marjanovic¹⁴,
 D.E. Marley⁹¹, F. Marroquim^{26a}, S.P. Marsden⁸⁶, Z. Marshall¹⁶, S. Marti-Garcia¹⁶⁷, B. Martin⁹²,
 T.A. Martin¹⁷⁰, V.J. Martin⁴⁸, B. Martin dit Latour¹⁵, M. Martinez^{13,r}, S. Martin-Haugh¹³²,
 V.S. Martoiu^{28b}, A.C. Martyniuk⁸⁰, M. Marx¹³⁹, A. Marzin³², L. Masetti⁸⁵, T. Mashimo¹⁵⁶,
 R. Mashinistov⁹⁷, J. Masik⁸⁶, A.L. Maslennikov^{110,c}, I. Massa^{22a,22b}, L. Massa^{22a,22b}, P. Mastrandrea⁵,
 A. Mastroberardino^{39a,39b}, T. Masubuchi¹⁵⁶, P. Mättig¹⁷⁵, J. Mattmann⁸⁵, J. Maurer^{28b}, S.J. Maxfield⁷⁶,
 D.A. Maximov^{110,c}, R. Mazini¹⁵², S.M. Mazza^{93a,93b}, N.C. Mc Fadden¹⁰⁶, G. Mc Goldrick¹⁵⁹,
 S.P. Mc Kee⁹¹, A. McCarn⁹¹, R.L. McCarthy¹⁴⁹, T.G. McCarthy³¹, L.I. McClymont⁸⁰, E.F. McDonald⁹⁰,
 K.W. McFarlane^{58,*}, J.A. McFayden⁸⁰, G. Mchedlidze⁵⁶, S.J. McMahon¹³², R.A. McPherson^{169,l},
 M. Medinnis⁴⁴, S. Meehan¹³⁹, S. Mehlhase¹⁰¹, A. Mehta⁷⁶, K. Meier^{60a}, C. Meineck¹⁰¹, B. Meirose⁴³,
 D. Melini¹⁶⁷, B.R. Mellado Garcia^{146c}, M. Melo^{145a}, F. Meloni¹⁸, A. Mengarelli^{22a,22b}, S. Menke¹⁰²,
 E. Meoni¹⁶², S. Mergelmeyer¹⁷, P. Mermod⁵¹, L. Merola^{105a,105b}, C. Meroni^{93a}, F.S. Merritt³³,
 A. Messina^{133a,133b}, J. Metcalfe⁶, A.S. Mete¹⁶³, C. Meyer⁸⁵, C. Meyer¹²³, J.-P. Meyer¹³⁷, J. Meyer¹⁰⁸,
 H. Meyer Zu Theenhausen^{60a}, F. Miano¹⁵⁰, R.P. Middleton¹³², S. Miglioranzi^{52a,52b}, L. Mijović²³,
 G. Mikenberg¹⁷², M. Mikestikova¹²⁸, M. Mikuž⁷⁷, M. Milesi⁹⁰, A. Milic⁶⁴, D.W. Miller³³, C. Mills⁴⁸,
 A. Milov¹⁷², D.A. Milstead^{147a,147b}, A.A. Minaenko¹³¹, Y. Minami¹⁵⁶, I.A. Minashvili⁶⁷, A.I. Mincer¹¹¹,
 B. Mindur^{40a}, M. Mineev⁶⁷, Y. Ming¹⁷³, L.M. Mir¹³, K.P. Mistry¹²³, T. Mitani¹⁷¹, J. Mitrevski¹⁰¹,
 V.A. Mitsou¹⁶⁷, A. Miucci⁵¹, P.S. Miyagawa¹⁴⁰, J.U. Mjörnmark⁸³, T. Moa^{147a,147b}, K. Mochizuki⁹⁶,
 S. Mohapatra³⁷, S. Molander^{147a,147b}, R. Moles-Valls²³, R. Monden⁷⁰, M.C. Mondragon⁹², K. Mönig⁴⁴,

J. Monk³⁸, E. Monnier⁸⁷, A. Montalbano¹⁴⁹, J. Montejo Berlingen³², F. Monticelli⁷³, S. Monzani^{93a,93b}, R.W. Moore³, N. Morange¹¹⁸, D. Moreno²¹, M. Moreno Llácer⁵⁶, P. Morettini^{52a}, D. Mori¹⁴³, T. Mori¹⁵⁶, M. Morii⁵⁹, M. Morinaga¹⁵⁶, V. Morisbak¹²⁰, S. Moritz⁸⁵, A.K. Morley¹⁵¹, G. Mornacchi³², J.D. Morris⁷⁸, S.S. Mortensen³⁸, L. Morvaj¹⁴⁹, M. Mosidze^{53b}, J. Moss¹⁴⁴, K. Motohashi¹⁵⁸, R. Mount¹⁴⁴, E. Mountricha²⁷, S.V. Mouraviev^{97,*}, E.J.W. Moyse⁸⁸, S. Muanza⁸⁷, R.D. Mudd¹⁹, F. Mueller¹⁰², J. Mueller¹²⁶, R.S.P. Mueller¹⁰¹, T. Mueller³⁰, D. Muenstermann⁷⁴, P. Mullen⁵⁵, G.A. Mullier¹⁸, F.J. Munoz Sanchez⁸⁶, J.A. Murillo Quijada¹⁹, W.J. Murray^{170,132}, H. Musheghyan⁵⁶, M. Muškinja⁷⁷, A.G. Myagkov^{131,ae}, M. Myska¹²⁹, B.P. Nachman¹⁴⁴, O. Nackenhorst⁵¹, K. Nagai¹²¹, R. Nagai^{68,z}, K. Nagano⁶⁸, Y. Nagasaka⁶¹, K. Nagata¹⁶¹, M. Nagel⁵⁰, E. Nagy⁸⁷, A.M. Nairz³², Y. Nakahama³², K. Nakamura⁶⁸, T. Nakamura¹⁵⁶, I. Nakano¹¹³, H. Namasivayam⁴³, R.F. Naranjo Garcia⁴⁴, R. Narayan¹¹, D.I. Narrias Villar^{60a}, I. Naryshkin¹²⁴, T. Naumann⁴⁴, G. Navarro²¹, R. Nayyar⁷, H.A. Neal⁹¹, P.Yu. Nechaeva⁹⁷, T.J. Neep⁸⁶, P.D. Nef¹⁴⁴, A. Negri^{122a,122b}, M. Negrini^{22a}, S. Nektarijevic¹⁰⁷, C. Nellist¹¹⁸, A. Nelson¹⁶³, S. Nemecek¹²⁸, P. Nemethy¹¹¹, A.A. Nepomuceno^{26a}, M. Nessi^{32,af}, M.S. Neubauer¹⁶⁶, M. Neumann¹⁷⁵, R.M. Neves¹¹¹, P. Nevski²⁷, P.R. Newman¹⁹, D.H. Nguyen⁶, T. Nguyen Manh⁹⁶, R.B. Nickerson¹²¹, R. Nicolaïdou¹³⁷, J. Nielsen¹³⁸, A. Nikiforov¹⁷, V. Nikolaenko^{131,ae}, I. Nikolic-Audit⁸², K. Nikolopoulos¹⁹, J.K. Nilsen¹²⁰, P. Nilsson²⁷, Y. Ninomiya¹⁵⁶, A. Nisati^{133a}, R. Nisius¹⁰², T. Nobe¹⁵⁶, L. Nodulman⁶, M. Nomachi¹¹⁹, I. Nomidis³¹, T. Nooney⁷⁸, S. Norberg¹¹⁴, M. Nordberg³², N. Norjoharuddeen¹²¹, O. Novgorodova⁴⁶, S. Nowak¹⁰², M. Nozaki⁶⁸, L. Nozka¹¹⁶, K. Ntekas¹⁰, E. Nurse⁸⁰, F. Nuti⁹⁰, F. O'grady⁷, D.C. O'Neil¹⁴³, A.A. O'Rourke⁴⁴, V. O'Shea⁵⁵, F.G. Oakham^{31,d}, H. Oberlack¹⁰², T. Obermann²³, J. Ocariz⁸², A. Ochi⁶⁹, I. Ochoa³⁷, J.P. Ochoa-Ricoux^{34a}, S. Oda⁷², S. Odaka⁶⁸, H. Ogren⁶³, A. Oh⁸⁶, S.H. Oh⁴⁷, C.C. Ohm¹⁶, H. Ohman¹⁶⁵, H. Oide³², H. Okawa¹⁶¹, Y. Okumura³³, T. Okuyama⁶⁸, A. Olariu^{28b}, L.F. Oleiro Seabra^{127a}, S.A. Olivares Pino⁴⁸, D. Oliveira Damazio²⁷, A. Olszewski⁴¹, J. Olszowska⁴¹, A. Onofre^{127a,127e}, K. Onogi¹⁰⁴, P.U.E. Onyisi^{11,v}, M.J. Oreglia³³, Y. Oren¹⁵⁴, D. Orestano^{135a,135b}, N. Orlando^{62b}, R.S. Orr¹⁵⁹, B. Osculati^{52a,52b}, R. Ospanov⁸⁶, G. Otero y Garzon²⁹, H. Otono⁷², M. Ouchrif^{136d}, F. Ould-Saada¹²⁰, A. Ouraou¹³⁷, K.P. Oussoren¹⁰⁸, Q. Ouyang^{35a}, M. Owen⁵⁵, R.E. Owen¹⁹, V.E. Ozcan^{20a}, N. Ozturk⁸, K. Pachal¹⁴³, A. Pacheco Pages¹³, C. Padilla Aranda¹³, M. Pagáčová⁵⁰, S. Pagan Griso¹⁶, F. Paige²⁷, P. Pais⁸⁸, K. Pajchel¹²⁰, G. Palacino^{160b}, S. Palestini³², M. Palka^{40b}, D. Pallin³⁶, A. Palma^{127a,127b}, E.St. Panagiotopoulou¹⁰, C.E. Pandini⁸², J.G. Panduro Vazquez⁷⁹, P. Pani^{147a,147b}, S. Panitkin²⁷, D. Pantea^{28b}, L. Paolozzi⁵¹, Th.D. Papadopoulou¹⁰, K. Papageorgiou¹⁵⁵, A. Paramonov⁶, D. Paredes Hernandez¹⁷⁶, A.J. Parker⁷⁴, M.A. Parker³⁰, K.A. Parker¹⁴⁰, F. Parodi^{52a,52b}, J.A. Parsons³⁷, U. Parzefall⁵⁰, V.R. Pascuzzi¹⁵⁹, E. Pasqualucci^{133a}, S. Passaggio^{52a}, Fr. Pastore⁷⁹, G. Pásztor^{31,ag}, S. Pataraia¹⁷⁵, J.R. Pater⁸⁶, T. Pauly³², J. Pearce¹⁶⁹, B. Pearson¹¹⁴, L.E. Pedersen³⁸, M. Pedersen¹²⁰, S. Pedraza Lopez¹⁶⁷, R. Pedro^{127a,127b}, S.V. Peleganchuk^{110,c}, D. Pelikan¹⁶⁵, O. Penc¹²⁸, C. Peng^{35a}, H. Peng^{35b}, J. Penwell⁶³, B.S. Peralva^{26b}, M.M. Perego¹³⁷, D.V. Perepelitsa²⁷, E. Perez Codina^{160a}, L. Perini^{93a,93b}, H. Pernegger³², S. Perrella^{105a,105b}, R. Peschke⁴⁴, V.D. Peshekhanov⁶⁷, K. Peters⁴⁴, R.F.Y. Peters⁸⁶, B.A. Petersen³², T.C. Petersen³⁸, E. Petit⁵⁷, A. Petridis¹, C. Petridou¹⁵⁵, P. Petroff¹¹⁸, E. Petrolo^{133a}, M. Petrov¹²¹, F. Petrucci^{135a,135b}, N.E. Pettersson⁸⁸, A. Peyaud¹³⁷, R. Pezoa^{34b}, P.W. Phillips¹³², G. Piacquadio¹⁴⁴, E. Pianori¹⁷⁰, A. Picazio⁸⁸, E. Piccaro⁷⁸, M. Piccinini^{22a,22b}, M.A. Pickering¹²¹, R. Piegaia²⁹, J.E. Pilcher³³, A.D. Pilkington⁸⁶, A.W.J. Pin⁸⁶, M. Pinamonti^{164a,164c,ah}, J.L. Pinfold³, A. Pingel³⁸, S. Pires⁸², H. Pirumov⁴⁴, M. Pitt¹⁷², L. Plazak^{145a}, M.-A. Pleier²⁷, V. Pleskot⁸⁵, E. Plotnikova⁶⁷, P. Plucinski⁹², D. Pluth⁶⁶, R. Poettgen^{147a,147b}, L. Poggioli¹¹⁸, D. Pohl²³, G. Polesello^{122a}, A. Poley⁴⁴, A. Pollicchio^{39a,39b}, R. Polifka¹⁵⁹, A. Polini^{22a}, C.S. Pollard⁵⁵, V. Polychronakos²⁷, K. Pommès³², L. Pontecorvo^{133a}, B.G. Pope⁹², G.A. Popeneciu^{28c}, D.S. Popovic¹⁴, A. Poppleton³², S. Pospisil¹²⁹, K. Potamianos¹⁶, I.N. Potrap⁶⁷, C.J. Potter³⁰, C.T. Potter¹¹⁷, G. Pouillard³², J. Poveda³², V. Pozdnyakov⁶⁷, M.E. Pozo Astigarraga³², P. Pralavorio⁸⁷, A. Pranko¹⁶, S. Prell⁶⁶, D. Price⁸⁶,

L.E. Price⁶, M. Primavera^{75a}, S. Prince⁸⁹, M. Proissl⁴⁸, K. Prokofiev^{62c}, F. Prokoshin^{34b},
 S. Protopopescu²⁷, J. Proudfoot⁶, M. Przybycien^{40a}, D. Puddu^{135a,135b}, D. Puldon¹⁴⁹, M. Purohit^{27,ai},
 P. Puzo¹¹⁸, J. Qian⁹¹, G. Qin⁵⁵, Y. Qin⁸⁶, A. Quadt⁵⁶, W.B. Quayle^{164a,164b}, M. Queitsch-Maitland⁸⁶,
 D. Quilty⁵⁵, S. Raddum¹²⁰, V. Radeka²⁷, V. Radescu^{60b}, S.K. Radhakrishnan¹⁴⁹, P. Radloff¹¹⁷,
 P. Rados⁹⁰, F. Ragusa^{93a,93b}, G. Rahal¹⁷⁸, J.A. Raine⁸⁶, S. Rajagopalan²⁷, M. Rammensee³²,
 C. Rangel-Smith¹⁶⁵, M.G. Ratti^{93a,93b}, F. Rauscher¹⁰¹, S. Rave⁸⁵, T. Ravenscroft⁵⁵, I. Ravinovich¹⁷²,
 M. Raymond³², A.L. Read¹²⁰, N.P. Readioff⁷⁶, M. Reale^{75a,75b}, D.M. Rebuzzi^{122a,122b}, A. Redelbach¹⁷⁴,
 G. Redlinger²⁷, R. Reece¹³⁸, K. Reeves⁴³, L. Rehnisch¹⁷, J. Reichert¹²³, H. Reisin²⁹, C. Rembser³²,
 H. Ren^{35a}, M. Rescigno^{133a}, S. Resconi^{93a}, O.L. Rezanova^{110,c}, P. Reznicek¹³⁰, R. Rezvani⁹⁶,
 R. Richter¹⁰², S. Richter⁸⁰, E. Richter-Was^{40b}, O. Ricken²³, M. Ridel⁸², P. Rieck¹⁷, C.J. Riegel¹⁷⁵,
 J. Rieger⁵⁶, O. Rifki¹¹⁴, M. Rijssenbeek¹⁴⁹, A. Rimoldi^{122a,122b}, M. Rimoldi¹⁸, L. Rinaldi^{22a}, B. Ristić⁵¹,
 E. Ritsch³², I. Riu¹³, F. Rizatdinova¹¹⁵, E. Rizvi⁷⁸, C. Rizzi¹³, S.H. Robertson^{89,l},
 A. Robichaud-Veronneau⁸⁹, D. Robinson³⁰, J.E.M. Robinson⁴⁴, A. Robson⁵⁵, C. Roda^{125a,125b},
 Y. Rodina⁸⁷, A. Rodriguez Perez¹³, D. Rodriguez Rodriguez¹⁶⁷, S. Roe³², C.S. Rogan⁵⁹, O. Røhne¹²⁰,
 J. Rojo^{aj}, A. Romaniouk⁹⁹, M. Romano^{22a,22b}, S.M. Romano Saez³⁶, E. Romero Adam¹⁶⁷,
 N. Rompotis¹³⁹, M. Ronzani⁵⁰, L. Roos⁸², E. Ros¹⁶⁷, S. Rosati^{133a}, K. Rosbach⁵⁰, P. Rose¹³⁸,
 O. Rosenthal¹⁴², N.-A. Rosien⁵⁶, V. Rossetti^{147a,147b}, E. Rossi^{105a,105b}, L.P. Rossi^{52a}, J.H.N. Rosten³⁰,
 R. Rosten¹³⁹, M. Rotaru^{28b}, I. Roth¹⁷², J. Rothberg¹³⁹, D. Rousseau¹¹⁸, C.R. Royon¹³⁷, A. Rozanov⁸⁷,
 Y. Rozen¹⁵³, X. Ruan^{146c}, F. Rubbo¹⁴⁴, M.S. Rudolph¹⁵⁹, F. Rühr⁵⁰, A. Ruiz-Martinez³¹, Z. Rurikova⁵⁰,
 N.A. Rusakovich⁶⁷, A. Ruschke¹⁰¹, H.L. Russell¹³⁹, J.P. Rutherford⁷, N. Ruthmann³², Y.F. Ryabov¹²⁴,
 M. Rybar¹⁶⁶, G. Rybkin¹¹⁸, S. Ryu⁶, A. Ryzhov¹³¹, G.F. Rzehor⁵⁶, A.F. Saavedra¹⁵¹, G. Sabato¹⁰⁸,
 S. Sacerdoti²⁹, H.F-W. Sadrozinski¹³⁸, R. Sadykov⁶⁷, F. Safai Tehrani^{133a}, P. Saha¹⁰⁹, M. Sahin soy^{60a},
 M. Saimpert¹³⁷, T. Saito¹⁵⁶, H. Sakamoto¹⁵⁶, Y. Sakurai¹⁷¹, G. Salamanna^{135a,135b}, A. Salamon^{134a,134b},
 J.E. Salazar Loyola^{34b}, D. Salek¹⁰⁸, P.H. Sales De Bruin¹³⁹, D. Salihagic¹⁰², A. Salnikov¹⁴⁴, J. Salt¹⁶⁷,
 D. Salvatore^{39a,39b}, F. Salvatore¹⁵⁰, A. Salvucci^{62a}, A. Salzburger³², D. Sammel⁵⁰, D. Sampsonidis¹⁵⁵,
 A. Sanchez^{105a,105b}, J. Sánchez¹⁶⁷, V. Sanchez Martinez¹⁶⁷, H. Sandaker¹²⁰, R.L. Sandbach⁷⁸,
 H.G. Sander⁸⁵, M. Sandhoff¹⁷⁵, C. Sandoval²¹, R. Sandstroem¹⁰², D.P.C. Sankey¹³², M. Sannino^{52a,52b},
 A. Sansoni⁴⁹, C. Santoni³⁶, R. Santonico^{134a,134b}, H. Santos^{127a}, I. Santoyo Castillo¹⁵⁰, K. Sapp¹²⁶,
 A. Sapronov⁶⁷, J.G. Saraiva^{127a,127d}, B. Sarrazin²³, O. Sasaki⁶⁸, Y. Sasaki¹⁵⁶, K. Sato¹⁶¹, G. Sauvage^{5,*},
 E. Sauvan⁵, G. Savage⁷⁹, P. Savard^{159,d}, C. Sawyer¹³², L. Sawyer^{81,q}, J. Saxon³³, C. Sbarra^{22a},
 A. Sbrizzi^{22a,22b}, T. Scanlon⁸⁰, D.A. Scannicchio¹⁶³, M. Scarcella¹⁵¹, V. Scarfone^{39a,39b},
 J. Schaarschmidt¹⁷², P. Schacht¹⁰², B.M. Schachtner¹⁰¹, D. Schaefer³², R. Schaefer⁴⁴, J. Schaeffer⁸⁵,
 S. Schaepe²³, S. Schaetzel^{60b}, U. Schäfer⁸⁵, A.C. Schaffer¹¹⁸, D. Schaile¹⁰¹, R.D. Schamberger¹⁴⁹,
 V. Scharf^{60a}, V.A. Schegelsky¹²⁴, D. Scheirich¹³⁰, M. Schernau¹⁶³, C. Schiavi^{52a,52b}, S. Schier¹³⁸,
 C. Schillo⁵⁰, M. Schioppa^{39a,39b}, S. Schlenker³², K.R. Schmidt-Sommerfeld¹⁰², K. Schmieden³²,
 C. Schmitt⁸⁵, S. Schmitt⁴⁴, S. Schmitz⁸⁵, B. Schneider^{160a}, U. Schnoor⁵⁰, L. Schoeffel¹³⁷,
 A. Schoening^{60b}, B.D. Schoenrock⁹², E. Schopf²³, M. Schott⁸⁵, J. Schovancova⁸, S. Schramm⁵¹,
 M. Schreyer¹⁷⁴, N. Schuh⁸⁵, M.J. Schultens²³, H.-C. Schultz-Coulon^{60a}, H. Schulz¹⁷, M. Schumacher⁵⁰,
 B.A. Schumm¹³⁸, Ph. Schune¹³⁷, A. Schwartzman¹⁴⁴, T.A. Schwarz⁹¹, Ph. Schwegler¹⁰²,
 H. Schweiger⁸⁶, Ph. Schwemling¹³⁷, R. Schwienhorst⁹², J. Schwindling¹³⁷, T. Schwindt²³, G. Sciolla²⁵,
 F. Scuri^{125a,125b}, F. Scutti⁹⁰, J. Searcy⁹¹, P. Seema²³, S.C. Seidel¹⁰⁶, A. Seiden¹³⁸, F. Seifert¹²⁹,
 J.M. Seixas^{26a}, G. Sekhniaidze^{105a}, K. Sekhon⁹¹, S.J. Sekula⁴², D.M. Seliverstov^{124,*},
 N. Semprini-Cesari^{22a,22b}, C. Serfon¹²⁰, L. Serin¹¹⁸, L. Serkin^{164a,164b}, M. Sessa^{135a,135b}, R. Seuster¹⁶⁹,
 H. Severini¹¹⁴, T. Sfiligoj⁷⁷, F. Sforza³², A. Sfyrla⁵¹, E. Shabalina⁵⁶, N.W. Shaikh^{147a,147b}, L.Y. Shan^{35a},
 R. Shang¹⁶⁶, J.T. Shank²⁴, M. Shapiro¹⁶, P.B. Shatalov⁹⁸, K. Shaw^{164a,164b}, S.M. Shaw⁸⁶,
 A. Shcherbakova^{147a,147b}, C.Y. Shehu¹⁵⁰, P. Sherwood⁸⁰, L. Shi^{152,ak}, S. Shimizu⁶⁹, C.O. Shimmin¹⁶³,
 M. Shimojima¹⁰³, M. Shiyakova^{67,al}, A. Shmeleva⁹⁷, D. Shoaleh Saadi⁹⁶, M.J. Shochet³³,

S. Shojaii^{93a,93b}, S. Shrestha¹¹², E. Shulga⁹⁹, M.A. Shupe⁷, P. Sicho¹²⁸, A.M. Sickles¹⁶⁶, P.E. Sidebo¹⁴⁸, O. Sidiropoulou¹⁷⁴, D. Sidorov¹¹⁵, A. Sidoti^{22a,22b}, F. Siegert⁴⁶, Dj. Sijacki¹⁴, J. Silva^{127a,127d}, S.B. Silverstein^{147a}, V. Simak¹²⁹, O. Simard⁵, Lj. Simic¹⁴, S. Simion¹¹⁸, E. Simioni⁸⁵, B. Simmons⁸⁰, D. Simon³⁶, M. Simon⁸⁵, P. Sinervo¹⁵⁹, N.B. Sinev¹¹⁷, M. Sioli^{22a,22b}, G. Siragusa¹⁷⁴, S.Yu. Sivoklokov¹⁰⁰, J. Sjölin^{147a,147b}, T.B. Sjursen¹⁵, M.B. Skinner⁷⁴, H.P. Skottowe⁵⁹, P. Skubic¹¹⁴, M. Slater¹⁹, T. Slavicek¹²⁹, M. Slawinska¹⁰⁸, K. Sliwa¹⁶², R. Slovak¹³⁰, V. Smakhtin¹⁷², B.H. Smart⁵, L. Smestad¹⁵, J. Smiesko^{145a}, S.Yu. Smirnov⁹⁹, Y. Smirnov⁹⁹, L.N. Smirnova^{100,am}, O. Smirnova⁸³, M.N.K. Smith³⁷, R.W. Smith³⁷, M. Smizanska⁷⁴, K. Smolek¹²⁹, A.A. Snesarev⁹⁷, S. Snyder²⁷, R. Sobie^{169,l}, F. Socher⁴⁶, A. Soffer¹⁵⁴, D.A. Soh¹⁵², G. Sokhrannyi⁷⁷, C.A. Solans Sanchez³², M. Solar¹²⁹, E.Yu. Soldatov⁹⁹, U. Soldevila¹⁶⁷, A.A. Solodkov¹³¹, A. Soloshenko⁶⁷, O.V. Solovyanov¹³¹, V. Solovyev¹²⁴, P. Sommer⁵⁰, H. Son¹⁶², H.Y. Song^{35b,an}, A. Sood¹⁶, A. Sopczak¹²⁹, V. Sopko¹²⁹, V. Sorin¹³, D. Sosa^{60b}, C.L. Sotiropoulou^{125a,125b}, R. Soualah^{164a,164c}, A.M. Soukharev^{110,c}, D. South⁴⁴, B.C. Sowden⁷⁹, S. Spagnolo^{75a,75b}, M. Spalla^{125a,125b}, M. Spangenberg¹⁷⁰, F. Spanò⁷⁹, D. Sperlich¹⁷, F. Spettel¹⁰², R. Spighi^{22a}, G. Spigo³², L.A. Spiller⁹⁰, M. Spousta¹³⁰, R.D. St. Denis^{55,*}, A. Stabile^{93a}, R. Stamen^{60a}, S. Stamm¹⁷, E. Stanecka⁴¹, R.W. Stanek⁶, C. Stanescu^{135a}, M. Stanescu-Bellu⁴⁴, M.M. Stanitzki⁴⁴, S. Stapnes¹²⁰, E.A. Starchenko¹³¹, G.H. Stark³³, J. Stark⁵⁷, P. Staroba¹²⁸, P. Starovoitov^{60a}, S. Stärz³², R. Staszewski⁴¹, P. Steinberg²⁷, B. Stelzer¹⁴³, H.J. Stelzer³², O. Stelzer-Chilton^{160a}, H. Stenzel⁵⁴, G.A. Stewart⁵⁵, J.A. Stillings²³, M.C. Stockton⁸⁹, M. Stoebe⁸⁹, G. Stoica^{28b}, P. Stolte⁵⁶, S. Stonjek¹⁰², A.R. Stradling⁸, A. Straessner⁴⁶, M.E. Stramaglia¹⁸, J. Strandberg¹⁴⁸, S. Strandberg^{147a,147b}, A. Strandlie¹²⁰, M. Strauss¹¹⁴, P. Strizenec^{145b}, R. Ströhmer¹⁷⁴, D.M. Strom¹¹⁷, R. Stroynowski⁴², A. Strubig¹⁰⁷, S.A. Stucci¹⁸, B. Stugu¹⁵, N.A. Styles⁴⁴, D. Su¹⁴⁴, J. Su¹²⁶, R. Subramaniam⁸¹, S. Suchek^{60a}, Y. Sugaya¹¹⁹, M. Suk¹²⁹, V.V. Sulin⁹⁷, S. Sultansoy^{4c}, T. Sumida⁷⁰, S. Sun⁵⁹, X. Sun^{35a}, J.E. Sundermann⁵⁰, K. Suruliz¹⁵⁰, G. Susinno^{39a,39b}, M.R. Sutton¹⁵⁰, S. Suzuki⁶⁸, M. Svatos¹²⁸, M. Swiatlowski³³, I. Sykora^{145a}, T. Sykora¹³⁰, D. Ta⁵⁰, C. Taccini^{135a,135b}, K. Tackmann⁴⁴, J. Taenzer¹⁵⁹, A. Taffard¹⁶³, R. Tafirout^{160a}, N. Taiblum¹⁵⁴, H. Takai²⁷, R. Takashima⁷¹, T. Takeshita¹⁴¹, Y. Takubo⁶⁸, M. Talby⁸⁷, A.A. Talyshev^{110,c}, K.G. Tan⁹⁰, J. Tanaka¹⁵⁶, R. Tanaka¹¹⁸, S. Tanaka⁶⁸, B.B. Tannenwald¹¹², S. Tapia Araya^{34b}, S. Tapprogge⁸⁵, S. Tarem¹⁵³, G.F. Tartarelli^{93a}, P. Tas¹³⁰, M. Tasevsky¹²⁸, T. Tashiro⁷⁰, E. Tassi^{39a,39b}, A. Tavares Delgado^{127a,127b}, Y. Tayalati^{136d}, A.C. Taylor¹⁰⁶, G.N. Taylor⁹⁰, P.T.E. Taylor⁹⁰, W. Taylor^{160b}, F.A. Teischinger³², P. Teixeira-Dias⁷⁹, K.K. Temming⁵⁰, D. Temple¹⁴³, H. Ten Kate³², P.K. Teng¹⁵², J.J. Teoh¹¹⁹, F. Tepel¹⁷⁵, S. Terada⁶⁸, K. Terashi¹⁵⁶, J. Terron⁸⁴, S. Terzo¹⁰², M. Testa⁴⁹, R.J. Teuscher^{159,l}, T. Theveneaux-Pelzer⁸⁷, J.P. Thomas¹⁹, J. Thomas-Wilsker⁷⁹, E.N. Thompson³⁷, P.D. Thompson¹⁹, A.S. Thompson⁵⁵, L.A. Thomsen¹⁷⁶, E. Thomson¹²³, M. Thomson³⁰, M.J. Tibbetts¹⁶, R.E. Ticse Torres⁸⁷, V.O. Tikhomirov^{97,ao}, Yu.A. Tikhonov^{110,c}, S. Timoshenko⁹⁹, P. Tipton¹⁷⁶, S. Tisserant⁸⁷, K. Todome¹⁵⁸, T. Todorov^{5,*}, S. Todorova-Nova¹³⁰, J. Tojo⁷², S. Tokár^{145a}, K. Tokushuku⁶⁸, E. Tolley⁵⁹, L. Tomlinson⁸⁶, M. Tomoto¹⁰⁴, L. Tompkins^{144,ap}, K. Toms¹⁰⁶, B. Tong⁵⁹, E. Torrence¹¹⁷, H. Torres¹⁴³, E. Torró Pastor¹³⁹, J. Toth^{87,ag}, F. Touchard⁸⁷, D.R. Tovey¹⁴⁰, T. Trefzger¹⁷⁴, A. Tricoli²⁷, I.M. Trigger^{160a}, S. Trincaz-Duvold⁸², M.F. Tripiana¹³, W. Trischuk¹⁵⁹, B. Trocmé⁵⁷, A. Trofymov⁴⁴, C. Troncon^{93a}, M. Trottier-McDonald¹⁶, M. Trovatelli¹⁶⁹, L. Truong^{164a,164c}, M. Trzebinski⁴¹, A. Trzupek⁴¹, J.C-L. Tseng¹²¹, P.V. Tsiareshka⁹⁴, G. Tsipolitis¹⁰, N. Tsirintanis⁹, S. Tsiskaridze¹³, V. Tsiskaridze⁵⁰, E.G. Tskhadadze^{53a}, K.M. Tsui^{62a}, I.I. Tsukerman⁹⁸, V. Tsulaia¹⁶, S. Tsuno⁶⁸, D. Tsybychev¹⁴⁹, A. Tudorache^{28b}, V. Tudorache^{28b}, A.N. Tuna⁵⁹, S.A. Tupputi^{22a,22b}, S. Turchikhin^{100,am}, D. Turecek¹²⁹, D. Turgeman¹⁷², R. Turra^{93a,93b}, A.J. Turvey⁴², P.M. Tuts³⁷, M. Tyndel¹³², G. Ucchielli^{22a,22b}, I. Ueda¹⁵⁶, R. Ueno³¹, M. Ughetto^{147a,147b}, F. Ukegawa¹⁶¹, G. Unal³², A. Undrus²⁷, G. Unel¹⁶³, F.C. Ungaro⁹⁰, Y. Unno⁶⁸, C. Unverdorben¹⁰¹, J. Urban^{145b}, P. Urquijo⁹⁰, P. Urrejola⁸⁵, G. Usai⁸, A. Usanova⁶⁴, L. Vacavant⁸⁷, V. Vacek¹²⁹, B. Vachon⁸⁹, C. Valderanis¹⁰¹, E. Valdes Santurio^{147a,147b}, N. Valencic¹⁰⁸, S. Valentinetto^{22a,22b},

A. Valero¹⁶⁷, L. Valery¹³, S. Valkar¹³⁰, S. Vallecorsa⁵¹, J.A. Valls Ferrer¹⁶⁷, W. Van Den Wollenberg¹⁰⁸, P.C. Van Der Deijl¹⁰⁸, R. van der Geer¹⁰⁸, H. van der Graaf¹⁰⁸, N. van Eldik¹⁵³, P. van Gemmeren⁶, J. Van Nieuwkoop¹⁴³, I. van Vulpen¹⁰⁸, M.C. van Woerden³², M. Vanadia^{133a,133b}, W. Vandelli³², R. Vanguri¹²³, A. Vaniachine⁶, P. Vankov¹⁰⁸, G. Vardanyan¹⁷⁷, R. Vari^{133a}, E.W. Varnes⁷, T. Varol⁴², D. Varouchas⁸², A. Vartapetian⁸, K.E. Varvell¹⁵¹, J.G. Vasquez¹⁷⁶, F. Vazeille³⁶, T. Vazquez Schroeder⁸⁹, J. Veatch⁵⁶, L.M. Veloce¹⁵⁹, F. Veloso^{127a,127c}, S. Veneziano^{133a}, A. Ventura^{75a,75b}, M. Venturi¹⁶⁹, N. Venturi¹⁵⁹, A. Venturini²⁵, V. Vercesi^{122a}, M. Verducci^{133a,133b}, W. Verkerke¹⁰⁸, J.C. Vermeulen¹⁰⁸, A. Vest^{46,ar}, M.C. Vetterli^{143,d}, O. Viazlo⁸³, I. Vichou¹⁶⁶, T. Vickey¹⁴⁰, O.E. Vickey Boeriu¹⁴⁰, G.H.A. Viehhauser¹²¹, S. Viel¹⁶, L. Vigani¹²¹, R. Vigne⁶⁴, M. Villa^{22a,22b}, M. Villaplana Perez^{93a,93b}, E. Vilucchi⁴⁹, M.G. Vincter³¹, V.B. Vinogradov⁶⁷, C. Vittori^{22a,22b}, I. Vivarelli¹⁵⁰, S. Vlachos¹⁰, M. Vlasak¹²⁹, M. Vogel¹⁷⁵, P. Vokac¹²⁹, G. Volpi^{125a,125b}, M. Volpi⁹⁰, H. von der Schmitt¹⁰², E. von Toerne²³, V. Vorobel¹³⁰, K. Vorobev⁹⁹, M. Vos¹⁶⁷, R. Voss³², J.H. Vossebeld⁷⁶, N. Vranjes¹⁴, M. Vranjes Milosavljevic¹⁴, V. Vrba¹²⁸, M. Vreeswijk¹⁰⁸, R. Vuillermet³², I. Vukotic³³, Z. Vykydal¹²⁹, P. Wagner²³, W. Wagner¹⁷⁵, H. Wahlberg⁷³, S. Wahrmund⁴⁶, J. Wakabayashi¹⁰⁴, J. Walder⁷⁴, R. Walker¹⁰¹, W. Walkowiak¹⁴², V. Wallangen^{147a,147b}, C. Wang^{35c}, C. Wang^{35d,87}, F. Wang¹⁷³, H. Wang¹⁶, H. Wang⁴², J. Wang⁴⁴, J. Wang¹⁵¹, K. Wang⁸⁹, R. Wang⁶, S.M. Wang¹⁵², T. Wang²³, T. Wang³⁷, W. Wang^{35b}, X. Wang¹⁷⁶, C. Wanotayaroj¹¹⁷, A. Warburton⁸⁹, C.P. Ward³⁰, D.R. Wardrop⁸⁰, A. Washbrook⁴⁸, P.M. Watkins¹⁹, A.T. Watson¹⁹, M.F. Watson¹⁹, G. Watts¹³⁹, S. Watts⁸⁶, B.M. Waugh⁸⁰, S. Webb⁸⁵, M.S. Weber¹⁸, S.W. Weber¹⁷⁴, J.S. Webster⁶, A.R. Weidberg¹²¹, B. Weinert⁶³, J. Weingarten⁵⁶, C. Weiser⁵⁰, H. Weits¹⁰⁸, P.S. Wells³², T. Wenaus²⁷, T. Wengler³², S. Wenig³², N. Wermes²³, M. Werner⁵⁰, P. Werner³², M. Wessels^{60a}, J. Wetter¹⁶², K. Whalen¹¹⁷, N.L. Whallon¹³⁹, A.M. Wharton⁷⁴, A. White⁸, M.J. White¹, R. White^{34b}, D. Whiteson¹⁶³, F.J. Wickens¹³², W. Wiedenmann¹⁷³, M. Wielers¹³², P. Wienemann²³, C. Wiglesworth³⁸, L.A.M. Wiik-Fuchs²³, A. Wildauer¹⁰², F. Wilk⁸⁶, H.G. Wilkens³², H.H. Williams¹²³, S. Williams¹⁰⁸, C. Willis⁹², S. Willocq⁸⁸, J.A. Wilson¹⁹, I. Wingerter-Seez⁵, F. Winklmeier¹¹⁷, O.J. Winston¹⁵⁰, B.T. Winter²³, M. Wittgen¹⁴⁴, J. Wittkowski¹⁰¹, S.J. Wollstadt⁸⁵, M.W. Wolter⁴¹, H. Wolters^{127a,127c}, B.K. Wosiek⁴¹, J. Wotschack³², M.J. Woudstra⁸⁶, K.W. Wozniak⁴¹, M. Wu⁵⁷, M. Wu³³, S.L. Wu¹⁷³, X. Wu⁵¹, Y. Wu⁹¹, T.R. Wyatt⁸⁶, B.M. Wynne⁴⁸, S. Xella³⁸, D. Xu^{35a}, L. Xu²⁷, B. Yabsley¹⁵¹, S. Yacoob^{146a}, R. Yakabe⁶⁹, D. Yamaguchi¹⁵⁸, Y. Yamaguchi¹¹⁹, A. Yamamoto⁶⁸, S. Yamamoto¹⁵⁶, T. Yamanaka¹⁵⁶, K. Yamauchi¹⁰⁴, Y. Yamazaki⁶⁹, Z. Yan²⁴, H. Yang^{35e}, H. Yang¹⁷³, Y. Yang¹⁵², Z. Yang¹⁵, W-M. Yao¹⁶, Y.C. Yap⁸², Y. Yasu⁶⁸, E. Yatsenko⁵, K.H. Yau Wong²³, J. Ye⁴², S. Ye²⁷, I. Yeletskikh⁶⁷, A.L. Yen⁵⁹, E. Yildirim⁸⁵, K. Yorita¹⁷¹, R. Yoshida⁶, K. Yoshihara¹²³, C. Young¹⁴⁴, C.J.S. Young³², S. Youssef²⁴, D.R. Yu¹⁶, J. Yu⁸, J.M. Yu⁹¹, J. Yu⁶⁶, L. Yuan⁶⁹, S.P.Y. Yuen²³, I. Yusuff^{30,as}, B. Zabinski⁴¹, R. Zaidan^{35d}, A.M. Zaitsev^{131,ae}, N. Zakharchuk⁴⁴, J. Zalieckas¹⁵, A. Zaman¹⁴⁹, S. Zambito⁵⁹, L. Zanello^{133a,133b}, D. Zanzi⁹⁰, C. Zeitnitz¹⁷⁵, M. Zeman¹²⁹, A. Zemla^{40a}, J.C. Zeng¹⁶⁶, Q. Zeng¹⁴⁴, K. Zengel²⁵, O. Zenin¹³¹, T. Ženiš^{145a}, D. Zerwas¹¹⁸, D. Zhang⁹¹, F. Zhang¹⁷³, G. Zhang^{35b,an}, H. Zhang^{35c}, J. Zhang⁶, L. Zhang⁵⁰, R. Zhang²³, R. Zhang^{35b,at}, X. Zhang^{35d}, Z. Zhang¹¹⁸, X. Zhao⁴², Y. Zhao^{35d}, Z. Zhao^{35b}, A. Zhemchugov⁶⁷, J. Zhong¹²¹, B. Zhou⁹¹, C. Zhou⁴⁷, L. Zhou³⁷, L. Zhou⁴², M. Zhou¹⁴⁹, N. Zhou^{35f}, C.G. Zhu^{35d}, H. Zhu^{35a}, J. Zhu⁹¹, Y. Zhu^{35b}, X. Zhuang^{35a}, K. Zhukov⁹⁷, A. Zibell¹⁷⁴, D. Ziemińska⁶³, N.I. Zimine⁶⁷, C. Zimmermann⁸⁵, S. Zimmermann⁵⁰, Z. Zinonos⁵⁶, M. Zinser⁸⁵, M. Ziolkowski¹⁴², L. Živković¹⁴, G. Zobernig¹⁷³, A. Zoccoli^{22a,22b}, M. zur Nedden¹⁷, G. Zurzolo^{105a,105b}, L. Zwalski³².

¹ Department of Physics, University of Adelaide, Adelaide, Australia

² Physics Department, SUNY Albany, Albany NY, United States of America

³ Department of Physics, University of Alberta, Edmonton AB, Canada

⁴ ^(a) Department of Physics, Ankara University, Ankara; ^(b) Istanbul Aydin University, Istanbul; ^(c)

- Division of Physics, TOBB University of Economics and Technology, Ankara, Turkey
- ⁵ LAPP, CNRS/IN2P3 and Université Savoie Mont Blanc, Annecy-le-Vieux, France
- ⁶ High Energy Physics Division, Argonne National Laboratory, Argonne IL, United States of America
- ⁷ Department of Physics, University of Arizona, Tucson AZ, United States of America
- ⁸ Department of Physics, The University of Texas at Arlington, Arlington TX, United States of America
- ⁹ Physics Department, University of Athens, Athens, Greece
- ¹⁰ Physics Department, National Technical University of Athens, Zografou, Greece
- ¹¹ Department of Physics, The University of Texas at Austin, Austin TX, United States of America
- ¹² Institute of Physics, Azerbaijan Academy of Sciences, Baku, Azerbaijan
- ¹³ Institut de Física d'Altes Energies (IFAE), The Barcelona Institute of Science and Technology, Barcelona, Spain, Spain
- ¹⁴ Institute of Physics, University of Belgrade, Belgrade, Serbia
- ¹⁵ Department for Physics and Technology, University of Bergen, Bergen, Norway
- ¹⁶ Physics Division, Lawrence Berkeley National Laboratory and University of California, Berkeley CA, United States of America
- ¹⁷ Department of Physics, Humboldt University, Berlin, Germany
- ¹⁸ Albert Einstein Center for Fundamental Physics and Laboratory for High Energy Physics, University of Bern, Bern, Switzerland
- ¹⁹ School of Physics and Astronomy, University of Birmingham, Birmingham, United Kingdom
- ²⁰ ^(a) Department of Physics, Bogazici University, Istanbul; ^(b) Department of Physics Engineering, Gaziantep University, Gaziantep; ^(d) Istanbul Bilgi University, Faculty of Engineering and Natural Sciences, Istanbul, Turkey; ^(e) Bahcesehir University, Faculty of Engineering and Natural Sciences, Istanbul, Turkey, Turkey
- ²¹ Centro de Investigaciones, Universidad Antonio Narino, Bogota, Colombia
- ²² ^(a) INFN Sezione di Bologna; ^(b) Dipartimento di Fisica e Astronomia, Università di Bologna, Bologna, Italy
- ²³ Physikalisches Institut, University of Bonn, Bonn, Germany
- ²⁴ Department of Physics, Boston University, Boston MA, United States of America
- ²⁵ Department of Physics, Brandeis University, Waltham MA, United States of America
- ²⁶ ^(a) Universidade Federal do Rio De Janeiro COPPE/EE/IF, Rio de Janeiro; ^(b) Electrical Circuits Department, Federal University of Juiz de Fora (UFJF), Juiz de Fora; ^(c) Federal University of Sao Joao del Rei (UFSJ), Sao Joao del Rei; ^(d) Instituto de Fisica, Universidade de Sao Paulo, Sao Paulo, Brazil
- ²⁷ Physics Department, Brookhaven National Laboratory, Upton NY, United States of America
- ²⁸ ^(a) Transilvania University of Brasov, Brasov, Romania; ^(b) National Institute of Physics and Nuclear Engineering, Bucharest; ^(c) National Institute for Research and Development of Isotopic and Molecular Technologies, Physics Department, Cluj Napoca; ^(d) University Politehnica Bucharest, Bucharest; ^(e) West University in Timisoara, Timisoara, Romania
- ²⁹ Departamento de Física, Universidad de Buenos Aires, Buenos Aires, Argentina
- ³⁰ Cavendish Laboratory, University of Cambridge, Cambridge, United Kingdom
- ³¹ Department of Physics, Carleton University, Ottawa ON, Canada
- ³² CERN, Geneva, Switzerland
- ³³ Enrico Fermi Institute, University of Chicago, Chicago IL, United States of America
- ³⁴ ^(a) Departamento de Física, Pontificia Universidad Católica de Chile, Santiago; ^(b) Departamento de Física, Universidad Técnica Federico Santa María, Valparaíso, Chile
- ³⁵ ^(a) Institute of High Energy Physics, Chinese Academy of Sciences, Beijing; ^(b) Department of Modern Physics, University of Science and Technology of China, Anhui; ^(c) Department of Physics, Nanjing University, Jiangsu; ^(d) School of Physics, Shandong University, Shandong; ^(e) Department of

Physics and Astronomy, Shanghai Key Laboratory for Particle Physics and Cosmology, Shanghai Jiao Tong University, Shanghai; (also affiliated with PKU-CHEP); ^(f) Physics Department, Tsinghua University, Beijing 100084, China

³⁶ Laboratoire de Physique Corpusculaire, Clermont Université and Université Blaise Pascal and CNRS/IN2P3, Clermont-Ferrand, France

³⁷ Nevis Laboratory, Columbia University, Irvington NY, United States of America

³⁸ Niels Bohr Institute, University of Copenhagen, Kobenhavn, Denmark

³⁹ ^(a) INFN Gruppo Collegato di Cosenza, Laboratori Nazionali di Frascati; ^(b) Dipartimento di Fisica, Università della Calabria, Rende, Italy

⁴⁰ ^(a) AGH University of Science and Technology, Faculty of Physics and Applied Computer Science, Krakow; ^(b) Marian Smoluchowski Institute of Physics, Jagiellonian University, Krakow, Poland

⁴¹ Institute of Nuclear Physics Polish Academy of Sciences, Krakow, Poland

⁴² Physics Department, Southern Methodist University, Dallas TX, United States of America

⁴³ Physics Department, University of Texas at Dallas, Richardson TX, United States of America

⁴⁴ DESY, Hamburg and Zeuthen, Germany

⁴⁵ Institut für Experimentelle Physik IV, Technische Universität Dortmund, Dortmund, Germany

⁴⁶ Institut für Kern- und Teilchenphysik, Technische Universität Dresden, Dresden, Germany

⁴⁷ Department of Physics, Duke University, Durham NC, United States of America

⁴⁸ SUPA - School of Physics and Astronomy, University of Edinburgh, Edinburgh, United Kingdom

⁴⁹ INFN Laboratori Nazionali di Frascati, Frascati, Italy

⁵⁰ Fakultät für Mathematik und Physik, Albert-Ludwigs-Universität, Freiburg, Germany

⁵¹ Section de Physique, Université de Genève, Geneva, Switzerland

⁵² ^(a) INFN Sezione di Genova; ^(b) Dipartimento di Fisica, Università di Genova, Genova, Italy

⁵³ ^(a) E. Andronikashvili Institute of Physics, Iv. Javakhishvili Tbilisi State University, Tbilisi; ^(b) High Energy Physics Institute, Tbilisi State University, Tbilisi, Georgia

⁵⁴ II Physikalisches Institut, Justus-Liebig-Universität Giessen, Giessen, Germany

⁵⁵ SUPA - School of Physics and Astronomy, University of Glasgow, Glasgow, United Kingdom

⁵⁶ II Physikalisches Institut, Georg-August-Universität, Göttingen, Germany

⁵⁷ Laboratoire de Physique Subatomique et de Cosmologie, Université Grenoble-Alpes, CNRS/IN2P3, Grenoble, France

⁵⁸ Department of Physics, Hampton University, Hampton VA, United States of America

⁵⁹ Laboratory for Particle Physics and Cosmology, Harvard University, Cambridge MA, United States of America

⁶⁰ ^(a) Kirchhoff-Institut für Physik, Ruprecht-Karls-Universität Heidelberg, Heidelberg; ^(b) Physikalisches Institut, Ruprecht-Karls-Universität Heidelberg, Heidelberg; ^(c) ZITI Institut für technische Informatik, Ruprecht-Karls-Universität Heidelberg, Mannheim, Germany

⁶¹ Faculty of Applied Information Science, Hiroshima Institute of Technology, Hiroshima, Japan

⁶² ^(a) Department of Physics, The Chinese University of Hong Kong, Shatin, N.T., Hong Kong; ^(b) Department of Physics, The University of Hong Kong, Hong Kong; ^(c) Department of Physics, The Hong Kong University of Science and Technology, Clear Water Bay, Kowloon, Hong Kong, China

⁶³ Department of Physics, Indiana University, Bloomington IN, United States of America

⁶⁴ Institut für Astro- und Teilchenphysik, Leopold-Franzens-Universität, Innsbruck, Austria

⁶⁵ University of Iowa, Iowa City IA, United States of America

⁶⁶ Department of Physics and Astronomy, Iowa State University, Ames IA, United States of America

⁶⁷ Joint Institute for Nuclear Research, JINR Dubna, Dubna, Russia

⁶⁸ KEK, High Energy Accelerator Research Organization, Tsukuba, Japan

⁶⁹ Graduate School of Science, Kobe University, Kobe, Japan

- ⁷⁰ Faculty of Science, Kyoto University, Kyoto, Japan
⁷¹ Kyoto University of Education, Kyoto, Japan
⁷² Department of Physics, Kyushu University, Fukuoka, Japan
⁷³ Instituto de Física La Plata, Universidad Nacional de La Plata and CONICET, La Plata, Argentina
⁷⁴ Physics Department, Lancaster University, Lancaster, United Kingdom
⁷⁵ ^(a) INFN Sezione di Lecce; ^(b) Dipartimento di Matematica e Fisica, Università del Salento, Lecce, Italy
⁷⁶ Oliver Lodge Laboratory, University of Liverpool, Liverpool, United Kingdom
⁷⁷ Department of Physics, Jožef Stefan Institute and University of Ljubljana, Ljubljana, Slovenia
⁷⁸ School of Physics and Astronomy, Queen Mary University of London, London, United Kingdom
⁷⁹ Department of Physics, Royal Holloway University of London, Surrey, United Kingdom
⁸⁰ Department of Physics and Astronomy, University College London, London, United Kingdom
⁸¹ Louisiana Tech University, Ruston LA, United States of America
⁸² Laboratoire de Physique Nucléaire et de Hautes Energies, UPMC and Université Paris-Diderot and CNRS/IN2P3, Paris, France
⁸³ Fysiska institutionen, Lunds universitet, Lund, Sweden
⁸⁴ Departamento de Fisica Teorica C-15, Universidad Autonoma de Madrid, Madrid, Spain
⁸⁵ Institut für Physik, Universität Mainz, Mainz, Germany
⁸⁶ School of Physics and Astronomy, University of Manchester, Manchester, United Kingdom
⁸⁷ CPPM, Aix-Marseille Université and CNRS/IN2P3, Marseille, France
⁸⁸ Department of Physics, University of Massachusetts, Amherst MA, United States of America
⁸⁹ Department of Physics, McGill University, Montreal QC, Canada
⁹⁰ School of Physics, University of Melbourne, Victoria, Australia
⁹¹ Department of Physics, The University of Michigan, Ann Arbor MI, United States of America
⁹² Department of Physics and Astronomy, Michigan State University, East Lansing MI, United States of America
⁹³ ^(a) INFN Sezione di Milano; ^(b) Dipartimento di Fisica, Università di Milano, Milano, Italy
⁹⁴ B.I. Stepanov Institute of Physics, National Academy of Sciences of Belarus, Minsk, Republic of Belarus
⁹⁵ National Scientific and Educational Centre for Particle and High Energy Physics, Minsk, Republic of Belarus
⁹⁶ Group of Particle Physics, University of Montreal, Montreal QC, Canada
⁹⁷ P.N. Lebedev Physical Institute of the Russian Academy of Sciences, Moscow, Russia
⁹⁸ Institute for Theoretical and Experimental Physics (ITEP), Moscow, Russia
⁹⁹ National Research Nuclear University MEPhI, Moscow, Russia
¹⁰⁰ D.V. Skobeltsyn Institute of Nuclear Physics, M.V. Lomonosov Moscow State University, Moscow, Russia
¹⁰¹ Fakultät für Physik, Ludwig-Maximilians-Universität München, München, Germany
¹⁰² Max-Planck-Institut für Physik (Werner-Heisenberg-Institut), München, Germany
¹⁰³ Nagasaki Institute of Applied Science, Nagasaki, Japan
¹⁰⁴ Graduate School of Science and Kobayashi-Maskawa Institute, Nagoya University, Nagoya, Japan
¹⁰⁵ ^(a) INFN Sezione di Napoli; ^(b) Dipartimento di Fisica, Università di Napoli, Napoli, Italy
¹⁰⁶ Department of Physics and Astronomy, University of New Mexico, Albuquerque NM, United States of America
¹⁰⁷ Institute for Mathematics, Astrophysics and Particle Physics, Radboud University Nijmegen/Nikhef, Nijmegen, Netherlands
¹⁰⁸ Nikhef National Institute for Subatomic Physics and University of Amsterdam, Amsterdam,

Netherlands

¹⁰⁹ Department of Physics, Northern Illinois University, DeKalb IL, United States of America

¹¹⁰ Budker Institute of Nuclear Physics, SB RAS, Novosibirsk, Russia

¹¹¹ Department of Physics, New York University, New York NY, United States of America

¹¹² Ohio State University, Columbus OH, United States of America

¹¹³ Faculty of Science, Okayama University, Okayama, Japan

¹¹⁴ Homer L. Dodge Department of Physics and Astronomy, University of Oklahoma, Norman OK, United States of America

¹¹⁵ Department of Physics, Oklahoma State University, Stillwater OK, United States of America

¹¹⁶ Palacký University, RCPTM, Olomouc, Czech Republic

¹¹⁷ Center for High Energy Physics, University of Oregon, Eugene OR, United States of America

¹¹⁸ LAL, Univ. Paris-Sud, CNRS/IN2P3, Université Paris-Saclay, Orsay, France

¹¹⁹ Graduate School of Science, Osaka University, Osaka, Japan

¹²⁰ Department of Physics, University of Oslo, Oslo, Norway

¹²¹ Department of Physics, Oxford University, Oxford, United Kingdom

¹²² ^(a) INFN Sezione di Pavia; ^(b) Dipartimento di Fisica, Università di Pavia, Pavia, Italy

¹²³ Department of Physics, University of Pennsylvania, Philadelphia PA, United States of America

¹²⁴ National Research Centre "Kurchatov Institute" B.P.Konstantinov Petersburg Nuclear Physics Institute, St. Petersburg, Russia

¹²⁵ ^(a) INFN Sezione di Pisa; ^(b) Dipartimento di Fisica E. Fermi, Università di Pisa, Pisa, Italy

¹²⁶ Department of Physics and Astronomy, University of Pittsburgh, Pittsburgh PA, United States of America

¹²⁷ ^(a) Laboratório de Instrumentação e Física Experimental de Partículas - LIP, Lisboa; ^(b) Faculdade de Ciências, Universidade de Lisboa, Lisboa; ^(c) Department of Physics, University of Coimbra, Coimbra; ^(d) Centro de Física Nuclear da Universidade de Lisboa, Lisboa; ^(e) Departamento de Física, Universidade do Minho, Braga; ^(f) Departamento de Física Teórica y del Cosmos and CAFPE, Universidad de Granada, Granada (Spain); ^(g) Dep Física and CEFITEC of Faculdade de Ciencias e Tecnologia, Universidade Nova de Lisboa, Caparica, Portugal

¹²⁸ Institute of Physics, Academy of Sciences of the Czech Republic, Praha, Czech Republic

¹²⁹ Czech Technical University in Prague, Praha, Czech Republic

¹³⁰ Faculty of Mathematics and Physics, Charles University in Prague, Praha, Czech Republic

¹³¹ State Research Center Institute for High Energy Physics (Protvino), NRC KI, Russia

¹³² Particle Physics Department, Rutherford Appleton Laboratory, Didcot, United Kingdom

¹³³ ^(a) INFN Sezione di Roma; ^(b) Dipartimento di Fisica, Sapienza Università di Roma, Roma, Italy

¹³⁴ ^(a) INFN Sezione di Roma Tor Vergata; ^(b) Dipartimento di Fisica, Università di Roma Tor Vergata, Roma, Italy

¹³⁵ ^(a) INFN Sezione di Roma Tre; ^(b) Dipartimento di Matematica e Fisica, Università Roma Tre, Roma, Italy

¹³⁶ ^(a) Faculté des Sciences Ain Chock, Réseau Universitaire de Physique des Hautes Energies - Université Hassan II, Casablanca; ^(b) Centre National de l'Energie des Sciences Techniques Nucléaires, Rabat; ^(c) Faculté des Sciences Semlalia, Université Cadi Ayyad, LPHEA-Marrakech; ^(d) Faculté des Sciences, Université Mohamed Premier and LPTPM, Oujda; ^(e) Faculté des sciences, Université Mohammed V, Rabat, Morocco

¹³⁷ DSM/IRFU (Institut de Recherches sur les Lois Fondamentales de l'Univers), CEA Saclay (Commissariat à l'Energie Atomique et aux Energies Alternatives), Gif-sur-Yvette, France

¹³⁸ Santa Cruz Institute for Particle Physics, University of California Santa Cruz, Santa Cruz CA, United States of America

- ¹³⁹ Department of Physics, University of Washington, Seattle WA, United States of America
¹⁴⁰ Department of Physics and Astronomy, University of Sheffield, Sheffield, United Kingdom
¹⁴¹ Department of Physics, Shinshu University, Nagano, Japan
¹⁴² Fachbereich Physik, Universität Siegen, Siegen, Germany
¹⁴³ Department of Physics, Simon Fraser University, Burnaby BC, Canada
¹⁴⁴ SLAC National Accelerator Laboratory, Stanford CA, United States of America
¹⁴⁵ ^(a) Faculty of Mathematics, Physics & Informatics, Comenius University, Bratislava; ^(b) Department of Subnuclear Physics, Institute of Experimental Physics of the Slovak Academy of Sciences, Kosice, Slovak Republic
¹⁴⁶ ^(a) Department of Physics, University of Cape Town, Cape Town; ^(b) Department of Physics, University of Johannesburg, Johannesburg; ^(c) School of Physics, University of the Witwatersrand, Johannesburg, South Africa
¹⁴⁷ ^(a) Department of Physics, Stockholm University; ^(b) The Oskar Klein Centre, Stockholm, Sweden
¹⁴⁸ Physics Department, Royal Institute of Technology, Stockholm, Sweden
¹⁴⁹ Departments of Physics & Astronomy and Chemistry, Stony Brook University, Stony Brook NY, United States of America
¹⁵⁰ Department of Physics and Astronomy, University of Sussex, Brighton, United Kingdom
¹⁵¹ School of Physics, University of Sydney, Sydney, Australia
¹⁵² Institute of Physics, Academia Sinica, Taipei, Taiwan
¹⁵³ Department of Physics, Technion: Israel Institute of Technology, Haifa, Israel
¹⁵⁴ Raymond and Beverly Sackler School of Physics and Astronomy, Tel Aviv University, Tel Aviv, Israel
¹⁵⁵ Department of Physics, Aristotle University of Thessaloniki, Thessaloniki, Greece
¹⁵⁶ International Center for Elementary Particle Physics and Department of Physics, The University of Tokyo, Tokyo, Japan
¹⁵⁷ Graduate School of Science and Technology, Tokyo Metropolitan University, Tokyo, Japan
¹⁵⁸ Department of Physics, Tokyo Institute of Technology, Tokyo, Japan
¹⁵⁹ Department of Physics, University of Toronto, Toronto ON, Canada
¹⁶⁰ ^(a) TRIUMF, Vancouver BC; ^(b) Department of Physics and Astronomy, York University, Toronto ON, Canada
¹⁶¹ Faculty of Pure and Applied Sciences, and Center for Integrated Research in Fundamental Science and Engineering, University of Tsukuba, Tsukuba, Japan
¹⁶² Department of Physics and Astronomy, Tufts University, Medford MA, United States of America
¹⁶³ Department of Physics and Astronomy, University of California Irvine, Irvine CA, United States of America
¹⁶⁴ ^(a) INFN Gruppo Collegato di Udine, Sezione di Trieste, Udine; ^(b) ICTP, Trieste; ^(c) Dipartimento di Chimica, Fisica e Ambiente, Università di Udine, Udine, Italy
¹⁶⁵ Department of Physics and Astronomy, University of Uppsala, Uppsala, Sweden
¹⁶⁶ Department of Physics, University of Illinois, Urbana IL, United States of America
¹⁶⁷ Instituto de Física Corpuscular (IFIC) and Departamento de Física Atomica, Molecular y Nuclear and Departamento de Ingeniería Electrónica and Instituto de Microelectrónica de Barcelona (IMB-CNM), University of Valencia and CSIC, Valencia, Spain
¹⁶⁸ Department of Physics, University of British Columbia, Vancouver BC, Canada
¹⁶⁹ Department of Physics and Astronomy, University of Victoria, Victoria BC, Canada
¹⁷⁰ Department of Physics, University of Warwick, Coventry, United Kingdom
¹⁷¹ Waseda University, Tokyo, Japan
¹⁷² Department of Particle Physics, The Weizmann Institute of Science, Rehovot, Israel

- ¹⁷³ Department of Physics, University of Wisconsin, Madison WI, United States of America
¹⁷⁴ Fakultät für Physik und Astronomie, Julius-Maximilians-Universität, Würzburg, Germany
¹⁷⁵ Fakultät für Mathematik und Naturwissenschaften, Fachgruppe Physik, Bergische Universität Wuppertal, Wuppertal, Germany
¹⁷⁶ Department of Physics, Yale University, New Haven CT, United States of America
¹⁷⁷ Yerevan Physics Institute, Yerevan, Armenia
¹⁷⁸ Centre de Calcul de l’Institut National de Physique Nucléaire et de Physique des Particules (IN2P3), Villeurbanne, France
^a Also at Department of Physics, King’s College London, London, United Kingdom
^b Also at Institute of Physics, Azerbaijan Academy of Sciences, Baku, Azerbaijan
^c Also at Novosibirsk State University, Novosibirsk, Russia
^d Also at TRIUMF, Vancouver BC, Canada
^e Also at Department of Physics & Astronomy, University of Louisville, Louisville, KY, United States of America
^f Also at Department of Physics, California State University, Fresno CA, United States of America
^g Also at Department of Physics, University of Fribourg, Fribourg, Switzerland
^h Also at Departament de Fisica de la Universitat Autonoma de Barcelona, Barcelona, Spain
ⁱ Also at Departamento de Fisica e Astronomia, Faculdade de Ciencias, Universidade do Porto, Portugal
^j Also at Tomsk State University, Tomsk, Russia
^k Also at Universita di Napoli Parthenope, Napoli, Italy
^l Also at Institute of Particle Physics (IPP), Canada
^m Also at National Institute of Physics and Nuclear Engineering, Bucharest, Romania
ⁿ Also at Department of Physics, St. Petersburg State Polytechnical University, St. Petersburg, Russia
^o Also at Department of Physics, The University of Michigan, Ann Arbor MI, United States of America
^p Also at Centre for High Performance Computing, CSIR Campus, Rosebank, Cape Town, South Africa
^q Also at Louisiana Tech University, Ruston LA, United States of America
^r Also at Institutio Catalana de Recerca i Estudis Avancats, ICREA, Barcelona, Spain
^s Also at Graduate School of Science, Osaka University, Osaka, Japan
^t Also at Department of Physics, National Tsing Hua University, Taiwan
^u Also at Institute for Mathematics, Astrophysics and Particle Physics, Radboud University Nijmegen/Nikhef, Nijmegen, Netherlands
^v Also at Department of Physics, The University of Texas at Austin, Austin TX, United States of America
^w Also at Institute of Theoretical Physics, Ilia State University, Tbilisi, Georgia
^x Also at CERN, Geneva, Switzerland
^y Also at Georgian Technical University (GTU), Tbilisi, Georgia
^z Also at Ochadai Academic Production, Ochanomizu University, Tokyo, Japan
^{aa} Also at Manhattan College, New York NY, United States of America
^{ab} Also at Hellenic Open University, Patras, Greece
^{ac} Also at Academia Sinica Grid Computing, Institute of Physics, Academia Sinica, Taipei, Taiwan
^{ad} Also at School of Physics, Shandong University, Shandong, China
^{ae} Also at Moscow Institute of Physics and Technology State University, Dolgoprudny, Russia
^{af} Also at Section de Physique, Université de Genève, Geneva, Switzerland
^{ag} Also at Eotvos Lorand University, Budapest, Hungary
^{ah} Also at International School for Advanced Studies (SISSA), Trieste, Italy
^{ai} Also at Department of Physics and Astronomy, University of South Carolina, Columbia SC, United States of America
^{aj} Associated at Department of Physics, Oxford University, Oxford, United Kingdom

ak Also at School of Physics and Engineering, Sun Yat-sen University, Guangzhou, China

al Also at Institute for Nuclear Research and Nuclear Energy (INRNE) of the Bulgarian Academy of Sciences, Sofia, Bulgaria

am Also at Faculty of Physics, M.V.Lomonosov Moscow State University, Moscow, Russia

an Also at Institute of Physics, Academia Sinica, Taipei, Taiwan

ao Also at National Research Nuclear University MEPhI, Moscow, Russia

ap Also at Department of Physics, Stanford University, Stanford CA, United States of America

aq Also at Institute for Particle and Nuclear Physics, Wigner Research Centre for Physics, Budapest, Hungary

ar Also at Flensburg University of Applied Sciences, Flensburg, Germany

as Also at University of Malaya, Department of Physics, Kuala Lumpur, Malaysia

at Also at CPPM, Aix-Marseille Université and CNRS/IN2P3, Marseille, France

* Deceased